TÉCNICO LISBOA

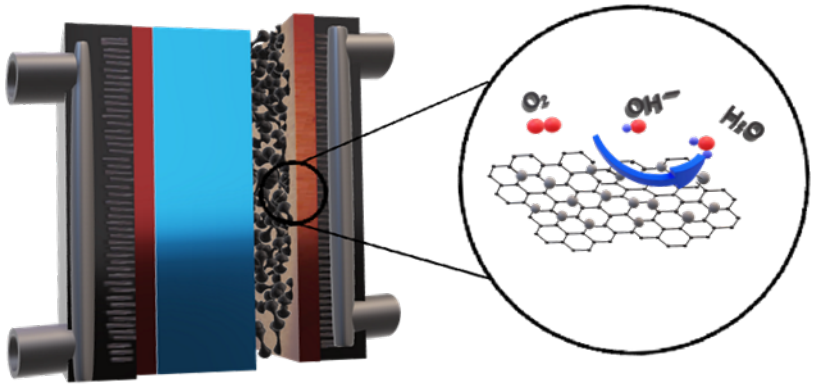

Electrochemical Characterization of Low and Non-Platinum Catalysts for Fuel Cell Applications in Gas Diffusion Electrode Setup

Talal Ashraf

Thesis to obtain the Master of Science Degree in

Energy Engineering and Management

Supervisors: Prof. Luísa Margarida Dias Ribeiro de Sousa Martins
Dr. Serhiy Cheverko

Examination Committee

Chairperson: Prof. Francisco Manuel Da Silva Lemos
Supervisor: Prof. Luísa Margarida Dias Ribeiro de Sousa Martins
Member of the Committee: Prof. Jorge Manuel Palma Correia

September 2020

Acknowledgments

The success of any project can only be possible with direct and indirect contributions. Through an amazing experience with all ups and down, challenges and moments of happiness and joy, I am concluding my degree with my thesis project for double degree Masters in Energy Transition. It is a time worth to mention the people and organizations with their valuable guidance, suggestion, support, facilities, and encouragement that enabled me to successfully complete this project. Firstly, I acknowledge my supervisors and mentors Konrad Ehelebe, Dr. Serhiy Cheverko, Professsor Dr. Luísa Margarida Martins and Professor Dr. Magdalena Dudek for their continuous support and help throughout the whole time. Without the contribution, idea, and development of GDE cell by Konrad with his continuous encouragement, this work would never come into realization. I pay special thanks to Helmholtz-Institut Erlangen-Nürnberg , Forschungszentrum Jülich for providing me excellent facilities, support, and platform within their outstanding infrastructure to perform my thesis. It is worth to mention that continuous support from teams in HIERN Electrochemical Energy Conversion group with their knowledge, mutual discussions and teamwork spirit and encouraging environment always motivated me to perform better and better. I would like to thank European Institute of Innovation and Technology and INNOENERGY for providing me best platform with mobility program which helped me to polish my profile for professional career. With all courses, trips, extracurricular activities, business startup challenges and support, entrepreneurial environment and learning by doing approach. I would like to acknowledge Prof. Dr. Karl Mayrhofer, Head of Electrocatalysis department and Alexander Hopf for their support for Pt/HGS catalyst and Prof Dr. Simon Thiele Electrocatalytic Interface Engineering department and his team especially Dominik Seeberger for their continuous support for Non PGM catalyst layer preparation and optimization. I also appreciate the administration officer Ewa Figorska from AGH University of Science and Technology and Rossella Leitao from Instituto Superior Técnico for helping me out through all administrative procedures in both universities. I also pay my gratitude to Dr. Karol Sztekler and Professor Dr Fatima Montemor, the directors of Energy Transition master program for providing me very demanding curriculum and gave me choice to choose extensive subjects and training courses.

Abstract

cell technology is taking the lead in energy transition for sustainable energy sources, but it is constrained by various factors, most importantly, the cost of precious catalysts. The advancement on the development and exploration of novel, cheap and highly effective and stable electrocatalyst tackling the challenges that are critical with ongoing research such as catalyse oxygen reduction reaction in the fuel cell. To benchmark the electrocatalyst, two conventional methods/device are used, i.e. RDE and MEA, which have several limitations. In this work, gas diffusion electrode GDE half-cell setup which is a novel optimised benchmarking tool is used to determine the ORR activity of electrocatalysts and aimed to bridge the gap between fundamental and applied electroanalytical devices as RDE and MEA. To investigate the versatility of GDE method, various catalysts were investigated to optimise the catalyst layer such as commercial Pt/C catalyst, advanced Pt/HGS catalyst and non PGM Fe-N-C catalyst. The Pt/C proved to be high performing catalyst with ECSA of 66.59 m^2/g_{pt} approaching the current density of 2 A/cm^2 at 0.63 V_{RHE} in 1.0 M $HClO_4$. As compared to $HClO_4$, the Pt/C suffered from severe degradation in 1.0 M H_2SO_4 facing mass transport limitation. The addition of membrane to commercial Pt/C in both electrolytes to mimic the conditions of PEMFC gave a comparable activity with less degradation. However, the Pt/C approached to extreme mass transport limitation in synthetic air due to the low concentration of O_2. The performance of Pt/C in alkaline was superior by achieving limiting current density of 2 A/cm^2 at 0.8 V_{RHE}, which was highest in comparison to literature and it is believed to be overestimated due to huge difference for forward and backward scan. Stress cycling of Pt nanoparticles confined highly graphitised spheres support Pt/HGS improved the catalyst activity. After subjecting to 10,000 and 30,000 cycles, the ORR activity enhanced up to 50 mV, and thus the catalyst layer was optimised accordingly. AEMFC conditions were also be mimicked in GDE cell with non PGM catalyst Fe-N-C which was investigated in 1.0 M KOH for the stability, ionomer activation and reproducibility. The catalyst layer was optimised with high ion exchange ionomers, and it has been found that the catalyst activity can be enhanced to approximately 80-100 mV by several breaking and time-based(max 48 hours) ionomer activation procedures. The Fe-N-C showed stability during ORR in O_2 but faced severe degradation in O_2 backed degradation cycling, which requires more investigations. Thus, GDE is proved to be a very effective method for quicker, reliable optimisation of electrocatalyst performance but with several challenges which are discussed in this work and it can be used to optimise the catalyst layer properties

with minimum efforts. The issues can be addressed by merging different characterisation mechanism and metal ions dissolution quantification techniques that will enable this method to be upgraded for fuel cell electrocatalyst research and development sector.

Keywords

Oxygen reduction reaction; Non precious metal group catalyst; Platinum confinement; Gas diffusion electrode; AEMFC; PEMFC.

Resumo

A tecnologia das células de combustível lidera a transição energética para fontes de energia sustentáveis, mas é limitada por vários fatores, principalmente por catalisadores de metais preciosos. O avanço no desenvolvimento e exploração de novos eletrocatalisadores altamente eficazes, estáveis e baratos, tem como objectivo superar os desafios que são críticos na investigação actual, tais como catalisar a reação de redução de oxigénio nas células de combustível. Para avaliar o eletrocatalisador, são utilizados dois métodos / dispositivos convencionais i.e., RDE and MEA que têm várias limitações. Neste trabalho, a configuração de semi-célula de eléctrodo de difusão gasosa, que é uma nova ferramenta de avaliação de eletrocatalisador utilizado otimizada para ORR, visa preencher a lacuna entre dispositivos eletroanalíticos fundamentais e aplicados tais como RDE e MEA. Para investigar a versatilidade do método GDE, foram investigados vários catalisadores para otimizar a camada catalítica, tais como o catalisador comercial Pt/C, o catalisador avançado Pt/HGS e o catalisador Fe-N-C não PGM. A Pt/C provou ser um catalisador de elevado desempenho com ECSA de 66,59 m^2/g_{pt} aproximando-se da densidade de corrente limite de 2 A/cm^2 a 0,63 V_{RHE} em $HClO_4$ 1,0 M. Em comparação com o $HClO_4$, a Pt /C sofreu elevada degradação em H_2SO_4 1,0 M enfrentando a limitação de transporte de massa. A adição de membrana a Pt/C comercial em ambos os eletrólitos para mimetizar as condições de PEMFC originou uma atividade comparável, com menor degradação. No entanto, a Pt/C aproximou-se da limitação de transporte de massa extrema em ar sintético devido à baixa concentração de O_2 e à contaminação do ar. O desempenho de Pt/C em meio alcalino foi superior ao atingir uma densidade de corrente limite de 2 A/cm^2 a 0,8 V_{RHE}, que foi a mais elevada em comparação com a literatura e se acredita que esteja sobre-estimada devido à enorme diferença nos varrimentos num sentido e no sentido contrário. O ciclo de tensão de nanopartículas de Pt confinadas e altamente grafitizadas Pt/HGS melhorou a atividade catalítica. Após sujeitar a 10000 e 30000 ciclos, a atividade ORR aumentou até 50 mV e, portanto, a camada de catalisador foi otimizada concordantemente. As condições de AEMFC também foram mimetizadas na célula GDE com catalisador Fe-N-C não PGM, que foi investigado em KOH 1,0 M relativamente à estabilidade, ativação de ionómero e reprodutibilidade. A camada de catalisador foi optimizada com ionómeros de elevada permuta iónica e verificou-se que a atividade do catalisador pode ser aumentada para aproximadamente 80 -100 mV por vários procedimentos de ativação de ionómero baseados em quebra e tempo (máximo de 48 horas). O Fe-N-C provou ser estável durante ORR em O_2, mas enfrentou degradação severa no ciclo de degradação

suportado em O_2. Assim, GDE provou ser um método muito eficaz para uma otimização mais rápida e confiável do desempenho do eletrocatalisador, mas com vários desafios que são discutidos neste trabalho e pode ser usado para otimizar as propriedades da camada de catalisador com um esforço mínimo. Estes problemas podem ser resolvidos através da fusão de diferentes mecanismos de caracterização e técnicas de quantificação de dissolução de iões metálicos que permitirão a utilização desse método para o setor de investigação e desenvolvimento de eletrocatalisadores de células de combustível.

Palavras Chave

Reação de redução de oxigênio; Catalisador de grupo de metais não preciosos; Confinamento de platina; Eletrodo de difusão de gás; AEMFC; PEMFC.

Contents

List of Figures

List of Tables

Acronyms

AFC	Alkaline Fuel Cell
AEM	Anion Exchange Membrane/Alkaline Exchange Membrane
AEMFC	Anion Exchange Membrane Fuel Cell/Alkaline Exchange Membrane Fuel Cell
AST	Accelerated Stress Test
CCM	Catalyst Coated Membrane
CV	Cyclic Voltammetry
ECSA	Electrochemical Surface Area
EIS	Electrochemical Impedance Spectroscopy
FET	Floating Electrode
FCV	Fuel Cell Vehicle
GDE	Gas Diffusion Electrode
GDL	Gas Diffusion Layer
HIEC	High Ion Exchange Capacity
HGS	Hollow Graphite Spheres
HOR	Hydrongen Oxidation Reaction
LIEC	Low Ion Exchange Capacity
MEA	Membrane Electrode Assembly
MCFC	Molten Carbonate Fuel Cell
OER	Oxygen Evolution Reaction
ORR	Oxygen Reduction reaction
OCV	Open Circuit Voltage
PAFC	Phosphoric Acid Fuel Cell

PEM	Proton Exchange Membrane/Polymer Electrolyte Membrane
PEMFC	Proton-Exchange Membrane Fuel Cells/Polymer Electrolyte Fuel Cell
PGM	Precious Group Metals
RDE	Rotating Disk Electrode
RHE	Reversible Hydrogen Electrode
SGEIS	Staircase Galvanic Impedance Spectroscopy
SOFC	Solid Oxide Fuel Cell
SA	Synthetic Air

1

Introduction

Contents

1.1 Motivation

In the era of Global warming, the mainstream concern for all countries is to stabilize greenhouse gases concentration caused by anthropogenic activities imposing drastic changes in eco and biosphere. The CO_2 emissions surged up to 1.7% of total emissions (33.1 Gt CO_2) in 2018 caused by high energy demand as energy production industries contributes to 30% of CO_2 emissions [1]. The focus of big economies is diverting towards sustainable environment under the framework of the Kyoto Protocol and Paris agreement [1]. According to Environmental Indicator Report for European Economic Area published in 2018, the objectives of green and low carbon economy constrained by greenhouse gases from transportation sector is unlikely to be achieved by 7^{th} Environmental Action Plan implementation (2014-2020). The transportation industry and businesses have a significant contribution in greenhouse gases emission as in 2017, nearly 27% of total EU emissions came from mobile vehicles, making it the second biggest pollutant emitter after energy production sector [2]. Fuel cell technology emerged as a significant technology to reduce the petroleum needs for transportation, stationary and cross-cutting applications with rapid progression.

From several decades, the research and development has been carried out to combat the challenges of fuel cell commercialization. The versatility of fuel cell broadens its scope to transportation and power generation sector from fuel cell electric vehicles to integrated combined heating and power systems and reformer systems [3]. The infrastructure for fuel cell vehicles (FCV) is growing to further advancement as more H_2 powered vehicles are being produced primarily in Germany, Japan and the USA. Japan has surpassed every other country with a massive infrastructure of 92 hydrogen refuelling stations. The automobile industry also stepped with a sustainable business model to produce fuel cell vehicles such as Toyota planned to produce 30,000 vehicles per year in 2020, Hyundai is targeting for 40,000 units per year production facility with 6.2 Billion US dollars investment [4]. In 2019, it was forecasted that the fuel cells shipped for transport purposes would reach a capacity of almost 907.8 megawatts. The most delivered fuel cells to customers belong to the transportation sector, and thus the supply has been increasing exponentially (see Figure 1.1). This trend shows the potential of zero-emission- fuel cell applications in the transportation sector and interest of the business community, but certain factors act a barrier for widely possible commercialization.

Fuel cell relies heavily on catalyst mainly platinum, which acts as a significant barrier to overcome the cost-related issues in a fuel cell and the potential depletion of platinum reserves worldwide. As per the breakdown analysis of fuell cell systems, the fuel cell catalyst costs around 41% of the total stack accounts for 500,000 units per year projected in 2017 [3]. The projected cost for the fuel cell system is nearly around 45 USD/kW with a target of 30 USD/kW by the US Department of Energy. From the past decade, the commercial (FCV) sector focused on the reduction of platinum loading, which eventually reduces the total cost of the system. The platinum consumption in the commercial sector is widely

varied for different numbers of applications. Auto-catalyst industries are major sectors in the market of platinum consumption to 34.33% of total available platinum in the market shown in Figure 1.1 as most of which is utilized in the fuel cell. Most of the platinum metal reserves available worldwide are present in South Africa nearly 63,000 metric ton which is 95% of total reserves available today in Earth crust (see Figure 1.1C). Increasing demand and depleting reserves of precious metal catalysts are one of the major concerns for fuel cell industrial applications. In 2017, the platinum loading targets had been reduced to 0.125 mg/cm^2 (around 10 g/vehicle) as compared to 1.0 mg/cm^2 (80 g/vehicle) in 2002 and even the 10 g of platinum will add the cost of 300 USD per vehicle. Over time, there is a parallel relation in fuel cell system cost and catalyst loading, which results in the reduction of 84% system cost and 88% platinum loading [4].

In the past years, extensive research has been carried out for electrocatalyst of fuel cell, especially in PEMFC. The commercialization of PEMFC is constrained by limited power density and stability [5], mostly a trade-off between efficiency and durability. The catalyst must be able to bear extensive potential cycling and shutdown events for over 5000 hours lifetime and produce at least 1-1.5 A/cm^2 at 0.6 V_{RHE} [6]. The high current density is limited by the sluggish kinetic reaction of ORR at the cathode for which high over-potentials are required to reach nearly to a theoretical value of open-circuit voltage OCV to 1.23 V_{RHE} [7]. Catalyst deactivation limits the efficiency of the fuel cell, and if performance loss exceeds to >10%, it would be a great challenge to meet the requirement of 8000 hours which is equivalent to 150,000-mile coverage in cars [5]. Due to the high price and scarcity of platinum metal, the better performance with engineered ultra-low loading catalysts (0.1 mg/cm^2) or other alternative is desirable. Advanced catalyst synthesis methods can overcome the cost-performance gap, such as modifying and controlling the composition and surface of platinum nanoparticles at the microscopic level or investigating the substitutes of Platinum metal groups PGM with similar performance and stability. The structural modification (nanowires and thin films) of pure platinum leads to higher stability while the different catalytic configuration (bimetallic or trimetallic) of platinum leads to higher activity. Two primary factors can classify the activity of the catalyst, i.e. specific activity and mass activity. The specific activity provides information to estimate the parameters (turn over frequency) for tuning the surface and electronic structure of catalyst [8].

To meet the technical targets, the research on ultra-low loading and non-Precious Group Metals (PGM) catalysts has increased, and several methods are used to investigate the electrocatalyst for fuel cell in laboratory [9]. The main approach is to use the minimum amount of catalyst in rapid screening with validated results. The benchmarking of electrocatalyst for the fuel cell is mainly done in Membrane Electrode Assembly MEA to estimate the actual realistic performance. The experiment is time-consuming and requires many parameters controlling procedures and electrode preparation for testing. Other methods like half-cell catalyst benchmarking tests provide electrocatalysis performance in less time with good

hydrodynamics for low loading catalysts [10]. The preferred half cell method to investigate fundamental catalytical performance is the rotating disk electrode RDE method, which eliminates the requirement of membrane assembly preparation complex procedures. Various groups determine the ORR and ECSA estimation with good reproducibility in thin-film RDE which leads to the adaptability of this technique for Pt on Carbon and Non-Carbon support catalyst, Pt/HGS, Nanoparticles, Pt alloys, Thins film, Non-PGM catalysts [11–14]. PEMFC faces several challenges with platinum as a catalyst due to corrosive conditions in the cell with very high overpotentials. An alternative fuel cell that works on less corrosive environments with effective performance is AEMFC which can help to investigate further development of non-PGM electrocatalysts. It will require an extensive amount of research to be done with numerous testing to benchmark new catalyst. Several methods are employed to benchmark electrocatalyst such as RDE, MEA, half cell GDE and floating electrode. The bottleneck for RDE technique is an unapproachable current density to real fuel cell conditions as the limiting current draws near to 6 mA/cm^2 at 1600 rpm. RDE measurements are usually performed at ambient temperature and 1 bar oxygen partial pressure that limits the oxygen solubility in electrolyte hence resulting in low current densities due to low concentration and diffusion coefficients of dissolved gases. Catalyst performance can differ to a broad range from 0.6-0.9 V_{RHE} due to mass transport phenomena inside the catalyst layer. It could lead to the misinterpretation of RDE results in which catalyst perform better at 0.9 V_{RHE} because the catalyst assembly is immersed in an electrolyte (oxygen saturated) providing superior access to electrons and protons while poor results for higher current densities in MEA. To overcome the gap and to take advantage of a fast and simplified method of RDE and high current densities of MEA, another method has been developed to benchmark catalyst in half cell gas diffusion electrode GDE setup for investigating the kinetics of electrocatalyst for ORR [15]. In this work, the standard and advanced PGM and non PGM electrocatalyst will be benchmarked for ORR in novel GDE half-cell to determine parameters affecting the performance of fuel cell in real-time.

1.2 Objectives

The objectives of this thesis are to investigate the catalytic activity for oxygen reduction reaction and to benchmarking the state of the art commercial, advanced, and non-platinum catalyst. Furthermore, the stability of electrocatalyst in oxygen and argon and synthetic air will also be investigated along with the degradation of the advanced platinum catalyst.

- Electrocatalyst benchmarking for ORR in GDE half cell which is used to bridge the gap between RDE and MEA method
- Investigation of the different electrolytes in PEMFC conditions for the commercial platinum catalyst in GDE half cell

- Investigation of the advanced platinum electrocatalyst Pt/HGS with activation and break-in procedures to analyze the most active state of electrocatalyst
- Testing of non-PGM electrocatalyst with different specialized ionomer for alkaline fuel cell along with an investigation of catalyst and ionomer activation time concerning stability in alkaline electrolyte
- Stability and reproducibility for Fe-N-C for AEMFC conditions in GDE Half cell
- Addressing the problems and errors for ORR performance in GDE half cell investigation

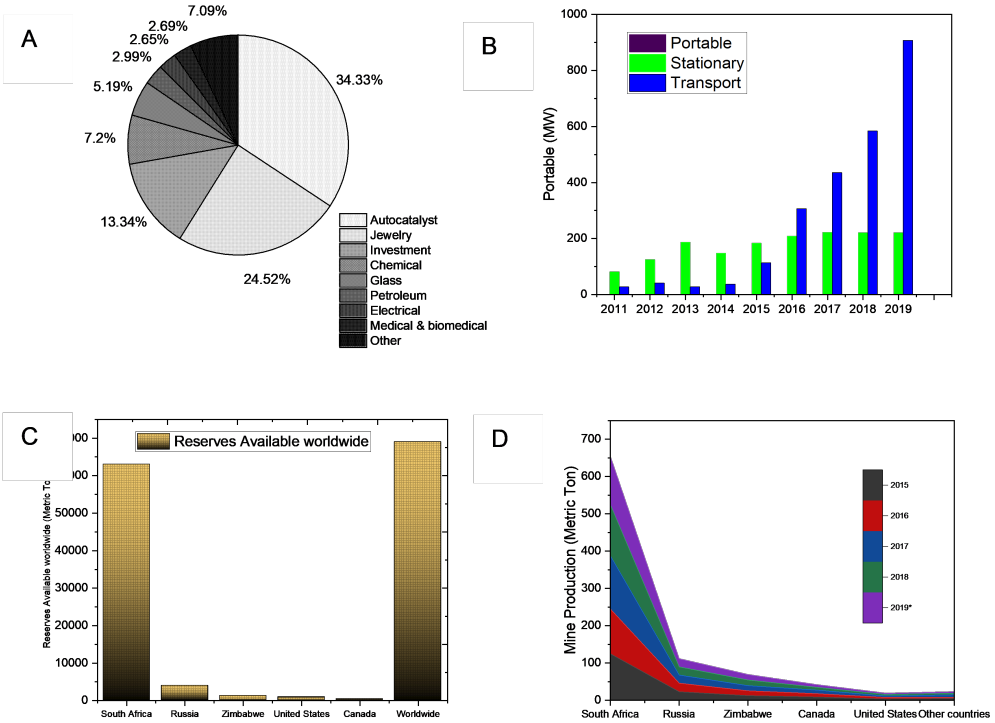

Figure 1.1: Statics of Platinum applications, demand, extraction, and reserves availability worldwide. A: Global platinum demand breakdown by the area of application in 2019. B: Global Capacity of fuel cell shipment from 2011-2019 worldwide for transportation section C: Estimated platinum metal reserves available globally. D: Global extraction of platinum from mines from 2015-2019 worldwide [16]

[0]Data is extracted from individual reports from different organizations and compiled together. Source:http://www.example.com/the

Table 1.1: DOE targets for electrocatalyst from 2015-2020 for transportation application [17]

Characteristics	Unit	2015 Target	2020 Target
PGM Content	g/kW	0.16	0.236
PGM loading	mg_{PGM}/cm^2	0.13	0.125
Mass Activity	A/mg_{PGM} at 900mV IR-Free	0.5	0.44
PGM free catalyst activity	A/cm^2 at 900mV IR-Free	0.016	>0.044
Performance Loss at 1.5A/cm^2	mV	65	>30
Initial activity loss	%mass activity loss	66	<40
Support Stability	%mass activity loss	41	<40

2

Literature Review and Fundamentals

Contents

The fuel cell is an electrochemical device that converts chemical energy into electrical energy with unique features of the one-step process as compared to multi-step combustion-based systems (chemical-thermal-mechanical-electrical) [18]. Due to the high energy conversion efficiency around 40% as compared to conventional power generation systems (photovoltaics, wind turbines and generators, reciprocating engine range from 6-40%), it is considered to be an up-and-coming solution with significant research in past decade [19]. The concept of fuel cell dated back to early 18^{th} century by the British chemist Humphry Davy who worked on the discovery of new metals by splitting common compounds with the help of voltaic pile. Taking the same concept of electrolysis, in 1839 the welsh chemist William Robert Groove also known as the father of fuel cell introduced a *"gas battery"* (known as a fuel cell) and demonstrated that the current could be generated by the reaction of hydrogen and oxygen through a reverse process. He defined his experiment by an expression ***"I cannot but regard the experiment as an important one..."***. Later in 1889, the British chemists Charles Langer and Ludwig Mond advanced the Grooves invention "gas battery" by introducing the three-dimensional porous electrodes with coal as fuel contrary to grooves argument that only pure hydrogen can be used as fuel in cell and began a new approach for electrochemical fuel systems [20]. In 1958, a British engineer Francis Thomas Bacon worked on the Langer and Mond cell and developed a fully operational fuel cell (Alkaline fuel cell AFC) which was later used by Apollo space mission and Harry Karl Ihrig farm field tractor. Since the development of new material Teflon in 1950, the material was then used for acid electrolyte and hence, at the end of 1950, two chemists from General Electric (GE), Willard Thomas Grubb and Leonard Niedrach designed the fuel cell (Polymer electrolyte membrane fuel cell PEMFC) which was then used by NASA and McDonnell Aircraft in the interim of Gemini space program [21–23]. Since the 19^{th} century until now, the fuel cell technology is emerging with better designs and efficiency for a broad range of commercial applications.

2.1 Fuel Cell Fundamentals

A fuel cell comprises of two electrodes anode (negative electrode) and the cathode (positive electrode) which are spatially separated by an electrolyte. In principle, two half electrochemical reactions are carried out in fuel cell, the fuel (hydrogen gas) is oxidized at anode resulting in the production of electrons and protons. The electrons flow through an electric circuit producing the current before making it to the cathode while the protons penetrating the membrane recombine with electrons and produce H_2O.

$$H_2 \rightleftharpoons 2H^+ + 2e^- \tag{2.1}$$

$$\frac{1}{2}O_2 + 2H^+ + 2e^- \rightleftharpoons H_2O \tag{2.2}$$

$$H_2 + \frac{1}{2}O_2 = H_2O \tag{2.3}$$

The critical component of the fuel cell is a unit cell, and different types of the fuel cell may vary in design, but they follow a similar working principle, as mentioned in Figure 2.1.

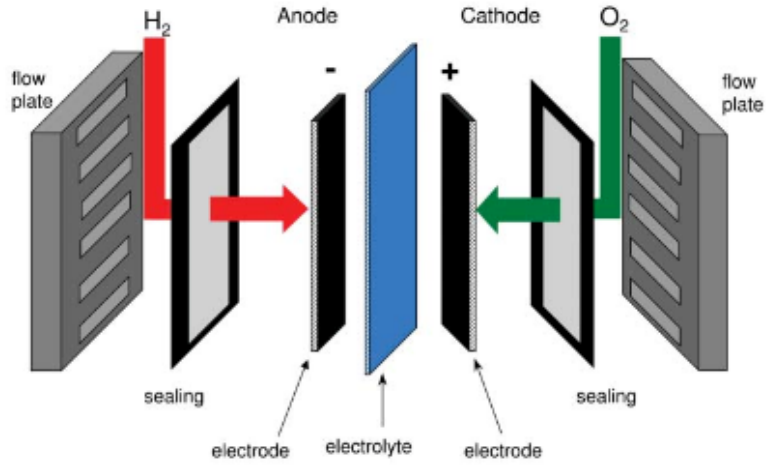

Figure 2.1: Illustration of single simple fuel cell. Reproduced with the permission from Royal Society of Chemistry [23]

Typical components of the fuel cell are bipolar plates, gas diffusion layer, catalyst layer and membrane. The bipolar plates which serve as flow channel/distributor made from metal or carbon composite. Their main functions are to act as a current collector from the circuit, distribution of oxidants across electrode and removal of the product(water) [24]. The micro-porous gas diffusion layers are an essential part of fuel cell assembly, usually made from carbon-based materials with high conductivity. GDL facilitates the diffusion of gases across catalyst layers and help to reduce the flooding due to hydrophobic properties [25]. The Oxygen reduction reaction (ORR) and Hydrogen oxidation reaction (HOR) occurs at the catalyst layer. The role of the catalyst is to catalyse the oxidation and reduction reaction. Usually, the catalysts (in nanoparticle forms of metal) are supported on a carbon base with high surface area to mass ratio, which increases the catalyst utilisation. The catalyst is combined with ionomer such as Nafion™which acts as a binder and helping protons to reach triple-phase boundary [26]. The membrane in fuel cell acts as a barrier to avoid intermixing of both gases (H_2 and O_2), allowing only protons to flow, the membrane is hydrophilic, absorbing the water [27] and hence increasing the conductivity forming protons conducting channels. All the elements of the fuel cell are pressed together, forming a single cell Membrane electrode assembly MEA, which are combined in the stack for practical applications [28–30]. Different fuel cell are available in the market which are categorized based on electrolytes but differ in the performance, efficiency, temperature range and applications. The classification of fuel cell is enlisted as below and the characteristics of these fuel cells are mentioned in section 2.8

- Alkaline fuel cell AFC

- Proton exchange membrane fuel cell PEMFC
- Phosphoric acid fuel cell PAFC
- Molten carbonate fuel cell MCFC
- Solid oxide fuel cell SOFC

Table 2.1: Fuel cell types characteristics based on their design and working principles

Type	Operating Temperature°C	Power kW	Efficiency	Capital Cost (USD/kW)	Lifetime [31]
AFC	100	1 - 100 kW	60%	200	10,000
PEMFC	<120	1 - 100 kW	60%	200	40,000
PAFC	150-200	5 - 400 kW	40%	3000	40,000
MCFC	600-700	300 kW - 3 MW	50%	1000	40,000
SOFC	500-1000	1 kW - 2 MW	60%	1500	40,000

This work is focused on fundamentals of PEMFC and AEMFC.

2.2 Fuel cell Kinetics and Thermodynamics

Since the fuel cell utilizes hydrogen as fuel, oxygen as an oxidizer with water as a product, the enthalpy of reaction in the fuel cell is estimated by the difference of heat of formation (Hf) and reaction in the cell by considering the reaction in Equation 2.4 and it can be calculated as follows.

$$\Delta H_{cell} = Hf_{H_2O} - Hf_{H_2} - \frac{1}{2}Hf_{O2} \tag{2.4}$$

The portion of enthalpy of reaction can be converted into fuel cell electricity as some entropy is produced by the reaction that cannot be converted into electricity which is correlated with Gibbs free energy.

$$\Delta G = \Delta H - T\Delta S \tag{2.5}$$

For Hydrogen/Oxygen fuel cell, the change in gibbs free energy is represented as

$$\Delta G_{fcell} = G_{fH_2O} - G_{fH_2} - \frac{1}{2}G_{fO_2} \tag{2.6}$$

The change in Gibbs free energy varies with both temperature and pressure

$$\Delta G_{fcell} = \Delta G^{\circ}_{fcell} - RTln\frac{p_{H2} * p_{O2}^{\frac{1}{2}}}{p_{H_2O}} \tag{2.7}$$

where ΔG°_{fcell} is the change in Gibbs free energy at standard pressure, which varies with the temperature T of the fuel cell in Kelvin, p_{H2}, p_{O2} and p_{H_2O} are the partial pressure of the hydrogen, oxygen, and

vapor, respectively. R is the universal gas constant (8.314 J/Kg K). When all the gibbs free energy converted into electrical energy, the fuel cell considered to be reversible and the voltage of fuel cell is related to the change in gibbs energy.

$$\Delta G_f = -nFE_{rev} \tag{2.8}$$

where F is Faraday constant (96485 coulombs) and E is the voltage of the fuel cell. The number n in the equation is the number of electrons. E_{rev} is called the reversible fuel cell potential, also known as the thermodynamic potential. Several operating conditions can effect the reversible fuel cell potential, for instance, the temperature dependence on the reversible voltage of fuel cell also known as Nernst voltage and it can be represented by the Nernst equation [32]. In the case of a hydrogen fuel cell, for each mole of hydrogen two moles of electrons pass around the external circuit (n =2). So the physical meaning of 2FE is the electrical work (charge *voltage).

$$E = -\frac{\Delta G_f}{2F} \tag{2.9}$$

$$E = -\frac{\Delta G^{\circ}_{fcell}}{2F} + \frac{RT}{2F} ln \frac{p_{H2} * p_{O2}^{\frac{1}{2}}}{p_{H_2O}} \tag{2.10}$$

At standard state (25 °C and 1 atm), the value of the term $-\frac{\Delta G^{\circ}_{fcell}}{2F}$ is given by

$$E = \frac{237.340 * J/mol}{2 * 96485 * A.s/mol} \tag{2.11}$$

$$E = 1.23V \tag{2.12}$$

The reversible fuel cell potential changes with different temperatures and standard pressures. The relation of change in Gibbs free energy, reversible cell voltage, and efficiency limit (high heating value HHV basis) of hydrogen fuel cell reaction at different temperatures can be observed from the literature [32]. The reversible or Nernst voltage of fuel cell is also known as theoretical open circuit voltage (OCV) which is effected by both temperature and pressure and it is represented by the difference of cathode and anode Nernst potential $E_c^r and E_a^r$ respectively.

$$E^{theo}_{OCV} = E^r_c - E^r_a \tag{2.13}$$

In PEMFC, for cathode reaction $O_2 + 4H^+ + 4e^- = H_2O$

$$E^r_c = E^{\circ}_c + \frac{RT}{4F} ln(p_{O2}[H^+]^4) \tag{2.14}$$

For anode reaction $H_2 = 2H^+ + 2e^-$

$$E_a^r = E_a^\circ + \frac{RT}{2F} ln \frac{[H^+]^2}{p_{H2}} \tag{2.15}$$

Where E_c° and E_a° are the standard cathode and anode potentials, respectively.

The theoretical OCV has the same value as the reversible cell potential. However, even when no current is drawn from a fuel cell, there is irreversible voltage loss, which means that the actual values of the OCV are always lower than the theoretically expected values. To date, a quantitative explanation for such OCV behavior has not been clear in the literature. The lower values of OCV is always interpreted by the mix potential which is the combined effect of several losses such as fuel cross over, internal shorts and parasitic oxidation reaction that occurs at cathode. These losses makes a difference between the measured OCV and the theoretical cell potential. So the actual OCV is represented as

$$E_{OCV} = E_{OCV}^{theo} - E_{cross} - E_{mix} \tag{2.16}$$

Where E_{cross} is loss of OCV by the crossover of the fuel through the electrolyte. The electrolyte transfer ions but in reality, some fuel also permeates to the membrane from anode to cathode. This fuel loss leads to the current loss and it can react with the oxidant resulting in a depression at cathode potential. It is believed that the H2 that has crossed over can form a local half-cell electrochemical reaction on the cathode.

In fuel cell, when all gibbs free energy is converted into electrical energy then the maximum theoretical efficiency of at at 25 °C is given by

$$\eta = \frac{\Delta G_{fcell}^\circ}{\Delta H^\circ} \tag{2.17}$$

$$\eta = \frac{237.1 Kj/mol}{286 Kj/mol} = 83\% \tag{2.18}$$

The theoretical efficiency is sometimes also known as the thermodynamic efficiency or the maximum efficiency limit The maximum efficiency of H_2/O_2 fuel cell is $\approx 83\%$ (theoretical) [33]. At the standard condition, the system reaches to the open circuit potential (theoretical) which is 1.23V [34]..

Kinetics of electrochemical reaction is different from the chemical reactions as it involves the transfer of electrons between an electrode and chemical spices while in chemical reactions , the reaction occurs without the liberation of electrons between two chemical species [32]. The electrochemical reactions are necessarily heterogeneous because it takes place at electrode electrolyte interface. Since the electrons are either consumed or generated during electrochemical reactions, the current i generated during the electrochemical reaction is the measure of rate of reactions. From the Faraday Law

$$i = \frac{dQ}{dt} \tag{2.19}$$

where Q is the charge (C) and t is time. Since the current is the rate of charge transfer and if the reaction results in transfer of n electrons then

$$i = nF\frac{dN}{dt} = nFv \tag{2.20}$$

where (dN/dt = v is the rate of the electrochemical reaction (mol/s) and F is Faraday's constant. As the electrochemical reactions are heterogeneous i.e. reaction occurs at electrode electrolyte interface, the current produced is related to the active area (A) of interface between electrode and electrolyte. This proportionality makes current density j more fundamental than current and expressed in amperes/square centimetre.

$$j = \frac{i}{A} \tag{2.21}$$

The electron energy is controlled by potential which is a measure of electron energy and can be determined by Fermi level. The direction of reaction is influenced by the control of electrode potential. Electrode potential can be manipulated to trigger reduction or oxidation. The thermodynamic equilibrium electrode potential (middle) corresponds to the situation where the oxidation and reduction processes are balanced.

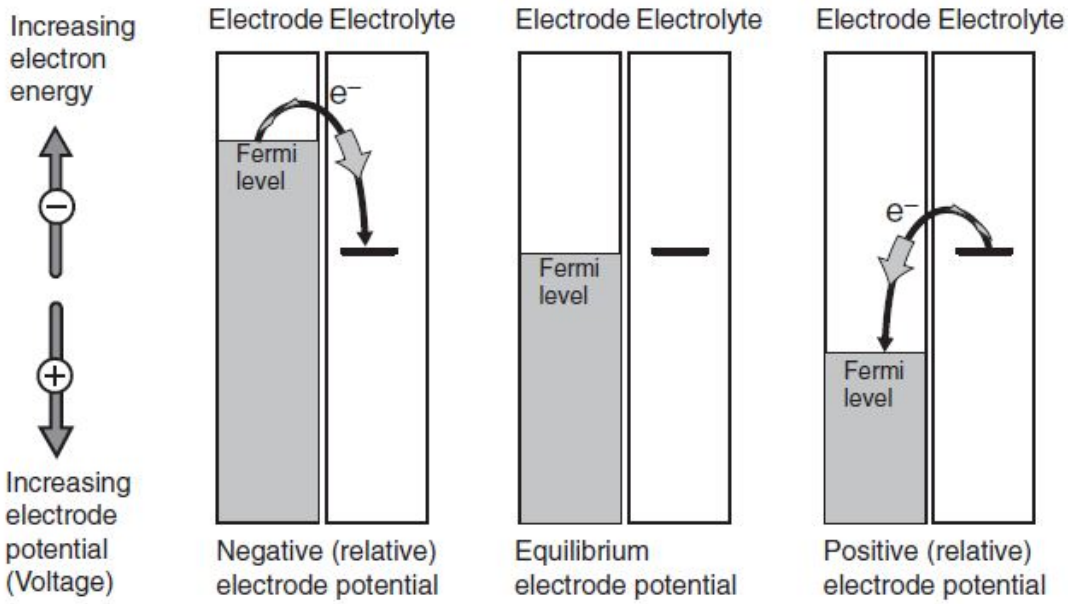

Figure 2.2: Influence on Fermi level by applied positive and negative potential for redox reaction . Reprinted from [35]

In general redox reactions, if the electrode potential is made to the negative than equilibrium, the reaction will leads to reduced forms of chemical specie, as negative electrode forces the electrons out of the electrode onto the electroactive species. By applying the positive potential than equilibrium potential, the reaction will lead to formation of oxidized species by attracting the electrons to electrode and pulling them out from electroactive species [35]. The current produced during an electrochemical reaction is limited as

the rate of any reaction is finite. In order to initiate the reaction, an activation barrier impedes the conversion of reactants to products. Only the species in the activated state can achieve the transition state to the products. For overall reaction, the net rate is the different of forward and reverse reactions and is defines as J = J1-J2, where J is the net reaction rate while J1 and J2 corresponds to the forward and reverse reactions rates. In general both reaction rates are not equal and the activation barrier for the forward reaction is much smaller than the activation barrier for the reverse reaction (G‡1 < G‡2). In this situation, it stands to reason that the forward reaction rate should be much greater than the reverse reaction rate. The net reaction rate can be written as

$$J = c(_R)f(_1) * e^{\frac{G‡1}{RT}} - c(_P)f(_2) * e^{\frac{G‡2}{RT}} \tag{2.22}$$

where $c(_R)$ is the reactant surface concentration, $c(_P)$ is the product surface concentration, G‡1 is the activation barrier for the forward reaction, and G‡2 is the activation barrier for the reverse reaction,$f(_1)$ is the decay rate of products and $f(_2)$ is the decay rate of reactants.

The reaction rates can be recasted to the current densities. At thermodynamic equilibrium, the forward and reverse current densities must balance so that there is no net current density (j = 0). In other words j_1=j−2=j°, j° is the exchange current density for the reaction. At equilibrium the net reaction rate is zero, both forward and reverse reactions are taking place at a rate which is characterized by j°; this is called dynamic equilibrium. As moving away from the equilibrium, the new current densities (forward and backward) can be rewrite by taking consideration of starting from j° to the change in direction of activation barrier.

$$j_1 = j^\circ e^{\frac{\alpha n F \eta}{RT}} \tag{2.23}$$

$$j_2 = j^\circ e^{-\frac{(1-\alpha) n F \eta}{RT}} \tag{2.24}$$

The net current density will be

$$j = j^\circ (e^{\frac{\alpha n F \eta}{RT}} - e^{-\frac{(1-\alpha) n F \eta}{RT}}) \tag{2.25}$$

α is known as transfer coefficient and its value depends on the symmetry of activation barrier, its value typically lies between 0 and 1. The Equation 2.25 is known as Butler-Volmer Equation and it is considered as the main equation for electrochemical kinetics [35]. The Butler–Volmer equation tells that the current produced during reaction increase exponentially with the activation over voltage which is the voltage loss to overcome the activation barrier. This represents that in practical application that to get more current from fuel cell, we have to bear more burden of voltage of loss. The activation polarization is split into two categories, one for the anode and other for the cathode. The anodic activation polarization is associated with HOR while the cathodic activation polarization is related to ORR. To achieve the maximum efficiency and performance, the polarization losses must be limited to much lower as possible.

One approach is to reduce the losses within the cell by selecting appropriate materials with higher conductivity. For example, the ohmic drop can be decreased by an ultra-thin membrane with 10 μm thickness, as investigated in Toyota Mirai by researchers [36]. One approach is to minimize the cell resistance in between by reducing the contact resistant or by improving the electrical conductivity of stack through appropriate material selection. Another approach is the proper designing of the gas distribution system and high conductive GDL and catalyst layers. In the fuel cell, the facile nature of redox can be overcome easily by appropriate electrocatalyst catalyst [37]. However, due to the higher-order and complexity of ORR, it is very challenging to overcome losses by activation polarization which can be dealt with by designing novel catalysts.

The Butler Volmer equation applies to all reactions in a fuel cell as different reactions produce different products. The kinetic parameters with low values impose sluggish kinetics which affects the performance. In the fuel cell, the HOR reaction is fast enough as compared to ORR, which occurs at the cathode. Therefore, the significant activation loss occurs at the cathode. ORR reactions are complicated because sluggish requires more steps and molecular re-organization [38].

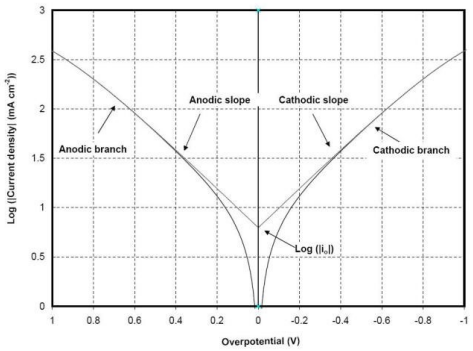

Figure 2.3: Tafel plot example with cathodic and anodic slopes. Reprinted from [39]

To achieve high current density, the fuel cell must be designed to operate with high efficiency possible.

Normally, the commercial fuel cells operate at 0.65-1.0 V_{RHE} within the efficiencies of 40-60% by providing enough power for respective applications [41]. The higher efficiency is restricted by losses in polarization and can be seen in Figure 2.5 in polarization curve for PEMFC with activation, ohmic and concentration polarization regions [40].

In respect to the fuel cell kinetics, the Butler-Volmer equation can be simplified into two different approximation and only applicable if the activation overpotential is either very large or very small. When activation overvoltage is too small (less than about 15 mV at room temperature or, more fundamentally, when j << j0),

$$j = j^{\circ}\frac{nF\eta_{(act)}}{RT} \tag{2.26}$$

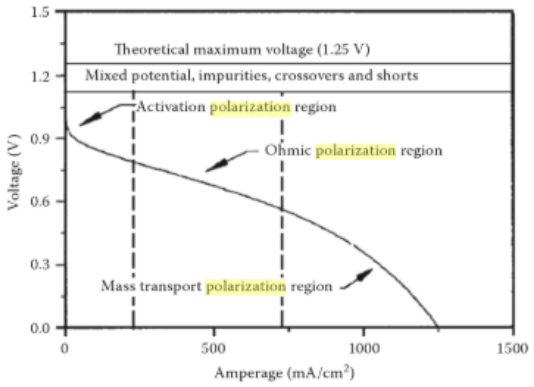

Figure 2.4: Polarization curve for PEMFC with activation, ohmic and concentration polarization regions . Reprinted from [40]

When activation potentials are higher in range of 50-100 mV, the second part of Butler-Volmar equation will be negligible and forward reaction dominates leading to irreversible reaction. The equation will be represented as

$$j = j^{\circ}(e^{\frac{\alpha n F \eta_{(}act)}{RT}}) \tag{2.27}$$

Solving this equation for $\eta_{(}act)$ results in

$$\eta_{(}act) = \frac{-RT}{\alpha nF} lnj^{\circ} + \frac{RT}{\alpha nF} lnj \tag{2.28}$$

The slope $\eta_{(}act)$ and lnj is straight line. If this equation is generalized in the form given as

$$\eta_{(}act) = a + blogj \tag{2.29}$$

This equation is known as the Tafel equation, and b is called the Tafel slope. This equation is important to electrochemical kinetics and predates the Butler–Volmer equation.

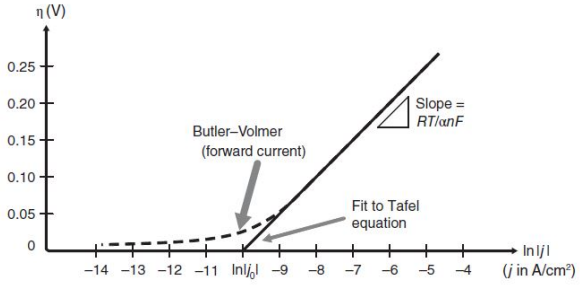

Figure 2.5: j−η representation of a hypothetical electrochemical reaction where at high overvoltages, a linear fit of the kinetics to the Tafel approximation allows determination of j° and α. Reprinted from [35]

2.3 Proton Exchange Membrane Fuel Cell(PEMFC)

The polymer electrolyte membrane fuel cell also known as Proton exchange membrane fuel cell is a H_2/air fed fuel cell that generates electricity through oxidation of hydrogen at the anode during the reduction of oxygen at the cathode. The first PEMFC (1 kW) was employed by NASA for space shuttles in the 1960s for the propose of drinking water system [42]. Due to high cost and poor stability, the PEMFC technology was out of the commercial scope during the 1970s. With the development of materials and catalyst, it comes back to commercial applications in 1980s [43]. The PEMFC utilizes the proton exchange membrane as the electrolyte. The reactions in PEMFC are kinetically promoted with the help of catalysts when the chemical energy of the fuel is converted into electrical energy at electrode-electrolyte interface [44]. The PEMFC stack is a unit of repetitive cells arranges parallel. Every single cell consists of two electrodes (cathode and anode) and capable of generating 0.6-0.7 V per cell.

Each cell is connected to other cells with the help of bipolar plates which functions as current collectors [45], the plates are also responsible for delivering reactant gases and removing exhaust gases and byproduct, i.e. water but at the same time availability of water in PEMFC can cause performance deterioration if the adequate water content is not available in the membrane. Due to the excess weight of bipolar plates (accounts for 80% of the total weight of single cell [46]), research has been carried out for an alternative lightweight, highly conductive and stable materials such as graphite, carbon-polymer composites and metallic materials such as titanium [47,48]. The carbon-based GDL with 100-200 micrometre thickness [49] helps to provide the uniform distribution of gases and also a decisive factor for water management [50]. The GDL has essential features which are porosity and permeability that can be optimized to enhance the performance [51]. The GDL is usually made of carbon with excellent strength, better electrical conductivity and corrosion-resistant. To prevent the flooding, a hydrophobic agent (ionomer) is added to a layer which also reduces the gas flow. In order to prevent the permeation of reactant gases, proton exchange membrane in PEMFC plays a vital role which is mostly based on perfluorosulfonic acid ionomer or Nafion™ [52]. It offers excellent stability and proton conductivity, but they are susceptible to degradation by water content and temperature changes. In PEMFC, the oxygen reduction reaction is six order slower than hydrogen oxidation reaction, therefore, less amount of catalyst needed at the anode in PEMFC as it has been stated that the platinum loading at anode could be reduced to 0.003 mg_{Pt}/cm^2 without affecting any performance of fuel cell. The most important part of the fuel cell is the cathode catalyst layer which is a complex structure of several materials such as carbon, ionomer, catalyst nanoparticles, catalyst support and water. The catalyst layer is the point of the triple-phase boundary where the oxygen, protons and electrons interface in the presence of a catalyst which eventually contributes to the stability, utilization and performance of fuel cell. The mass scale application of PEMFC is still limited due to several challenges such as high cost due to the platinum catalyst, bipolar plates, and membrane. Yet, the recent research and reviews showed that alternative materials have potential to

reduce the cost of the PEMFC to DOE target($30/kW with 8000 hours operation) and therefore, makes it applicable to commercialization [53–56].

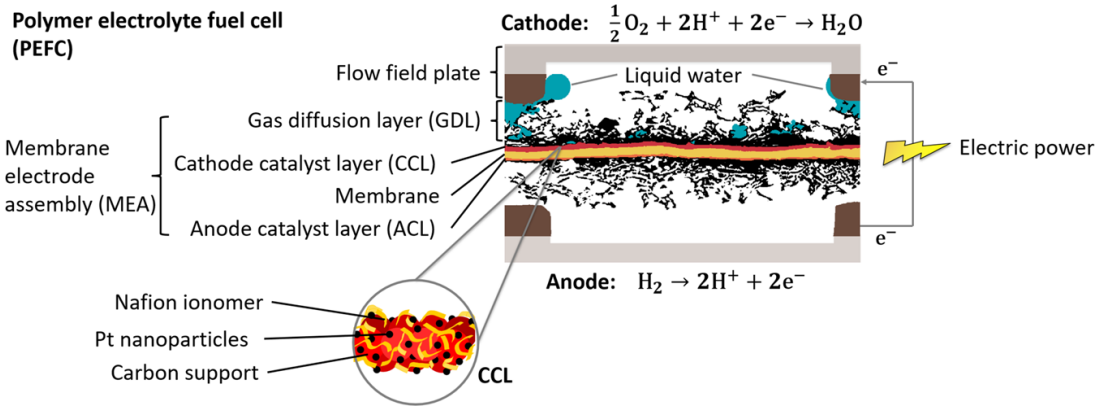

Figure 2.6: PEMFC Membrane electrode assembly structure with Gas diffusion layer and membranes. Reprinted from [57]

2.4 Alkaline Exchange Membrane Fuel Cell(AEMFC)

The alkaline fuel cell is one of the oldest low temperature (60-80°C) fuel cell that generates electricity through a redox reaction. The OH^- ions generated at cathode reacts with hydrogen at the anode side. The formation of hydroxyl ions is continuous as the water produced diffuses to the cathode and reacting with oxygen [58]. The transfer of water is carried out from cathode to anode employing electro-osmotic drag, due to complex dynamics, the AFC faces more challenges during fuel cell operations as compared to PEMFC and yet imposing a significant barrier for commercialization. Alkaline fuel cell AFC was first adopted for practical application as a power source for tractors by Allis Chalmers-US manufacturer in 1950s. Later in the 1970s, the first AFC stack was developed for personal transportation (car) by Karl Kordech based on the current systems designed by Union Carbide Corp. (UCC) for General Motors. Generally, the electrolyte used in AFC is KOH at 70°C started with the power range of 1-10 kW in the 1950s for NASA space program "Apollo" with a performance of 470 mA/cm^{-2} at 0.88 V [59, 60]. Due to the functionality of AFC at high pH, the conditions in the cell enables the application of non PGM catalyst. The modified form of AFC is AEMFC in which liquid electrolyte is replaced to reduce ohmic losses by the introduction of anion exchange membrane in basic form AEM, which can affect the cost and performance of the cell. The AEM provides permeation of hydroxyl and bicarbonate anions (OH, HCO_3 and CO_3^{-2}) while preventing the excess protons from flowing. The electro-kinetics of the catalyst mainly non PGM is much better in alkaline rather than acid which faces stability issues, but the primary concern of AEMFC is the carbonate formation by atmospheric CO_2 which can block the pores of electrodes but

also precipitates in the cell causing mechanical degradation [61].

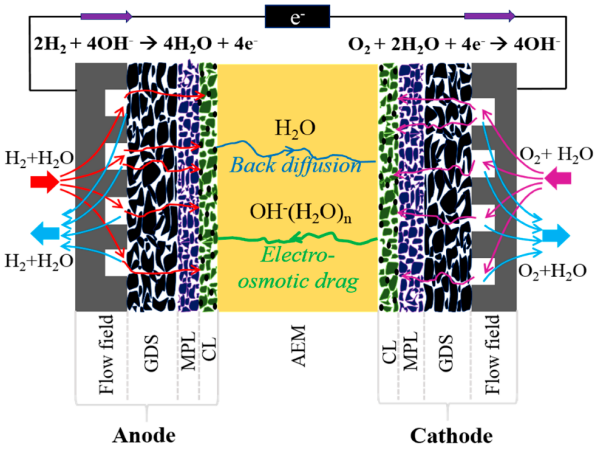

Figure 2.7: Alkaline exchange membrane fuel cell with a systematic flow diagram of reactions on cathode and anode. Reprinted from [62]

Several approaches have been carried out in the past to improve the efficiency and stability of fuel cell such as AEMFC is preferred to AFC due to restricted electrolyte selection and controlling parameters and exploring new ionomers and membranes. The KOH is more suitable electrolyte as compared to NaOH because of higher conductivity and less solubility products [63]. In advanced systems, the KOH is circulated continuously to avoid impurities, less exposure to CO_2 which can poison the electrolyte and ease in thermal and water management, less gradient of OH ions concentration and gas bubbles in between electrodes [59]. These issues are not available for AEMFC as ionomer and membrane development for the alkaline solution in OH^- form is one of the strategies that can maximize the ionic contact to catalyst sites so that mobility of hydroxide ion will be faster. In previous years, various AEM and ionomer materials with polymers of arylene piperidinium, styrene, propylene, ether have been synthesized with different cationic groups such as benzimidazolium, quaternary ammonium and pyridinium for high conductivity [64]. One of the main problems in AEMFC is the risk of carbonation of AEM and ionomers, which reduces the conductivity. Notably, at ambient conditions, the quaternary ammonium group are unstable due to their affinity to CO_2, which is convertible to carbonates and bicarbonate and the large radius of anions will restrict their mobility.

The conductivity is drastically decreased from fully OH- form to fully carbonated from 100 to 70%; therefore, it is desirable to operate AEMFC in a CO_2 free environment [65, 66]. Following Figure 2.7 depicts the systematic view of AFC fed with H_2/Air and KOH as an electrolyte, the products are electricity, water and heat, the water is then utilized at the cathode in a stoichiometric ratio which could avo-aid the possibility of flooding at the cathode side. Anion exchange membranes are an important part of AFC, which typically consists of polymer with fixed ionic sites. The mobility of hydroxide ions through

the membrane from cathode to anode is possible only due to these ionic groups. These polymers include Polyvinyl chloride (high tensile strength, ionic conductivity, cheap) [67,68], Poly-arylene-ether(high conductivity and stability) [69], Poly-tetra-fluoroethylene-PTFE (high chemical and thermal stability, less water absorption and non-toxic) [70–72]. Functional groups are also used in AEM such as quaternary ammonium (less mechanical degradation, high ionic conductivity and low overpotential) [73,74], imidazolium (efficient OH^- transport and ion exchange capacity) [75,76]. AEM have a well-defined structure with two phases. One can uptake water and OH^- ions in the hydrophilic phase of the membrane while other hydrophobic regions maintain stability by weakening nucleophilic attack [64]. However, the AEM is prone to degradation by the effect of carbonation and irradiation. Flooding in the fuel cell is also an issue, and the possibility of flooding is very negligible in AEMFC as water produced at the anode and consumed at the cathode. However, if the balance of water management is not sustained, then there is a problem of flooding at anode or catalyst layer drying out cathode [77]. One of the advantages of AFC is that it is very tolerant to non PGM catalyst and thus opening a pathway to explore more cheap electrocatalyst that can equate the performance of PGM catalyst.

Nevertheless, there are certain limitations for AEMFC to approach to industrial applicability such as "CO_2 syndrome" [78], low anode pH causing by the deficiency of electrolyte "KOH", low conductivity of membrane, fuel cross over at cathode and reduced catalyst utilization. The catalyst layer and membrane thickness, ionomer content can also affect the performance of AEMFC, for instance, the high ionomer content can impact the mass transport and could lead the catalyst and carbon particles to be electron isolated [79]. However, there are still some challenges need to be addressed such as electrocatalyst for the anode, although HOR reaction is simple and platinum and alloy been used for acid media but due to AEMFC compatibility with non PGM, a highly active electrocatalyst is needed [80]. The carbonate issues with solid electrolyte membrane is an open research area that has proved to be preferable as it eliminates the possibility of carbonates precipitation [81,82].

2.5 Reaction Pathways for Oxygen Reduction Reaction ORR

The oxygen reduction reaction is one of the most important reaction at the cathode in the fuel cell, and it is ineluctably more complex and critical than hydrogen oxidation reaction. In aqueous solution, ORR follows two reaction pathways with parallel reaction mechanism and much larger overpotentials, highly irreversible with multiple adsorption/desorption of species such as O, OH, O_2^-, HO_2^-, and H_2O_2 [83]. The two different pathways are four electrons reductions from O_2 to H_2O and two-electron reduction from O_2 to H_2O_2, which are dependent on the interaction of oxygen with the catalyst surface. In acid electrolyte, the ORR at standard condition (25 °C) with thermodynamic potentials are presented in equations below.

$$O_2 + 4H^+ + 4e^- \rightleftharpoons 2H_2O \qquad E^\circ = 1.229V_{RHE} \qquad \text{(Direct four electron pathway)} \tag{2.30}$$

$$O_2 + 2H^+ + 2e^- \rightleftharpoons H_2O_2 \qquad E^\circ = 0.67V_{RHE} \qquad \text{(Indirect two electron pathway)} \tag{2.31}$$

The indirect reduction is usually followed two other steps

$$H_2O_2 + 2H^+ + 2e^- \rightleftharpoons 2H_2O \qquad E^\circ = 1.77V_{RHE} \qquad \text{(two electron reduction)} \tag{2.32}$$

or

$$2H_2O_2 \rightleftharpoons 2H_2O + O_2 \qquad E^\circ = 1.77V_{RHE} \qquad \text{(direct decomposition)} \tag{2.33}$$

In alkaline electrolyte, the ORR mechanism is described by equations

$$O_2 + H_2O + 4e^- \rightleftharpoons 4OH^- \qquad E^\circ = 0.401V_{RHE} \qquad \text{(four electrons reduction)} \tag{2.34}$$

$$O_2 + H_2O + 2e^- \rightleftharpoons HO_2^- + OH^- \qquad E^\circ = 0.080V_{RHE} \qquad \text{(two electrons reduction)} \tag{2.35}$$

and

$$HO_2^- + H_2O + 2e^- \rightleftharpoons +3OH^- \qquad E^\circ = 0.880V_{RHE} \tag{2.36}$$

he oxidation-reduction reaction proceeds through two pathways in acid and alkaline media with two electrons with H_2O_2 and four electrons transfer with H_2O. Damjanovic et al. introduced the mechanism of ORR, and later Wroblowa et al. [84] improvised the proposition by presenting a complete sequential analysis for ORR mechanism at a metal surface. The first step occurs at the surface region by the diffusion of oxygen from the bulk phase to the electrode, leading to parallel pathways with a comparable rate of reaction. At the electrode-electrolyte interface, the oxygen can follow two way of reduction process through path K_1 which involves the $4e^-$ or K_2 involving $2e^-$ with H_2O_2 as an intermediate which further reduced to water in an additional step K_3. The decomposition of H_2O_2 to O_2 and H_2O can occur via K_4 pathway, the desorption and adsorption into solution or diffused back to the bulk through K_5 and K_6 routes respectively.

The kinetics of Pt redox reaction is much complex, considering the example of ORR on Pt which is favoured by $4e^-$ pathway by inter-molecular distance shortening of Pt-Pt promoted by geometric effect, increasing d-band vacancies by altering the electronic structure or surface roughness. The potential profile and sites blocking by anion adsorption can adversely affect ORR activity. The ORR pathways can be altered easily by transport and double layer effect (depends on particle size) [85]. Considering the example of Pt ORR in acid electrolyte ($HClO_4$), the decomposition of H_2O_2 is limited by mass transport in the potential range of 0.2-1.5 V_{RHE} [86]. As the decomposition rate of H_2O_2 decreases with time, the hydrogen peroxide is not able to be detected in the electrolyte as it triggers reactions on Pt surface such as OH_{ads} production during interaction with reduced atom surface and oxidation by reducing on

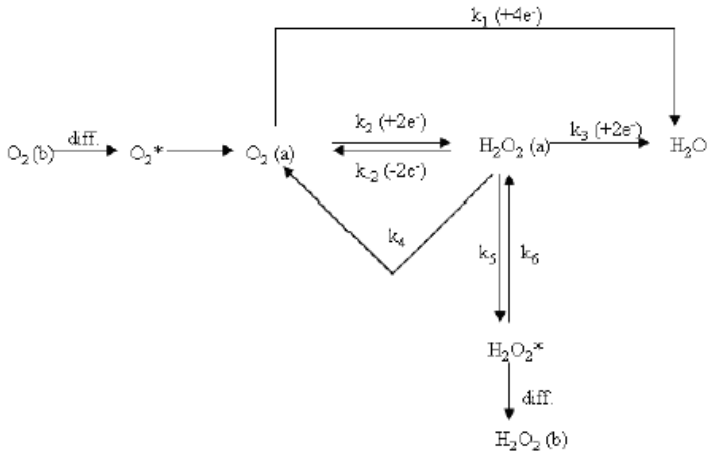

Figure 2.8: Reaction Mechanism of ORR proposed by Wroblowa et al. Reprinted from [84]

the surface. This makes H_2O_2 unstable on Pt and will lead to dissociation to OH. At OH free Pt surface, the H_2O_2 dissociate on active platinum sites to OH_{ads}, because OH is not stable on Pt, the regeneration of surface sites will occur leading to reduction steps and the desorbed OH free Pt sites will be available again to dissociate other OH molecules. Oxides free Pt which is not yet stable properly will be re-oxidised and become available for H_2O_2 oxidation [86]. At large overpotential (0.7 V_{RHE}-equilibrium voltage for peroxide) [87], there is possibility of H_2O_2 production during ORR, even though H_2O_2 is not relevant to the Pt catalyst based ORR, but it must be taken into consideration that the oxidizing agent along with acid electrolyte can deteriorate the PEM in fuel cell. During the reaction intermediates, the oxygen will bind to the surface and yet, more losses will be induced by using the catalyst optimised for oxygen evolution reaction OER and ORR [88]. Various models are available to analyse the oxygen reduction on Pt such as Bridge, Griffith and Pauling model which are difficult to address and beyond the scope of the thesis.

2.6 Electrocatalysts for Oxygen Reduction Reaction ORR

To catalyze ORR, numerous catalysts have been used since the past, and they are categorized into precious and non-precious group metal catalyst.

2.6.1 PGM State of the Art Pt/C Electrocatalyst

The widely commercialized and state of the art catalyst for fuel is platinum nanoparticles support on carbon and yet it is still known to be the best metal to catalyze ORR [41]. The electronic structure of Pt benefits for OH and O_2 binding energies that help this single metal catalyst for ORR than any other metals (Ag, Pd, Ir, Ru). The crystallographic structure of platinum is an essential factor for ORR as

redox reaction is sensitive to surface orientation. The crystal structure of Pt is oriented to face centre cubes with plane index (111),(100) and (110) [85], due to irreversible surface oxidation which affects the durability of catalyst, the platinum nanoparticles structure have a large number of defective active sites which reduces the kinetics of redox reaction. Kinetics of Platinum catalyst has been under observation through shape control and surface modification. Non-spherical shapes are more preferred to spherical shapes which are difficult to create due to high symmetry of Pt cubic crystals, and the efficiency of tetrahedron Pt nanoparticle is reported to be much higher than spherical nanoparticles [89].

The use of platinum as the electrode was started in 1839 by William Grove for water electrolysis. Since from the beginning, the Pt black nanoparticle was used as a catalyst on both anode and cathode. Due to the benefits of high stability and durability, the higher amount of Pt was used due to large overpotentials. The Pt particles are suspended on the support (Carbon- Vulcan or Ketjen black), which is essential to avoid the agglomeration of Pt particles that reduces the performance of the catalyst. The efficiency of Pt nanoparticles is highly dependent on shape, size and morphology, which can be optimized and control during synthesis for the advanced platinum catalyst. The morphology of nanoparticles can be tuned into cubical, spherical to octahedron and tetrahedron structures, and different facets enclose each structure. The commercial Pt/C is enclosed with low index facets (111) and (100) as these facets have strong interaction to O_2 molecules as indicated in the previous studies for ORR in $HClO_4$ [90]. Pt/C comes in different shapes from the single metal catalyst, monolayer 1D(nanotubes and nanowires) and two-dimensional shapes. Control methods used to be employed to achieve excellent shape and facets. For catalytic reaction, the electrochemical surface area and mass activity are significant factors that rely on the catalyst size. Usually, the smaller Pt nanoparticles have been preferred to catalyze ORR reactions.

Commercial Pt/C catalyst has been synthesized through different methods such as nano capsules [91], under-potentially deposition [92] and electron reduction [93], resulting in the particles with the range of 2-5nm [94]. The carbon support provides a high surface area, better conductivity and stability for Pt nanoparticles (2-5nm). Due to issues like carbon corrosion at high potential values, the graphitized carbon was used as support instead of carbon black which helped in delaying carbon oxidation, but graphitization leads to low mass activity due to dispersion [95]. Several types of carbon support are used for commercial Pt catalyst such as Carbon black(Vulcan), nanotubes, nanofibers, nano horns, mesoporous, carbon shells colloid imprinted carbon, microemulsion templated carbon, hollow graphite spheres and graphene ranging from 1-100 nm particle size with a high surface area of 50-2000 m^2/g [96]. There are also carbon-free supports available for electrocatalyst such as oxides, carbides and nitrides with high stability, but due to their low conductivity, they face challenges for the performance of fuel cell [97].

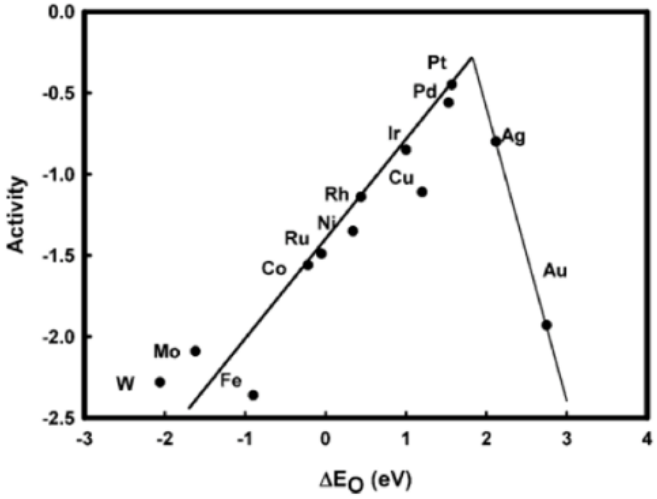

Figure 2.9: Platinum alloy volcano plot for ORR. Reprinted with permission from [98]. Copyright 2019 Springer Nature

2.6.2 Advanced Platinum Alloy Electrocatalysts

Platinum alloys proved to be superior electrocatalyst for ORR as compared to single metal Pt/C, and it was utilized in fuel cell since 1980s [41, 88]. They were classified as second-generation fuel cell catalyst. Due to their higher activity and durability than a pure platinum catalyst, there are used in the application for commercial fuel cell vehicle (Toyota Mirai) [36]. The activity of Pt alloys (bimetallic, ternary and quaternary) is better due to different mechanisms such as structural effect [99, 100]. The bond distance between platinum and transition metal is shorter due to compressive strains which makes the adsorption of oxygen more favourable to active sites [101]. Due to the significant effect, the transition metals alloyed with platinum such as (PtCo, PtNi, PtAg, PtAu, PtFe, PtAl, PtNi) were able to achieve comparable and even higher activity than the pure platinum [102–107].

In some studies, it has been demonstrated that due to the smaller atomic size of a transition metal, lattice contraction will occur resulting in reducing the bond distance of Pt-M. The other phenomena which make the Pt alloys superior are the formation of oxides on the surface as the structural properties of alloys prevent the poisoning species (OH and OOH) by debilitating the adsorption process [108, 109]. The changing of d-band vacancy and downshifting of Pt is considered to be an essential strategy to increase the ORR activity [110] because the Pt-M alloy balances itself in such a way for reducing surface oxide coverage through strain(increasing overlap between d-orbitals) and ligand effect(weakening the binding of adsorbates) [111]. The Pt-M alloys are also stable in acidic electrolyte due to "Pt-surface skeleton", a phenomenon that buildup a mono-layer surface over the bulk alloy protecting sub-surfaces from oxidation. Since the active phase of a bulk alloy is the 1-2nm over-layer of roughly pure platinum makes

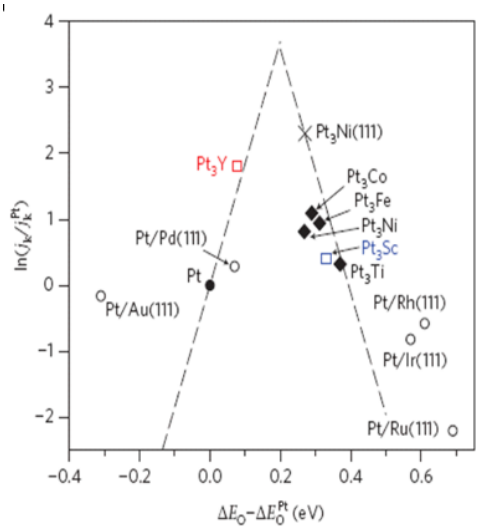

Figure 2.10: Platinum alloy volcano plot for ORR. Reprinted with permission from [98]. Copyright 2019 Springer Nature

a "Pt skin" by providing more protection to the bulk catalyst [110, 112]. In the past years, significant studies have been done to investigate the synthesis and composition control parameters of platinum alloys such as synthesis of PtCox by annealing method and variation in composition by the amount of metal precursor, Pt-Ni alloy by altering the d band through solid-state chemistry method. It has been found that various compositions of binary metal alloys showed significant higher ORR activities as compared to commercial Pt/C. The face effect also inspired research after the discovery of PtNi(111) which is ten times more active for ORR than Pt/C(111) and demonstrate the effect of morphology control during the synthesis process. The thermodynamics and kinetics of the facet growth mechanism can influence the morphology properties during particles growth [113, 114]. Tri-metallic and quaternary Pt alloys are optimized with the help of high throughput and density function theory DFT calculations by introducing different elements for adsorption and desorption of oxygenated species. This is resulting in higher ORR activity of ternary alloys such as Pt-Fe-Co, Pt-Fe-Ni(3.5 times high mass activity), Pt-Pd-Cu(4.7 times high mass activity) as compared to some bimetallic and Pt/C electrocatalyst [115, 116]. Despite the high activity, Pt alloys still face several challenges such as corrosion, degradation and leaching. Base metal leaching can impose a drastic effect (less oxygen diffusion, high resistance) on the fuel cell performance. Due to the high affinity of metal cations to the sulfonic group leads to poisoning of ion exchange sites in the membrane, which will restrict the movement of the proton. The leaching of metal can be caused by several reasons as reported [41] including the excess deposition of base metal on a carbon support, insufficient admits of alloys due to temperature variation and thermodynamic stability of base metals at different conditions. In the fuel cell, the loss of activity of Pt alloys during potential cycling is mostly due to de-alloying, which has been studied for PEMFC by several researchers. In acidic electrolyte, the

alloyed metal at the surface of catalyst dissolves at high potential as the potential at PEMFC cathode is higher than dissolution potential [117]. At the high potential, there will be much more possibilities for the strong interaction between adsorbed species and solute metal ions. For Pt alloys, the surface oxide formation will be a problem as some of the oxides do not have tendencies to reduce back to metallic form such as NiOx and CoOx [118, 119]. The specific activity of Pt alloy is also prone to degradation due to Ostwald ripening. Due to the converse effect, the dissolute platinum particles will redeposit causing a thick layer formation on nano particles [120].

2.6.3 Core Shell Structures

In the case of bulk platinum catalyst, the Pt utilization is not subjected to comply fully with 70% of the catalyst utilization [121]. Core-shell approach is highly regarded as efficient as compared to bulk platinum by utilizing monolayer of Pt nanoparticles on other less expensive metal catalysts with higher activities (Pt-AuNi, Pt-Cu, Pt-Pd) along with that it can influence in re-positioning of the d-centre band and lattice parameters of thin Pt shells [122, 123]. The core-shell approach also helps to design a Pt-alloy based catalysts in such a way to minimize the Pt loading along with overcoming of the stability and activity issues.
Several methods are available to synthesize the core-shell structures such as etching(electrochemical/chemical) in which the less noble metal surface is covered with Pt layer, chemical reduction, vapour deposition and electrodeposition. The monolayer of Pt can also be deposited on the non-platinum alloys (IrNi, PdFe, etc.) with significantly higher activity and stability than single metal due to extra lattice strain and alteration of properties. This shows that both parameters are highly influenced by synthesis procedure, structure and composition of cores [124, 125].

These cores are tuned with ligand (short-range electron charge transfer) and geometric effects (altering the lattice constants) [127]. There have been 700 core shells identified by density function theory calculations DFT with 2nm nanoparticles based on bonding and segregation energies for ORR [128]. For the single metal core Fe, Co and VIII B group elements are more reliable for the core of catalyst due to their similar properties to Pt. The mass activity of these core-shell catalyst has significant for ORR, which is 4-22 times better than bulk platinum. Other metals having similar properties to those found in the peak of volcano chart are also a promising candidate for core of catalysts, such as Cu, member of IB group with similar properties of gold and silver [129]. For the typical fuel cell, the application of core shells such as Ni-Pt, Co-Pt and Fe-Pt restricted due to complicating synthesis but favoured by high magnetism. This facilitates the recovery of catalyst and for low price bulk platinum, and the overall effect is due to poor kinetics and cost limitations [130]. There is still room for improvement to enhance the stability

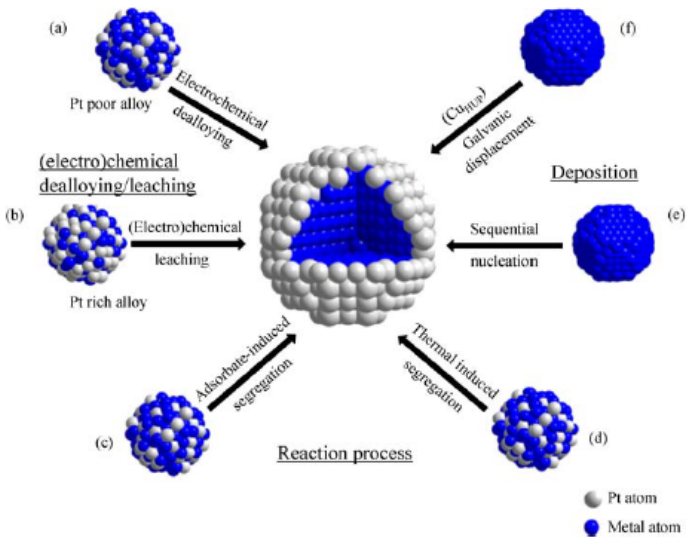

Figure 2.11: Core shell nano particles synthesis approach. Reprinted with permission from [126] Copyright 2013 American Chemical Society

and catalytic ability of Pt-based core-shell nanoparticles by modifying the core composition, core-shell elements redistribution and shell thickness [107]. Besides extra steps in synthesis, the core-shell approach is preferred for economic reason as the high surface area of active metal can be utilized with less amount of precious metals [131] but also it tends to approach to the fuel cell commercialization level. Several issues regarding durability and activity of the core-shell catalyst are yet to be addressed [132, 133].

2.6.4 Non PGM Electrocatalyst

Due to the competitiveness of fuel cell technology, it is always a primary concern to search for alternatives that can replace expensive Pt catalysts. Transition metal oxides are one of the non PGM group materials that can achieve good ORR activity, and these include nitrides, oxides, and carbides [134, 135]. As compared to other electrocatalysts, transition metals oxides are stable in acid due to oxidized state and oxygen vacancies in their structure which are believed to be the reason for higher activity. However, these materials suffer from poor conductivity and complexity in a synthesis which is still very challenging [136]. Several years of research emphasized on exploring metallic and non-metallic electrocatalyst such as carbon, nitrogen-doped metal-carbon, non-metallic hetero-atom doped carbon, transition metal oxides, nitrides and phosphides that can compete with the platinum to its activity and stability for commercial applications [137, 138]. The most promising PGM free catalyst for ORR is metal-nitrogen-transition metal complex supported on an inexpensive carbon support and indicated as M-Nx-C (where M is the 4^{th} period transition metals= Fe, Co, Ni etc. and x = number of atoms coordinating the metal). These transition metals are abundant in nature and have been studied for four decades for redox reac-

tion [139, 140]. M-N-C catalysts are classified into two states such as pyrolyzed with inorganic state and non-pyrolyzed with the organic state. Non-pyrolyzed state gives M-N-C a well-defined structure with simple synthesis process while pyrolyzed M-N-C catalyst undergoes a high-temperature treatment and provides better activity for catalytic reactions by enabling the formation of active sites [141, 142]. Each element has a different function to support these reactions, the nitrogen-containing molecule helps the formation of N atoms matrix to the carbonaceous material in the support. The nitrogen precursors are in the form of small organic molecules pyrrole, melamine, bipyridine or gases such as NH_3. It is essential to achieve high activity because the active sites are atomically dispersed in MNx moieties for ORR [143]. In alkaline electrolyte, the M-N-C catalysts can be stable with negligible reduction for their ORR activity while in acid, the catalysts may be unstable in metallic form and stabilization will be required by nitrogen in order to retain stability and activity, this investigation will be addressed through a different approach in this thesis. The most promising catalyst in the category of M-N-C is Fe-N-C catalyst with application into a broad range of pH.

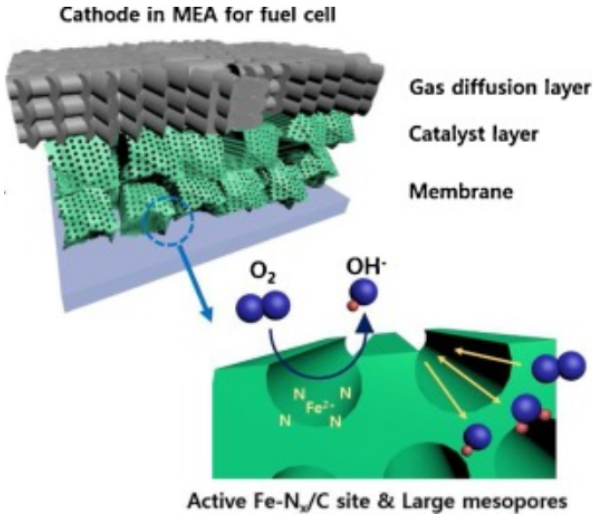

Figure 2.12: Systematic representation of Fe-N-C active sites. Reprinted with permission from Elsevier [144] Copyright 2018 Applied Catalysis B: Environmental

Fe-N-C is synthesized by the pyrolysis of Fe and nitrogen precursor on carbon support at a high temperature which helps the coordination of Fe for adjusting the electronegativity that helps to retain ORR activity [145]. Other transition metals such as non-precious catalysts (Fe, Ni-Co and Cu), he trooped Fe-N-C catalyst performed higher activity because of additional amount of iron by hetrodoping technique. Even with 0.24% of iron, Fe-N-C catalytic activity could be higher to more positive onset with higher stability in electrochemical measurements [146], N stabilized metal centre either in the form of N_2 or N_4 favours the formation of active sites. At the same time, iron also acts as growth supporter during

synthesis. The activity loss in Fe-N-C can be due to low pyridine or unapproachable iron active sites. With reaction to acid, the iron of Fe-N-C tends to leach providing the evidence that active sites contain iron [147]. The activity of M-N-C also depends on the porous structure of catalyst support. In order to select the best candidate for catalyst support, three considerations were taken as approaches such as the amount of carbon, the diameter of particles and size of graphene layers.

2.7 Electrocatalyst Activity and Stability Methods for ORR Evaluation

2.7.1 Cyclic Voltammetry (CV)

Several investigation techniques can help for the determination of electrocatalyst activity and stability during the redox process in electrochemical systems. Among them, the voltammetry technique is one of the widely applied techniques which works on the function of current response at a different potential. It is developed by the discovery of Polarography by Czech chemist Jaroslav Heyrovsky in 1992 [148], A polarization curve at steady state will be produced as a result, and it gives a high current density. Cyclic voltammetry CV technique is one of the techniques of voltammetry used to examine the redox process at the molecular level of electron transfer to initiative chemical reaction for initial catalysis qualitative studies [149]. The voltammogram is the diagram obtained after CV technique which works on different scan rate depends on the requirement. The potential is swept back and forth in a varied defined voltage range with a suitable scan rate and current as a response in the cyclic region which represents the cathodic and anodic reactions taken place. This technique is applied on different occasions, usually before, during and after experiments to determine the condition of catalyst layers. The scan rate can be reduced to absolute values in order to reduce specific capacitance. For non PGM catalyst (Fe-N-C), the curve gives information about the capacitive current which shows the information of the specific surface area of catalyst (as double-layer capacitance is proportional to an electrochemical specific area) in the absence of Faradic reaction. The benefit of CV is the rapid results and sufficient information related to the redox process (thermodynamics, the kinetics of electron transfer reaction, Gibbs free energy and diffusion coefficients). The CV technique is based on potential sweep between two potential limits at a known scan/sweep rate. The signal of excitation of each scan is in a triangle form; the peak in the curve at their own potential shows the point where reactions are taking place on the electrode. For oxidation, a positive potential is applied, and the electroactive species loose electron, which results in the rise of anodic peak current [150]. When potential is applied in a negative direction, cathodic current peaks will be observed giving information about the reduction step, and these steps start from a point when species are not active. CV data is represented by two conventions such as IUPAC or US convention with

just change in direction to 180°. In principle, if energy is provided to atom or molecule, it will have a tendency to oxidized or reduced. Electrochemically active molecules are those who have lone pairs or multiple bonds. CV informs about the kinetics of reactions at the electrode surface with the reaction mechanism. In voltammogram, the magnitudes of peaks (both anodic and cathodic) are an essential point of concern [39]. As the beginning of the experiment, the potentials are lower to a level that no reduction conversion takes place to oxidized state as the bulk solution contains reduced species. When the redox potential is positive enough that reduced species oxidizes at the electrode surface, then the current will depend on mass transfer to the surface of the electrode. If no peaks are observed in the CV curve, then the reaction will be referred to reversible, and the specific capacitance will be observed. Strong reductant can be determined by switching the scanning to a negative direction while strong oxidant is determined by applying a potential to positive scan [150]. The peak potential is the difference of anodic and cathodic peak potential which are needed to get information about redox since redox reactions are not reversible and this makes CV process more attractive due to non-ideality of the situation and the area to diagnose properties [39].

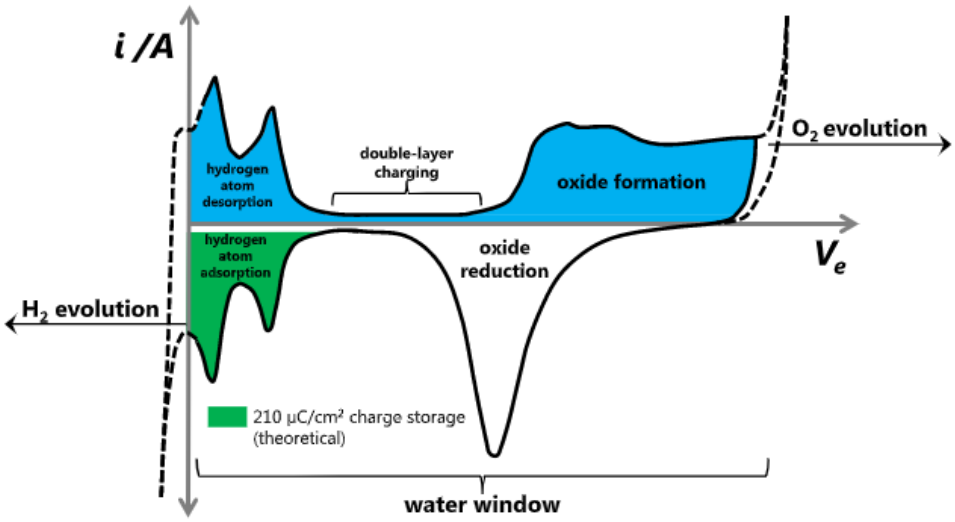

Figure 2.13: Pt Cyclic voltammogram in acid electrolyte .Reproduced from [151]

Figure 2.13 depicts the CV of Pt/C electrocatalyst, the CV comprises of six regions which are hydrogen evolution, hydrogen adsorption, hydrogen desorption, double layer region, Pt oxidation and Pt-O reduction region. In acidic electrolyte, protons (H+) are adsorbed reversibly by forming a monolayer at the potential range of 0.05 to 0.4 V_{RHE}. This process is reversible as adsorption and desorption take place during a complete cycle with forwarding and backward sweep simultaneously. All these regions are linked to the potential applied and its direction [39]. The three regions hydrogen adsorption and desorption lie in the range of 0-0.35 V_{RHE}. The double-layer capacitance is in the potential range of 0.3-0.8 V_{RHE}

and the oxide region. The hydrogen adsorption/desorption is the H_{upd} or also known as underpotential deposited region, and it is important to determine the electrochemical surface area and refers to adsorbed hydrogen monolayer on the catalyst surface [149]. The peaks of voltammogram providing information about the reactions happening at the surface, the most prominent and sharp peaks lie in the H_{upd} region, which is a matter of interest for researchers. Each peak in the hydrogen desorption region is related to the reactions at a different surface facet of Pt such (110) and (100) [152]. Integrating the desorption area with constant charge value gives an estimation of the monolayer of hydrogen, which will help to determine the electrochemical surface area and catalyst utilization. The double-layer region is the area where current is non-faradic, and the electrode is polarizable lies in the range of 0.35-0.8 V_{RHE}, and no redox reaction takes place in this region [152]. The oxidation region is beyond 0.8 V_{RHE} where the Pt atoms exchange with O_{ad} and the growth of PtOx takes place with the formation of bulk oxides. More concepts of CV techniques are addressed in this literature [153]. In this work, the cyclic voltammetry with triangular sweep cycles technique will be used.

2.7.2 Electrochemical Impedance Spectroscopy EIS

Electrochemical impedance spectroscopy is one of the powerful diagnostic techniques to measure the ohmic losses in the three-electrode setup in a steady-state condition. The first reported locally observation of electrochemical impedance spectroscopy was given in 2003 by Brett et al. over a wide range of frequency from 0.1Hz-10kHz for solid polymer fuel cell [154] which was later modified and patented by Schneider and Scherer with their key classification experiments [34]. At constant current or constant potential, the electrodes are excited in the variable frequency to achieve a sinusoidal response. The response of perturbation gives quick information about electrode-electrolyte resistance, capacitance, and mass transport. In order to achieve a suitable uniform response, the EIS system needs to behave linearly, which can be implemented by letting the magnitude of perturbation too small. This technique involves control over the frequency in a concept that all responses can be views together. The response of the system is represented by Nyquist or Bode plot by applying harmonic perturbation resulting in kinetics and transport properties [155]. For electrochemical cell, the impedance is described by the ratio of the transfer function of potential and current.

$$Z(\omega) = \frac{E(\omega)}{I(\omega)} \tag{2.37}$$

In this equation E and I are the Laplace transform of potential and current function, $Z(\omega)$ is representing the complex function whose real and imaginary part are $Re(\omega)$ and $lm(\omega)$ respectively. The magnitude of complex function is estimated by the modulus of $Z(\omega)$.

$$|Z(\omega)| = \sqrt{ReZ(\omega)^2 + lmZ(\omega)^2} \tag{2.38}$$

The phase angle between each signal is calculated by the following equation

$$\phi = arctan\frac{lmZ(\omega)}{ReZ(\omega)} \tag{2.39}$$

In a system, the electrochemical can be represented by resistive and capacitive elements with an additional element for mass transport effect known as the impedance of resistance. In the ideal system model, the impedance of resistance is based on Ohms law.

$$Z(\omega) = R \tag{2.40}$$

The current that pass across the resistor will be

$$\delta I(t) = \frac{E}{R} * sin(\omega t) \tag{2.41}$$

Where R is resistance in ohms. The impedance of capacitance element will be

$$Z(\omega) = -j\omega C \tag{2.42}$$

Here J is the imaginary component and capacitance is represented by C; the resistive element can indicate the resistance of solution. The resistive element can also represent the charge transfer while the capacitive element can demonstrate the double-layer capacitance. Due to the non-ideal nature of systems that can be based on electrode structure, high porosity which makes the EIS more sophisticated, a constant phase element can be introduced. The redox reaction mass transport impedance also known as Warburg, by taking concentration effect at the electrode and stagnant solution with no fixed diffusion layer can be estimated by

$$Z(\omega) = \sigma(1-j)\sqrt{\omega} \tag{2.43}$$

$Z(\omega)$ is dependent on frequencies, and is the concentration and diffusion coefficient of reactants. The final impedance of all components in series will be estimated by using Kirchoff law and equals to the summation of all impedance $Z_t = Z_1 + Z_2 + \ldots Z_n$, for parallel components these individual components impedance value will go reciprocal.

The plot of the real part of impedance vs imaginary part is known as Nyquist plot Figure 2.15 with a complete circuit of PEMFC can be seen in Figure 2.14 which helps in the quantification of resistance, capacitance, and mass transport behaviour. As mentioned before that impedance spectroscopy can work on a different arrangement of circuits, the Randles-Ershler circuit will produce semicircle of Nyquist plot offsite to real axis [157]. Starting from the first point intercepting the real part caused by solution resistance. Then this intercept follows the semicircle path when the arrangement if the resistor is parallel

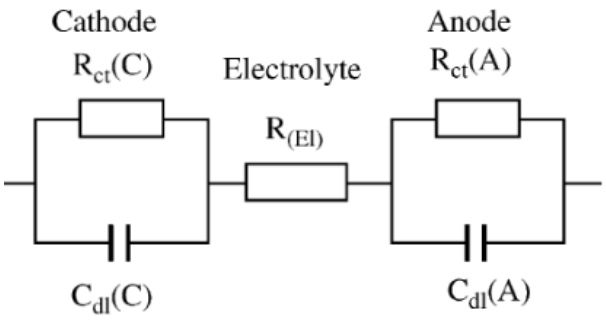

Figure 2.14: A complete circuit illustration for PEMFC for Nyquist Plot. Reprinted with permission from Elsevier [156] Copyright 2018 International Journal of Hydrogen Energy

with a capacitor for double-layer capacitance and faradic charge transfer. Sometimes the system cannot be modelled with an ideal capacitor, in such case constant phase element is used as it will help for practical fitting purposes. The magnitude of the semicircle is positioned for the frequency [158].

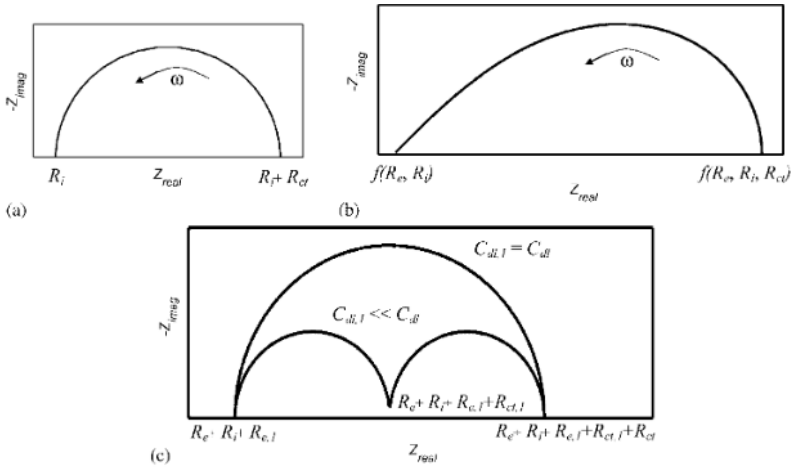

Figure 2.15: Nyquist Plot(a) half cell with catalyst layer in planner form (b) half cell with catalyst layer in porous form (c) full PEMFC. Reprinted with permission from John Wiley and Sons [159] Copyright 2005 International Journal of Energy Research

The smaller semicircle will be observable at higher frequencies if the reaction is facile. At low frequencies, the mass transfer resistance will be observed. If there is a fixed thickness of the diffusion layer, the second semicircle will have appeared, if the diffusion layer grows, then the semicircle will follow a straight line at an angle of 45°. If there are no species of the reactant with a fixed thickness of the diffusion layer, then the curve will surge to 90° line with an increase in impedance. Nyquist plots are used mostly to evaluate the impedance parameters based on the number of arches, but Nyquist plots do not relate to indicate frequency which makes the information incomplete [160]. On the other hand, bode plots demonstrate the magnitude and phase angle vs frequency.

Due to the versatility of the electrochemical cell modelling to a wide range of circuit with a different combination of passive elements, it is easy to measure EIS results for different criteria. In EIS, the mass transfer process is limited and directed in the low-frequency region while the charge transfer process is dominated in the high-frequency region. The Bode plot is also used for EIS measurements and helps to find a relation between phase shift and modulus of impedance. [39, 161] In our work, we used the Nyquist plot for EIS measurement in our three-electrode set up to determine the uncompensated resistance for 100% data correction.

2.8 Degradation Investigation via Accelerated Stress Test AST

The wide operating range of fuel cell in the potential limit of 0-1.5 $V_{RHE}$with the various break-in and start-up steps, dynamic load cycling, humidity effect and temperature variations can cause performance degradation. The degradation of performance is still challenging is focused on research, since these mechanisms are unavoidable. Therefore it is essential to understand the failure and degradation behaviour of fuel cell (more specifically catalyst layer). During cycling, these mechanisms can lead to severe bad results in the form of physical and changes [162]. These mechanisms include Ostwald ripening, catalyst dissolution, poisoning, ionomer and membrane degradation and support oxidation [163]. Due to widely research area of interest for the degradation mechanism of electrocatalyst, it is not feasible to operate fuel cell for thousands of hours to analyze the impact. Accelerated Stress Test "AST" is one of the most preferable and fast methods that helps to identify the key issues of electrocatalyst problems in shot time to address the durability issues. AST method follows a specific protocol in a way to gather enough data with comparability. Due to the advancement of material by design approach, novel electrocatalysts are being developed, which requires an extensive effort to test with a suitable protocol. The AST protocol can speed up the reliability test by skipping the detailed examination, but the protocol is subjected to realistic fuel cell conditions in order to eliminate new failure mechanisms. Catalyst layer degradation is crucial and utmost for the stability of fuel cell; it can be affected by both physical degradation and chemical degradation [164]. These phenomena include the cracking of catalyst layer, catalyst poisoning and washout, catalyst particles growth and migration [165–167]. Carbon oxidation (corrosion) is related to the carbon-based support of catalyst [168]. In the electrochemical system, the carbon oxidation starts at 0.207 V_{RHE} [43], but its severity is negligible with potentially less than 1.1 V_{RHE} in a fuel cell, as the kinetics of corrosion process is very slow [169]. The carbon corrosion happens when there is a non-uniform distribution of fuel and cross over issues during start-up and shutdown procedure. Nevertheless, this reaction is catalyzed by the Pt catalyst mostly used in PEMFC by lowering the carbon oxidation potential [170]. The gas diffusion layer is also one of the most important parts of MEA and GDE which is also prone to degradation since it consists of carbon which is subjected to oxidation but also subjected to the mechanical degradation and ionomer decomposition [171, 172]. The degradation of GDL

results in alteration of structuring properties of GDL and hydrophobic loss and thereby affecting the mass transport [173, 174]. To develop AST protocols with reduced experimental time and components interaction, the failure mode has to be analyzed thoroughly. The AST method gives the advantage to understand completely the degradation mechanism not different to the one encountered in the fuel cell, but with certain limitations such as different degradation behaviour needs a different AST protocol with specific conditions and cycles. Two organizations DOE and US Fuel cell council (USFCC) had extensively developed AST protocols with specific standard operating procedures. Both organizations similarly aligned the standardization of AST protocol, but AST protocols used in research is mostly adopted in the context of DOE set of standards while USFCC AST protocol is applicable for long term applications. These protocols for individual degradation mechanism is already presented in the literature with AST for carbon supportGDL, operational degradation, membrane and catalyst layer [163, 175, 176]. Most of the protocol available are valid for PGM and Non PGM electrocatalyst for PEMFC and yet the protocols for AEMFC for individual degradation mechanism is yet to be developed and standardized.

Table 2.2: US FCTT AST protocol for PEMFC fuel cell electrocatalyst. Adopted from [177]

AST Cycling for Electrocatalyst		
Conditions		
Temperature	80°C	
Relative Humidity	Hydrogen/N_2-100%	
Pressure	Atmospheric Pressure	
Fuel/Oxidant	Hydrogen/N_2	
Cycling		
Number	30,000 cycles	
Time per cycle	16 second	
Sweep	Triangle sweep cycles from 0.6-1.0V_{RHE} at 50mV/sec	
Parameters	**Frequency**	**Target**
Mass activity	Initial and Final	$\leqslant$ 40%loss of initial activity
Polarization curve	0,1K,5K.10K and 30K	$\leqslant 30mV$ loss at 0.8A/cm^2
ECSA	10,100,1K,3K,10K,20K and 30K	$\leqslant$ 40%loss of initial area

2.9 Recent Advancement of Electrocatalyst for ORR and Characterization Methods

Although the AEMFC research has been increased over the past decade for exploring non PGM catalyst with a lower cost to compete with PEMFC, PEMFC is still favourable due to the performance gap. Now, the activity of Pt in alkaline is much of an interest to see the performance of the high-cost catalyst in low cost operating AEMFC. The water optimisation can enhance the performance of AEMFC catalyst by adjusting the gas diffusion electrodes, Omasta et al. expressed that capacity of anion exchange ionomer

with Pt in AEMFC with high potential of 0.75 V_{RHE} at 2 A/cm^2 [178]. Similarly, addressing the water management issue in AEMFC by optimising ionomer ratio, catalyst loading for enhancing the water back diffusion characteristics, the same research group achieved the activity of 0.75 V at 2 A/cm^2 for platinum in AEMFC [179]. The impact of high ion exchange capacity and type of ionomer can address the water transport issues and stability of Pt in alkaline, the platinum exhibited high activity with 0.75 V_{RHE} at 2 A/cm^2 in fuel cell testing [180, 181]. Just like mesoporous encapsulated Pt/C catalyst have high activity as compared to Pt on Vulcan, same way Nitrogen-doped carbon encapsulated non-noble metals are also auspicious. Nevertheless, there are more efficient materials that can be doped with carbon for better performance. For instance, NFC@Fe/Fe_3C catalyst under alkaline conditions are very much stable with loss of $\approx$ 26 mV per 50,000 cycles and at half-wave potential with better activity than commercial Pt/C catalyst (16 mV higher) as demonstrated by Karuppannan et al [182]. The same catalyst performed less in acid conditions with $\approx$ 27 mV decay at 30000 cycles. In most of the research, The nitrogen-doped catalyst has higher stability in the alkaline environment as compared to the commercial Pt/C in the fuel cell tests [183, 184]. With the help of polymerisation techniques, scientists were able to develop mesoporous carbon microspheres for Fe-N-C by citing the higher activity with a half-wave potential ($E_{1/2}$) of 0.86 V_{RHE} in RDE experiments, due to stabilised adduct formed in alkaline media promoted by HO_2^-. This is quite the opposite to stabilisation in acid media which is effected by the protonation of H_2O_2 leading to high overpotentials for ORR [185]. The catalytic activity of Fe-N-C for ORR is promising due to carbonisation of catalyst for the mesoporous structure to provide metal ions a promoted pathway to adsorbed O_2 for comparability to Pt/C but still very challenging. Non PGM such Ag and Pd have also widely studied electrocatalyst in replacement of Pt, Wang et al. worked on a new mechanism for radiation grafted membranes which improved the shelf life of the catalyst, although the Ag/C catalyst achieved a high activity of 0.6 V_{RHE} at 2 A/cm^2 but still the performance is lower to that of Pt [186]. In another research, Wang et al. observed the same trend that has been observed by trying to optimise the Ag/C and Pt/C electrocatalyst with newly drafter ionomer poly(ethylene-co-tetrafluoroethylene) but faced issues with high gas crossover rates [187]. Similar trends with Pd and its alloy has been demonstrated by Omasta et al. in AEMFC, the performance(0.5 V_{RHE} at 2 A/cm^2) of catalyst was still lower than Pt/C in alkaline but with slow degradation [188]. It has also been examined that the Pd based alloys at the anode can improve the performance of non-Pt/C catalyst in AEMFC, which also shows that the there is still a gap for exploration of non-platinum catalysts for the anode in AEMFC [189]. For non PGM catalyst, the full understanding of catalyst stability and material properties issue is still yet to be addressed, which requires special protocol and advanced characterisation techniques such as MEA. Although, there is a possibility to use existing developed protocols for PGM with addition stressors such as GDL ageing with different gases, humidification and temperature [190–192]. For instance, the performance loss of GDL is less aggressive with nitrogen as compared to air [193]. The humidification can lead to decrease the

electrode hydrophobicity and high ionomer degradation after intensive operation of 1600Hrs [194, 195]. AEMFC is also widening the possibility of extensive research in material chemistry and several non PGM catalysts that come into competition within the past years, showing promising high stability over several hours of operation in RDE and MEA. In non PGM electrocatalyst, Fe-N-C is widely researched catalyst for bothPEMFC and AEMFC. Firouzjaiei et al. [196] explained the conditions of Fe-N-C that the main concern is not about activity but stability even though they approached 0.6 V_{RHE} at 2 A/cm^2 with Fe-N-C at the cathode and Pt alloy (Pt-Ru) at the anode and it can even worse in PEMFC due to Fentons reagent reaction. Nevertheless, as compared to Wang et al. [197] with Ag as AEMFC cathode with performance loss of 50-100 mV, the Fe-N-C is still better than their counterpart non PGM. Previously, various attempts have been made with the modified Fe-N-C by carbon capsuling, nanotubes and graphene nanosheet but their performance (0.1-0.3 V_{RHE} at 375 mA/cm^2-1.6 A/cm^2) was not comparable to the recent studies [198–201]. However, since, Fe-N-C ORR in alkaline is still an open topic, various studies are yet to come by optimisation of catalyst layer properties. Fe-N-C ORR in the acidic electrolyte has also been studied in the past decade exhibiting the high performance but not comparable to commercial Pt/C ORR in PEMFC. Proietti et al. first investigated the Fe-N-C in PEMFC, despite a good performance of 0.45 V_{RHE} at 1 A/cm^2, the decay rate was found to be faster as compared to Pt catalyst [202]. Later then, Fe-N-C was optimised with carbon nanofibers, and it was able to achieve slightly better performance with 7-8 mV loss after 35000 cycles of operation [203]. There are lots of other efforts have been done to improve the performance of Fe-N-C in acid through modified superficial support, doping Fe into zeolite framework, by introducing more nitrogen-rich precursors but still the catalyst activity is not up to the mark in the range of 0.3-0.5 V_{RHE} at 1 A/cm^2 [9, 204–207]. The performance of Pt/C is well known in PEMFC and can be found in various research papers [96, 208–212], most of the test were carried out in RDE and MEA, both results can differ due to mass transport by gases in MEA, and low practical current density approach of RDE.Some researchers worked on optimisation of RDE or development of other methods such as Fleige et al. improved the design of RDE by coupling magnetic drive to the electrochemical cell in an autoclave to enable high temperature (140°C) and pressure conditions (100 bars). These elevated conditions boosted the limiting current densities due to better solubility of reacting gases in liquid electrolyte [212]. Generally, the data from RDE is extrapolated to PEMFC relevant densities (0.6 V$_{RHE}$ at 1.5–2.0 A/cm^2) usually approaches to significant errors [7]. Floating electrode FET in the half cell is another alternative method for RDE that implements the approach of high mass transport to the realistic fuel cell conditions. Zlatis et al. investigated the ORR activity for 60 wt% Pt/C and approached to the geometric current density of 800 mA/cm^2 at 0.38 V$_{RHE}$ which is two orders higher than RDE in the new FET technique. However, the current density is still limited to approach the realistic fuel cell conditions. Even though, FET provides higher ORR current densities but the compatibility of mass activity at 0.9 V$_{RHE}$ is differ in all techniques (RDE, FET and MEA) [213]. There was a gap that a new

method could be introduced providing fast and reliable results approachable to limiting current density of MEA and accuracy of RDE with low cost and less time consuming which will help researchers to optimise and investigate the catalyst layer quickly. GDE in the half cell is one of the methods that can be regarded as intermediate of RDE and MEA. Jia et al. investigated the platinum on Vulcan X-72 carbon support in GDE setup and approached to 600 mA/cm^2 limiting current density [214]. Pinuad et al. [215] enabled to close this gap by introducing a graphite flow field channel for forced convection which approached to 1.75 A/cm^2 limiting current density for platinum catalyst in 1.0 M $HClO_4$ comparable to single-cell test. The key feature for their GDE half-cell assembly is **Modularity** which simplifies the component assembling and disassembling [215]. Inaba et al. introduced a modified GDE half-cell with a temperature-controlled system and able to mimic the realistic fuel cell conditions and expected to bridge the performance gap of fundamental research to fuel cell. They were able to achieve 1 A/cm$^2_{geo}$ at 60°C with 100% relative activity and results were comparable to MEA by utilising Pt/C catalyst with ultra-low loading (0.05mg/cm^2). Due to kinetic current determination without extrapolation and the comparability with MEA makes this technique an edge over TF-RDE [216]. As Pinuad et al. [215] approached the realistic conditions without any transportation limit at higher current densities, Ehelebe et al. [15] further optimised the GDE design and were able to achieve 2 A/cm^2, which is highest approachable current density achieved until yet in GDE half cells. Instead of fully immersing the compressed catalyst layer into the flow channel, they introduced a separate attachable compartment confined to the geometric area of catalyst up to 2.01 cm^2 without any active sides pressed facing to the electrolyte. They were able to get reproducible and comparable GDE results to MEA and hence concluded that GDE half-cell measurements can serve as an intermediate between Thin film-RDE and MEA [15]. As GDE method is already validated for Pt/C evaluation, it is yet to be explored for the catalyst layer optimisation of non PGM and AEMFC, which will be covered in this thesis.

3

Materials and Methodology

Contents

The experiment of catalyst layer investigation for ORR in GDE half requires series of steps which are presented as below

3.1 Catalyst Coated GDL Electrodes Preparation

Multiple sets of GDEs were prepared in the laboratory at Helmholtz-Institut Erlangen-Nürnberg. The focus of this research work was to investigate the ORR for commercial Pt/C, advanced Pt/HGS and non PGM (Fe-N-C) catalyst. All samples with the similar loading tested in a set of two samples in order to see reproducibility of results. The method of GDEs electrodes preparation is as following:

3.1.1 Commercial Pt/C

The commercial Pt/C was purchased from Fuel Cell Store consists of 40% of Pt on Carbon with loading 0.3 mg_{pt}/cm^2, surface area of 60 m^2/g, 2% moisture content. The material type of gas diffusion layer is carbon paper fibre with a pore size of 215 ±20 microns, the thermal conductivity of 0.3W and roughness of 7.2μm. The resistivity of GDL is < 10 mΩ/cm^2 with 5% Nafion content and < 10 ppm of impurities (Fe, Co, Ni). The samples were withdrawn from the layers with manual punching tool in a circular shape of 2.01cm (diameter). Some of the GDLs were hotpressed with Nafion™211 to mimic the conditions of fuel cell electrode.

3.1.2 Advanced Platinum Catalyst Pt/HGS

The catalyst ink for GDE was prepared from Pt/HGS powder, the ink was comprised of 1 wt% of solid in of 20 wt% isopropyl alcohol (IPA) in H_2O. The ionomer Nafion520; DuPont to catalyst ratio (I/C-gravimetric) was 1.05 wt%. The catalyst in glass crucible was placed in an ultrasonic bath, and the IPA water solution was added to it dropwise. Later the ionomer was added in a similar manner, and the ink was left for 2 minutes. The catalyst ink was then homogenized via ultrasonic horn (Hielscher) at 0°C 60W for 20 minutes. The gas diffusion electrodes were prepared by spray coating using the catalyst ink onto gas diffusion media Freudenberg H23C8 (thickness 230 μm, resistivity 8 mΩ/cm^2 and weight of 135 g/m^2) via ultrasonic spray coater (Biofluidix) on a heated platform at 85°C. In order to achieve a deposition rate of 6 $\mu g_{Pt}/cm^2$ per cycle, the spray head was controlled for ink flow rate and movement speed. The catalyst was prepared for two different loadings, i.e. 0.04 mg/cm^2_{Pt} and 0.1 mg/cm^2_{Pt} through additional spray coating for high loading sample.

3.1.3 Non PGM Fe-N-C catalyst

The non PGM catalyst (Fe-N-C) for high pH GDE was prepared with two different ion exchange capacity i.e. High ion exchange capacity (HIEC) GDE and Low ion exchange capacity (LIEC) GDE with

a total composition of 20wt% solids in 1-propanol. The composition of catalyst ink is 70wt% FeNC (PMF-011904,commercial Pajarito Powder) is infused with the 30wt% of commercial ionomer for alkaline conditions (Aemion™HNN5-00-X) with ion exchange capacity of average 1.6 meq/g LIEC and 2.4 meq/g for HIEC. The ionomer was first dissolved in the solvent, and later Fe-N-C powder was added to the solution. The solution ink was homogenized by mechanical stirring for one hour, and then it was placed for an additional one hour in an ultrasonic bath. Later, the ink was homogenized via stirrer all overnight and then sonicated again for on the hour on the next day. Before depositing the ink onto GDL, the ink was stirred again. The deposition of ink on Freudenberg H23C8 GDL was done via doctor blading method in an automatic film applicator (ZAA 2300, Zehnter). The thickness of the wet film was determined via adjustment of gap height on the doctor blade. The gap height was adjusted to 170μm, resulting in the average loading of 1.3-1.65mg/cm^2. The wet samples were later dried at 40°C for 2 hours, the first hour with atmospheric pressure and the second hour with reduced pressure. The weight difference of samples measured the loading of Fe-N-C before and after catalyst ink deposition and solvent evaporation by a weight balance (Sartorius Cubis®, 0.001 mg). Later then samples were punched for a circular shape of 2.01cm^2 area, in order to study the activation of samples, some samples of LIEC were immersed into 1M KOH(Ensure) liquid for the period of without activation, 2*20 minutes, 24, 48 and 72 hours.

3.2 GDE half-cell measurements

To investigate the ORR activity of Fe-N-C catalyst, we operated the modified GDE half-cell developed by Ehelebe et al. [15] which was already used to benchmark platinum catalyst without any mass transport limitation and mimicked fuel cell conditions. The Figure 3.1 shows the schematic CAD view of GDE and cross-sectional view of electrode-electrolyte interface. The cell is made up of PTFE which has very high chemical resistance and strength [217]. The Viton O-rings were used for coupling the gas chamber to the electrolyte chamber. It provides better sealing due to high compressibility. The cell is comprised of two compartments, i.e. gas chamber and electrolyte compartment. The electrolyte compartment (holdup volume 250 ml) is comprised of two chambers, one for reference electrode and other for working electrode and electrolyte. The reference electrode compartment is connected to electrolyte compartment and working electrode interface by lugging capillary in symmetrically oriented position (1mm apart from the electrode-electrolyte interface) to reduce ohmic resistance between the working and reference electrode (Ag/AgCl Metrohm). It does not impose any effect on electric field between working and counter electrode (expanded mesh of Ir/Ta mixed metal oxide [AN45272] on Ti, (METAKEM)). To limit the temperature variation up to 4 K, the distance between the counter and working electrode is kept to minimum 1cm to depreciate cell resistance. The gas chamber comprised of low resistive (13 µΩ m) graphite flow field (R8710, SGL CARBON) with channelling to ensure distributive gas flow over the

gas diffusion electrode. The exposed area (2.01 cm^2) of gas diffusion electrode to the electrolyte is not compressed and supported by flow field from the back which also serves as a current distributor. For unhindered conduction, the GDL is subjected to humidified gases (Air Liquid with purity 99.998% Ar, O_2, HO_2 and synthetic air with 20% O_2 in NO_2) in both electrolyte and gas compartment by commercial humidifier (Low Flow Humidification System, Fuel Cell Technologies, Inc) with mass flow controllers (EL-Flow Se- lect, Bronckhorst) at 3 bar. Biologic potentiostats (VSP-300) with two 2A booster cables was used for data acquisition and parameters control (potential, current) for all experimental investigations of GDE half-cell.

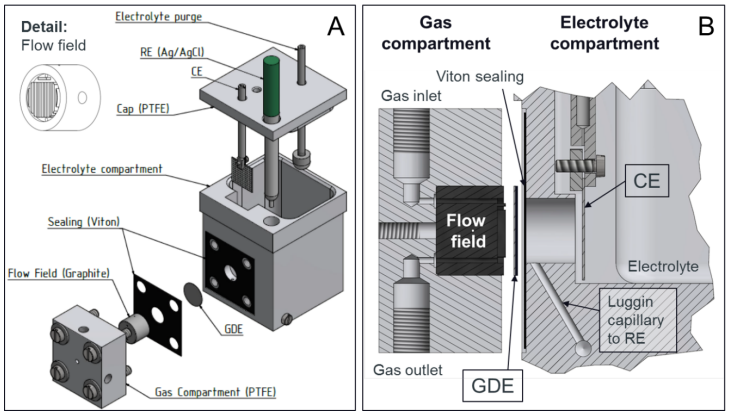

Figure 3.1: Schematic view of gas diffusion electrode GDE half cell assembly. A Detailed demonstration of all GDE parts with the configuration. B: Cross sectional view of electrode electrolyte interface with flow channels. Reprinted from [15]

3.2.1 Electrochemical Testing Protocol for GDE

Before every experiment, the cell cleaning procedure was carried out in order to reduce the contamination as we are using a high concentration of electrolyte ($\sim$ 1.0 M) so there is a possibility of high impurities [218]. The choice of high concentration of the electrolyte is to avoid any significant resistance by solution and their respective errors [219]. The electrolyte was changed after every experiment to avoid electrolyte decomposition and generation of ions such as chlorides from $HClO_4$. The new cell was first cleaned with soap and ultrapure water (18.2 MΩcm at 25°C, <1.7 ppb TOC water, Milli-Q IQ 7000 Merck). Then the cell was boiled once in 1% HNO_3 (Suprapure) and three times in ultra-pure water. The water is drained after each boiling and replaced it with the freshwater. All parts of the cell were immersed in a large beaker filled with saturated $KMnO_4$ solution for overnight cleaning. The cell is then neutralized with 96% H_2SO_4 and 30% H_2O_2 (30ml) to ensure full dissolution of MnO_2 to Mn^{+2} and then boiled three times in ultrapure water to remove peroxide traces. After finishing each experiment, the GDE assembly was rinsed three-time and boiled one time for the next experiment. Before every experiment, all components

of GDE assembly were dried in air. The reference electrode was calibrated for the reversible hydrogen electrode (RHE) before every experiment, and the potential of the reference electrode in RHE was shifted accordingly. The test protocol was developed according to the parameters required for the investigation of catalyst. The evaluation of commercial Pt/C was carried out to show that how GDE and (catalyst coated membrane) CCM can be used to evaluate the catalyst layer properties for ORR. Firstly, the catalyst was purged for 10 min with humidified Ar. Even though, the GDE and CCM measurement in our half cell are less sensitive to contamination as compared to RDE due to large surface samples (2.01cm^2 vs 0.2 cm^2) and high loading (0.3 mg/cm^2 vs 0.020 mg/cm^2) [215]. The cleaning cycles were performed (30-50) till the cyclic features remain stable with the potential sweep of 0.05-1.2V_{RHE}. The GDE cell developed by Ehelebe et al. [15] used for this study which is an optimized version of Pinuad et al. [215] cell which requires at least 100-200 cleaning cycles to reach to a stable state. The cyclic voltammetry was carried out at the scan rate of 50,100 and 200 mV/sec, within the potential range of 0.05-1.2 V_{RHE}. The electrochemical surface area ECSA of the catalyst was determined by integrating the hydrogen desorption curve region and theoretical value of Pt surface H_{upd} value of 210 µC/cm^2. However, there is a possibility of overestimation of the surface area when correcting the baseline and enhanced peaks due to hydrogen evolution reaction. This issue will be discussed later in the next section of this thesis**??**. So during ECSA determination, the flow of Ar gas was stopped as it has been demonstrated in previous research that the flow of gas through catalyst layer will prevent the hydrogen from accumulating at catalyst surface and thus due to hydrogen evolution the potential will be shifted [220]. During the data processing, the CVs were corrected to 100% by the following formula.

$$E_{corrected} = E_{uncorrected} + E_{Ag/AgCl} - R_u * 1 - (1 - (Correction factor iR)/100) \tag{3.1}$$

To determine the ECSA and catalyst utilization, we need charge which is obtained by integrating the area under the curve Next step is to find charge

$$q_H = Area\ measure - Area\ capacitance \tag{3.2}$$

The real surface is the ratio of charge to the hydrogen desorption charge density of bulk Pt (hydrogen adsorbed onto the monolayer of Pt)

$$S_{real} = \frac{q_H}{q_{HPt}} \tag{3.3}$$

The ECSA can be determined by

$$\text{ECSA} = \frac{S_{real}}{Catalyst\ loading * S_{geo}} \tag{3.4}$$

Where S_{real} is real surface area, S_{geo} is the geometric area, q_H is the charge bulk density, $E_{Ag/AgCl}$ is

potential of reference electrode Ag/AgCl and Ru is the uncompensated resistance Since our GDE half-cell can approach to high current density $2A/cm^2$, therefore, to avoid errors during ORR determination, the uncompensated resistance between reference and working electrode must be determined which is the sum of all resistance (electrolyte, GDL, contact, flow field and catalyst layer resistance). The importance of realization of uncompensated resistance was addressed by Ehelebe et al. that at 1 A, the difference of 10 mΩ can deviate the 10 mV in applied potential [15]. The ORR data was corrected by the following equation.

$$E_{corrected} = E_{uncorrected} + E_{Ag/AgCl} - \frac{I_{uncorrected}(mA)}{1000} * R_u * (1 - (Correctionfactori R)/100) \quad (3.5)$$

The catalyst layer is purged with Argon from the back (through gas diffusion layer) to remove any dissolved oxygen for ten minutes. All experiments have been carried out in 1.0 M $HClO_4$ and H_2SO_4 for Pt/C, 1.0 M $HClO_4$ for Pt/HGS and 1.0 M KOH for Fe-N-C LIEC, Fe-N-C HIEC and Fe-N-C Nafion electrocatalyst for optimal conductivity at room temperature. Cyclic voltammetry measurements were being carried out in Ar saturated solution at 100mV/s with the potential range of 0.05 to 1.2 V_{RHE} and reported with 100% correction (95% in-situ and 5% post-processing compensation). All the voltages were referenced to V_{RHE}, which was measure before every experiment (around 0.015 to 0.026 V_{RHE} for $HClO_4$ and 1.015-1.026 V_{RHE} for KOH). The cell also equipped with mesh counter electrodes and Ag-AgCl as the reference electrode. For ORR, spectroscopic galvanic impedance spectroscopy(SGEIS) technique has been carried out with O_2 flow (250 mln/min) from -0.1 mA to -4 A in both directions (forward and backward) within the range of 10kHz to 10 Hz with 100% post-correction of iR compensation. The step was repeated until the achievement of reproducible results. After that, degradation cycles were carried out (5000-30000 cycles, depends on the requirement) within the potential limit of 0.6-1.0 V_{RHE} in Argon saturated environment at a flow rate of 250 mln/min and SGEIS ORR was carried out again to see the stability of Fe-N-C after degradation cycles. More details of the protocol are mentioned in flowcharts for each catalyst system.

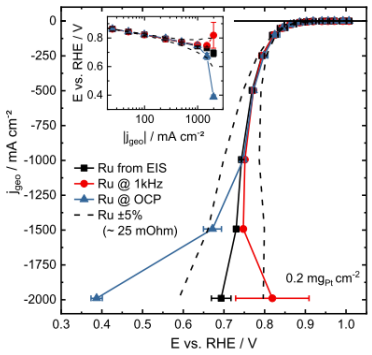

Figure 3.2: Different methods of uncompensated resistant determination for ORR and the deviation at high current densities.Reprinted from [15]

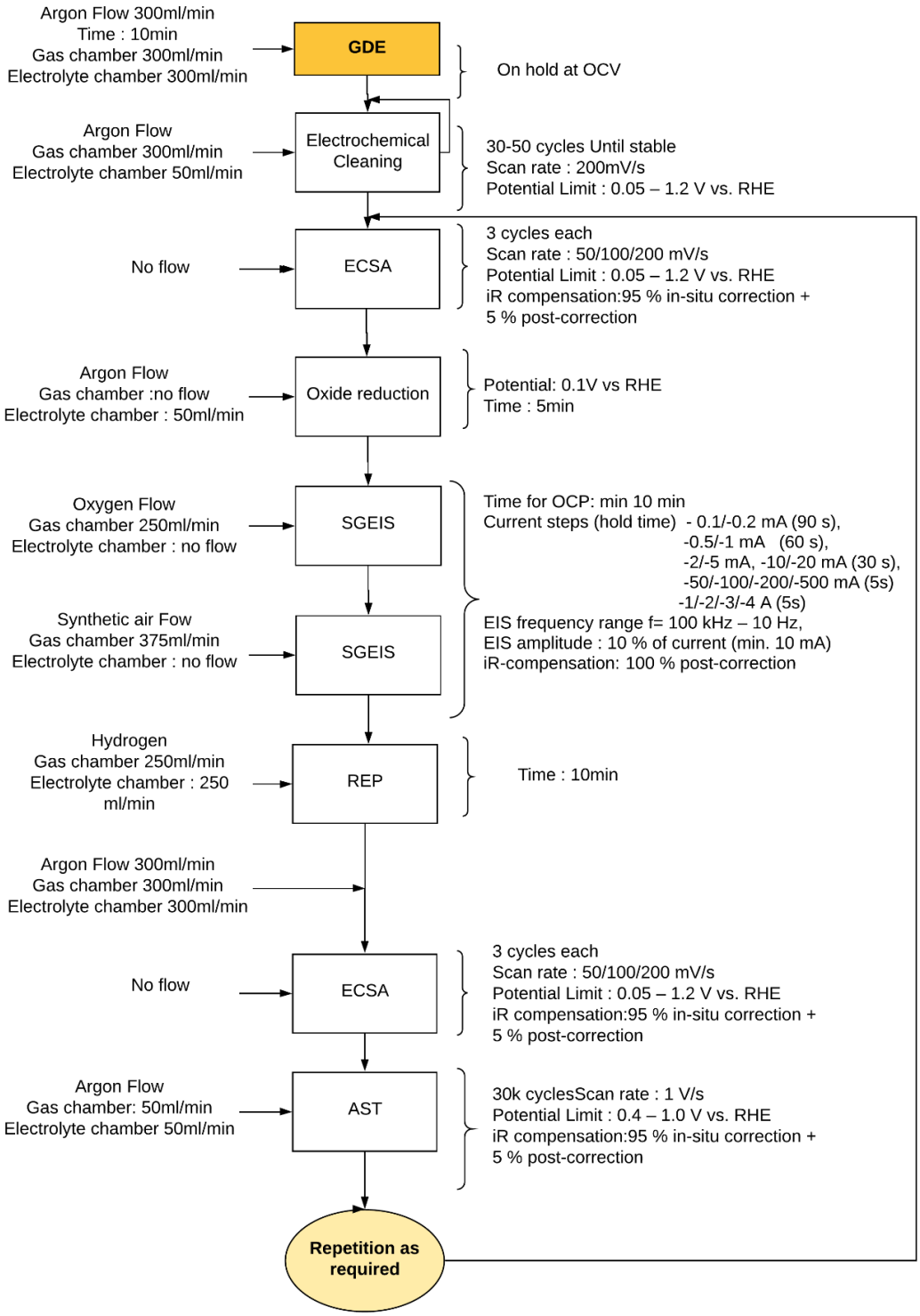

Figure 3.3: Complete protocol for commercial Pt/C activity determination in ORR for PEMFC based GDE half cell

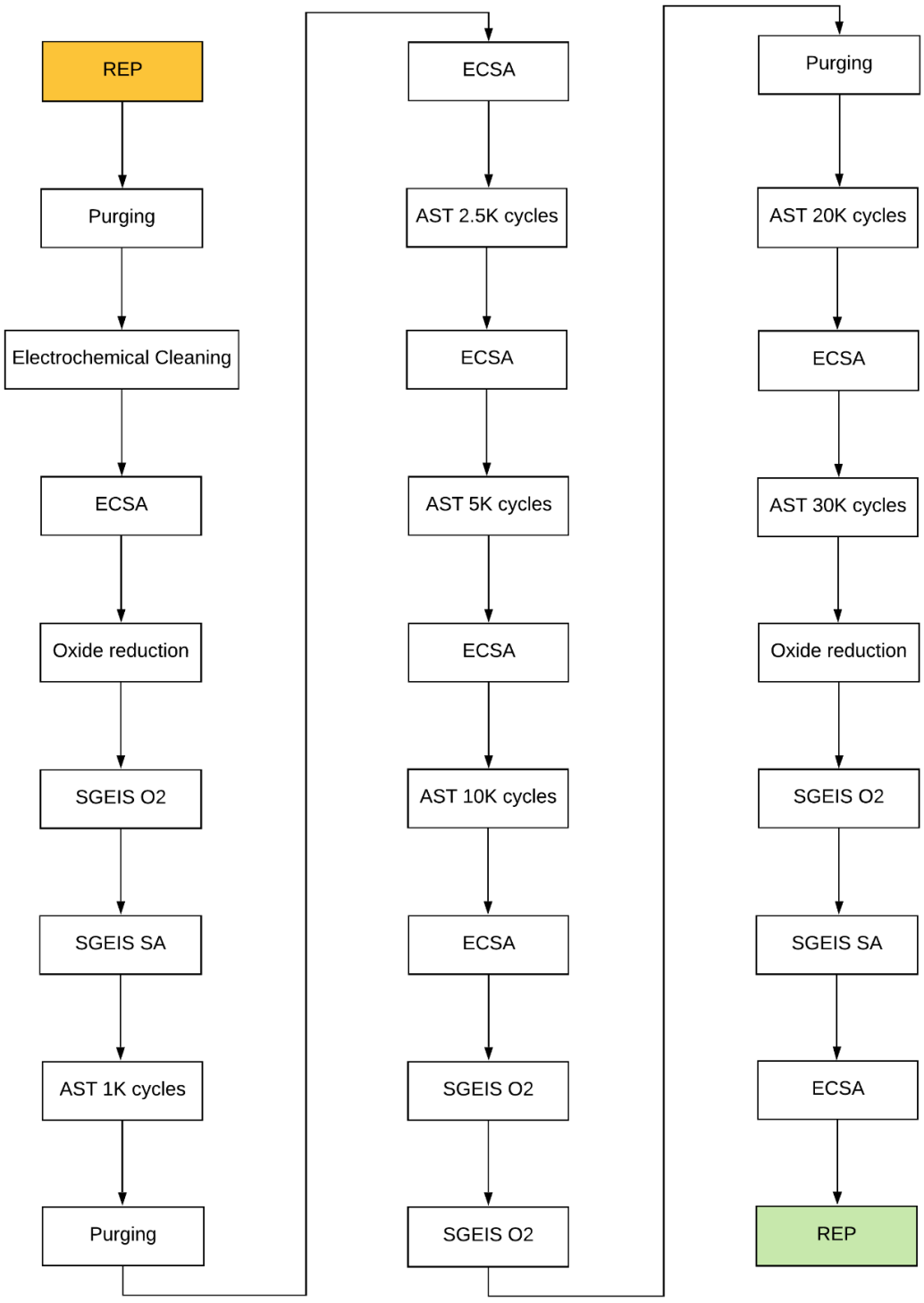

Figure 3.4: Modified protocol for maximum activity for Pt/HGS in $HClO_4$ after several stress test cycles with interval of 1000,2500,5000,10000 and 30000 cycles

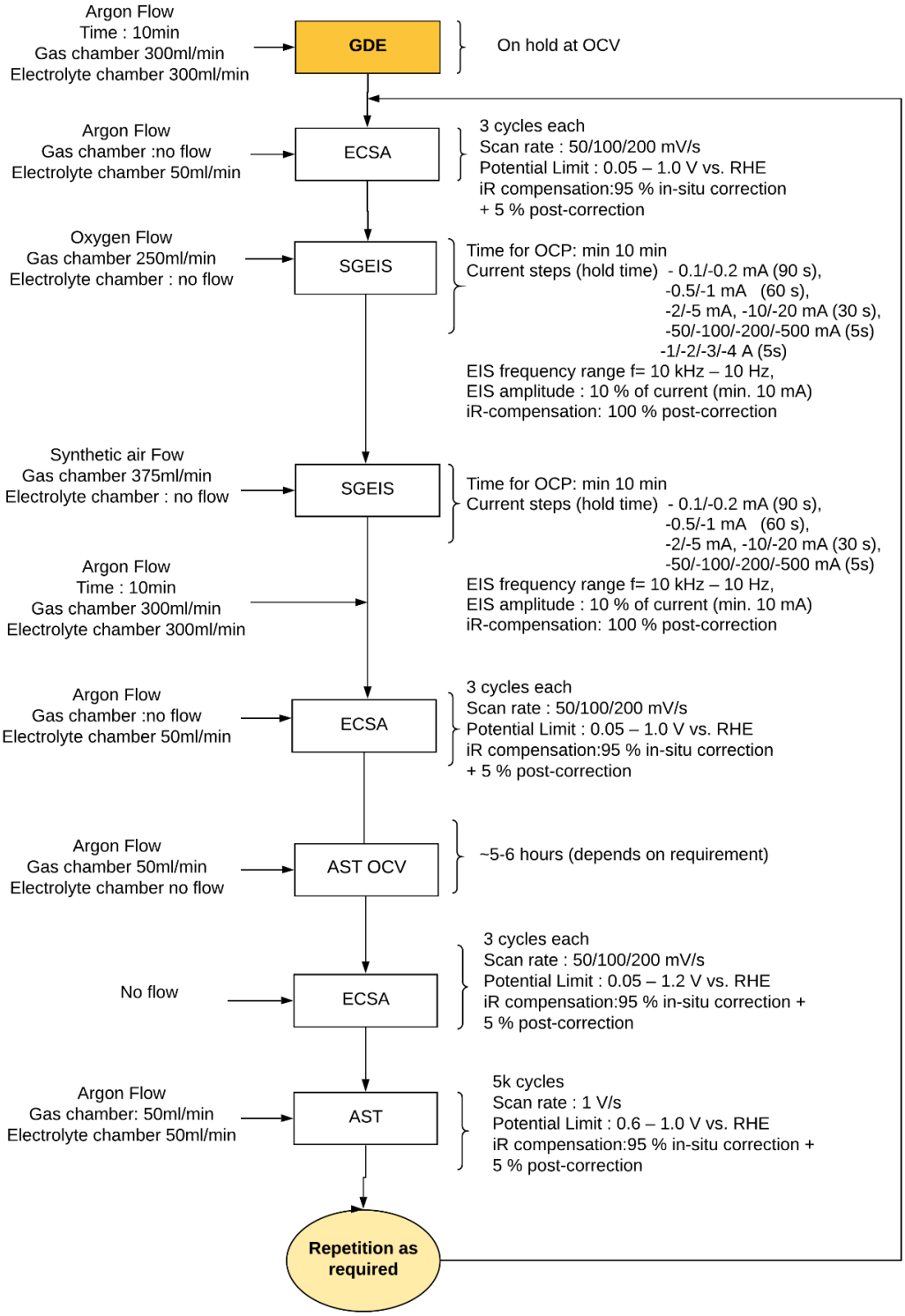

Figure 3.5: Protocol for Fe-N-C in investigation for AEMFC in GDE for stability and activation studies

4

Results and Discussions

Contents

Fuel cell electrocatalyst research is mainly based on improving the cathode catalyst layers, and several cathode electrocatalysts have been developed in the past and discussed in previous chapter 2. The central aspect of catalyst development is an extensive series of quick evaluation methods for comparison and investigation of newly developed catalysts. All the testings in fuel cell stack are time-consuming and complex, and the various methods have been discussed in the previous chapter 2. GDE method was chosen for this study, and it is employed to investigate the ORR phenomena, degradation and stability studies for the state of the art commercial platinum catalyst, advanced platinum catalyst (platinum nanoparticles in hollow graphite spheres) and non-platinum catalyst (Fe-N-C with different ionomers). The GDE half-cell provides full control in a mimic fuel cell environment with the possibility of imitating the electrode conditions with potential cycling, start/stop control and acceleration degradation study AST. This method anticipates generating reproducible and comparable results to the literature within a series of experiments..

4.1 State of the art Platinum Catalyst supported on Carbon

The state-of-the-art platinum catalyst for PEMFC consisted of nanoparticles dispersed over high surface area support, namely carbon/carbon black. The carbon/carbon black generally sourced from different materials produced from petrochemicals or biomass through methods of partial oxidation and thermal cracking [221–223]. During the synthesis, the carbon carries out contaminants within it, and those impurities can be traced in the carbon support of fuel cell. During the synthesis of the commercial catalyst, several other contaminants such as organic impurities from different reducing agents by platinum precipitation or inorganic impurities from the platinum salt can influence the electrocatalyst performance. Before starting the ORR procedure, the catalyst was subjected to cleaning cycles in the potential range of 0.05-1.2 V_{RHE}.

The appropriate cleaning cycles used for this investigation were limited to 30-50 due to the observation that prolonging the cleaning cycles may result in carbon corrosion [224]. To a certain extent, the carbon oxidation in our GDE cell is quite negligible due to the controlled environment (scan rate 200 mV/s at room temperature) This is according to the literature that carbon corrosion in insignificant until and unless fast scan rate at 500 mV/s is applied in the potential regime of 0.6-1.5 V_{RHE} [225]. The influence of impurities can be seen in CVs (Figure 4.1) by a distinctive difference between the first and 50^{th} cleaning cycle. In the first cycle, the suppressed peaks of oxidation are visible, and the current density is continuously increasing after continuous cycling due to the oxidation of organic impurities. At the high constant scan rate of 200 mV/sec, the process of impurities oxidation is faster that helps in cleaning the platinum surface by adsorption of hydrogen and oxygen species and removal of organic impurities which is an essential factor for further testing of catalyst.

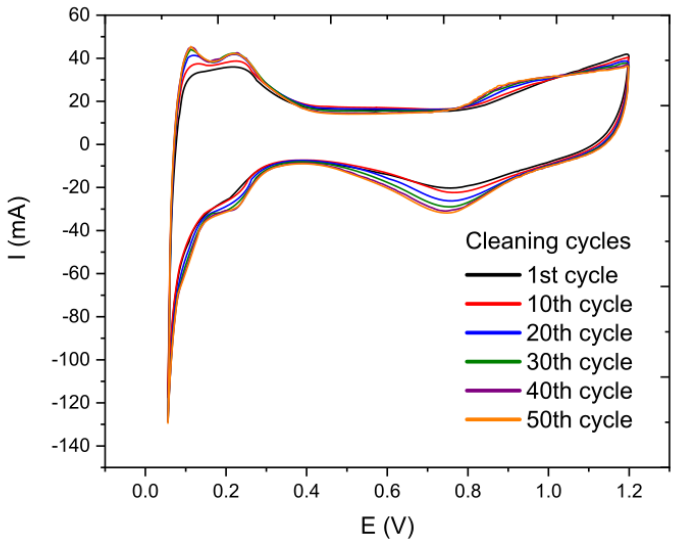

Figure 4.1: Cleaning cycles for Pt/C HISPEC 4000 in GDE half-cell for PEMFC

The area of H_{upd} also increased with each cycle which can be possible due to growth of the surface area as the organic impurities remove from surfaces leading to more empty active sites of the catalyst. Therefore, cleaning cycles help to further investigation of electrochemical surface area by cleaning the active sites without much interference of catalyst itself [226]. This attribute of potential cycling leads to real surface area exposure for better electrochemical reactions. However, there is a possibility of platinum dissolution over the range of 0.85 V_{RHE} as investigated by Cherevko et al. [227]. Although the activation of the electrode depends on the cleaned surface, potential cycling also leads to structural changes in the catalyst, which could affect the activation procedure.

4.1.1 Impact of non-membrane and membrane coated GDL catalyst layer on ECSA

The commercial state of the art Pt/C catalysts were tested in the acid electrolyte with a concentration of 1.0 M for $HClO_4$ and 1.0 M for H_2SO_4. The CVs were determined at different scan rates, i.e. 50, 100 and 200 mV/s and only the results for a faster scan rate of 200 mV/s as shown in Figure 4.2 demonstrated in this section. At 0.09 V_{RHE}, the hydrogen desorption peak is visible, which is related to Pt with (110) facets, whereas the peak emerges at 0.23 V_{RHE} relates to Pt (100) facets in agreement to literature [228]. Pt (110) sites are affinitive to weak bounded hydrogen while the Pt (100) corresponds to strong bond hydrogen to active sites. The CVs were obtained without the gases purged from the back of GDE as it has been reported that inert gas flow can lead to underestimation of ECSA by shifting the hydrogen evolution reaction to a more positive potential [220]. The peak values of potential

are very similar to the literature [229] exhibiting the normal CVs for the acid electrolyte. In H*upd* region i.e. hydrogen underpotential region ranging from (0.05-0.3 V_{RHE}), the double-layer region of pseudocapacitance (0.3–0.7 V_{RHE}) and oxides formation and reduction region (>0.7 V_{RHE}). The intensity of peaks exemplifies the oxidation and reduction of species. Also, there is an increase in the double layer capacitance area due to surface roughness or high-water dipoles molecule concentration near to electrode-electrolyte interface.

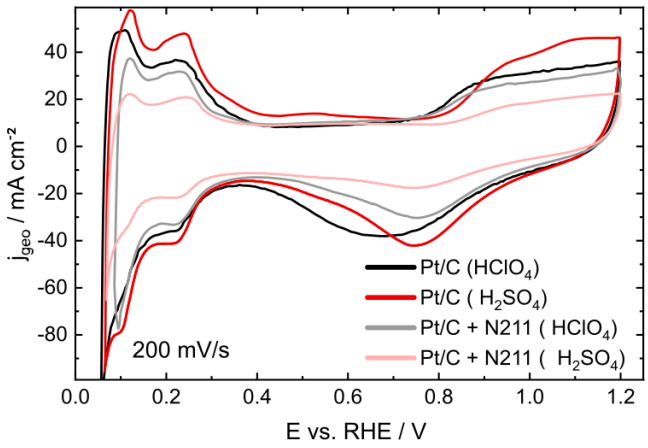

Figure 4.2: Comparison of CVs for commercial Pt/C catalyst with $0.3 mg_{Pt}/cm^2$ in $HClO_4$ and H_2SO_4 with and without membranes

The GDE half-cell test is reliable and has been investigated by a few other researchers [15, 215, 230] observing reproducible results in a way that the similar experiments performed in a relatable environment. Hence, several other factors must be taken into consideration to optimize the GDE cell such as reported by Ehelebe et al. [15] to determine ECSA through experiments with low or no gas flows from the back of GDE. An approach was given to flood GDE with water from the back, which could alter the effects at gas electrolyte interface or with the minor gas flow. So, in these experiments, the ECSA was conducted with Ar flow of 50 mln/min. In the CVs, the oxidation current is higher for samples without a membrane (H_2SO_4 > $HClO_4$) with an onset voltage ≃0.8 V_{RHE} in the positive scan. It can be related to the formation of species (Oxygenated) on Pt such Pt-OH. In the negative scan, the reduction peaks are visible, leading to the reduction of Pt oxides. The onset voltage of Pt/C catalyst in H_2SO_4 for the formation of oxygenated species shifted the peak current mainly caused by anion adsorption with a difference of 0.8 V_{RHE} for $HClO_4$ to 0.85 V_{RHE} for H_2SO_4 possibly due to the strong bisulfate adsorption [231]. The CVs were obtained in the oxygen-free environment, but the presence of O_2 in the electrolyte is visible at 0.75 V_{RHE} affecting the redox reaction of Pt/C. The samples without membranes were least affected by the reduction, and there is a significant increase in reduction currents for GDL without membranes.

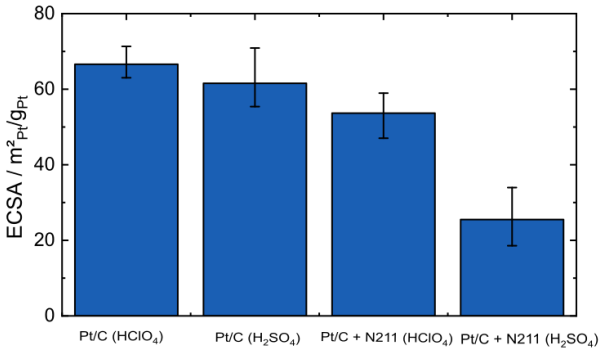

Figure 4.3: Electrochemical surface area of commercial Pt/C with and without membrane in GDE

Due to the nanoparticles of catalyst, the surface area of Pt/C was determined through the electrochemical method, as the total surface area (Pt nanoparticles and carbon support) is proportional to capacitive current. The adsorption and desorption of protons are specific to platinum. The electrochemical surface area of Pt/C electrocatalyst is found to be as 66.59 m^2/g_{pt} in $HClO_4$,61.55 m^2/g_{pt} in H_2SO_4, 53.67 m^2/g_{pt} in $HClO_4$(with membrane) and 25.49 m^2/g_{pt} in H_2SO_4 (with membrane). The sequential order ECSA is similar to the CVs area, but the possibility of uneven estimation of ECSA could be subjected the large error.

Although, this ECSA can be varied by the cleaning cycles which can decontaminate the catalyst layer from impurities. There is also the possibility of overestimation of surface area due to baseline correction of H*upd* region. The charge value of H*upd*, i.e. 210 $\mu C/cm^2$ is also under debatable, and other researchers might use different values which make it difficult for comparability. The specific ECSA of Pt/C-HISPEC 4000 is around $60m^2/g_{pt}$ which somehow satisfies our calculated ECSA except for the catalyst in H_2SO_4 with membrane mainly due to degradation mechanism. This estimation tells us the durability and vast application for GDE, as CVs performed in RDE at lower scan rate and the possibility of some contamination on rings could alter the results. However, in half-cell, the iR correction is very crucial, and sometimes it becomes substantial due to the high current density approach which is addressed by compensation to achievable level (though 100% correction is not approachable due to potentiostats limitation to run the system stably) through the feedback system. The difference between the electrochemical surface area for Pt/C with same conditions but in the different electrolytes ($HClO_4$ and H_2SO_4) is not similar can be seen in Figure 4.3.

Until, it is still not clear that what will be the possibility of difference between ECSA; however, both sets of experiments showed a similar trend, which means that results are reproducible. There might be several reasons that can justify this difference, such as perchlorate or persulfate anion properties or difference in impurities in both electrolytes. However, the possibility of acid strength can be neglected as both electrolytes used with the same concentration of 1.0 M. Several reports have demonstrated that morphological changes of Pt/C catalyst are much higher in H_2SO_4 as compared to $HClO_4$ because of the high absorbing

capability of sulfate ions on the platinum surface as compared to perchloric ions causing platinum ion dissolution and inhibiting redeposition [208, 232]. The influence of pH can also be one the primary factor for this difference as H_2SO_4 is diprotic acid and can lead to a decrease in pH value from 1 to 0.96. Future studies on the pH influence and different electrolytes for PEMFC with advanced tools can reveal more information. Liquid electrolytes such as perchloric acid and sulfuric acid are the conventional electrolytes used in PEMFC. However, each electrolyte has a different tendency for electrocatalytic activity. The adsorption on platinum catalyst surface for perchlorate anions are weaker as compared to sulfate anions can be related to the difference in activities limited by the active site's blockage [233]. In CVs, the onset of platinum oxidation shifts towards more positive potential while the hydrogen adsorption peak to more negative for H_2SO_4 with and without membrane. It shows that H_2SO_4 is more prone to catalyst stability as compared to $HClO_4$ in similar conditions. The Cl- ions are common impurities, but the sulfate ions can produce substantial retardation for the formation of the oxide. These anions can typically block the active sites, causing limiting transport of protons [222, 234]. Another possible impact is that the samples with membrane have a less active area which could happen by distortion of the physical structure and active sites damage due to hot pressing at high temperature and pressure. More experiments will be required to validate the outcomes of this investigation which is beyond the scope of this thesis.

4.1.2 ORR performance in O_2 purged cathode in $HClO_4$ and H_2SO_4

The polarization curve and Tafel plot during ORR determined in oxygen via SGEIS technique with forward and a backward scan was showing the typical redox behaviour of electrocatalyst in O_2 in Figure 4.4 and Figure 4.5. The samples were tested with and without membrane in both $HClO_4$ and H_2SO_4. The activity was compared with literature to analyze the effect of a bonded membrane to ORR activity. In Figure 4.4, it is revealed that the Pt/C in $HClO_4$ approached to high current density of 2 A/cm^2 from 0.607-0.633 V_{RHE}. At 0.66 V_{RHE} and 1.5 A/cm^2, both polarization curves of Pt/C with and without membrane showed a similar trend. Later then the divergence appears in polarization curves with a difference of $\simeq$26 mV. However, both samples exhibited the same onset and half-wave potential onset (E_{onset} 0.871 V_{RHE}, $E_{1/2}$ 0.706 V_{RHE}). The difference can be regarded as flooding at the catalyst surface, which can be minimized with more additional potential cycles. In comparison to other GDE study, the results agree with other researchers [15, 215]. It was already perceived to see the different behaviour of catalyst coated membrane and GDE, as GDE is interfaced directly to the bulk electrolyte solution with the produced water to went back to the solution while CCM acted as a barrier for water transport. The Pt/C in H_2SO_4 with and without membrane showed less performance with more negative onset as compared to $HClO_4$.

The sample without membrane approached to more positive onset as compared to sample with membrane

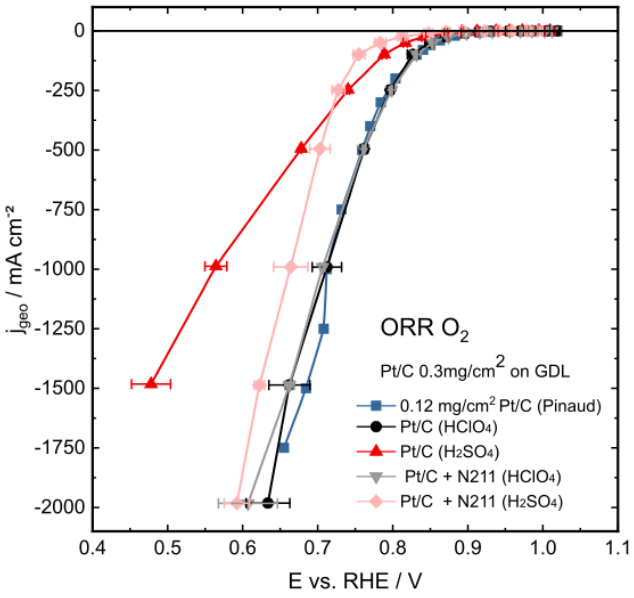

Figure 4.4: Polarization curve of commercial Pt/C for ORR in O_2 obtained via SGEIS

and thus to require low activation energy which makes sense that the membrane can add additional resistance that could lead to losses. However, approaches to the high current density the sample without membrane showed a proximate increase in degradation and approached to limiting current of 1.5 A/cm^2 at 0.477 V_{RHE}.

Due to the direct contact to the bulk electrolyte, there is a possibility of sulfate ions positioning and blocking the active sites of catalyst as H_2SO_4 is a harsh acid with high concentration 1.0 M used in this study. With the membrane, the Pt/C required high activation energy, but the performance was batter and approachable to high performing Pt/C in $HClO_4$. The sample approached the current density of 2 A/cm^2 at 0.59 V_{RHE}. The better performance is due to the restriction imposed by membrane for sulfate ions to deposit on the active sites of catalyst as compared to sample without membrane interfacing directly to the bulk electrolyte. The degradation of catalyst in H_2SO_4 can also be mitigated by higher temperatures, as approaching to high current densities, which can weaken the specific adsorption of SO_4^{-2} ions and this would be another research to determine the effect. In the 1.0 M concentration of electrolyte (both $HClO_4$ and H_2SO_4), it was expected to achieve a high current density due to enough H^+ transport, as compared to the test done in RDE in the literature previously [212]. It demonstrates that transport will not be a limiting factor for our GDE catalyst. However, if the activity will be decreasing for a high concentration of electrolyte, the catalyst layer will be subjected to the poising due to more impurities.

In O_2, the achieved Tafel slope shown for all samples (Figure 4.5, as Pt/C exhibited the same activity with and without membrane, their slope is similar. In the low current density region of 1 µA/cm$^2_{Pt}$ to 1 mA/cm$^2_{Pt}$, the Tafel slope of 47.9 mV/dec is achieved. The higher slope of 84.43 mV/dec is achieved

in the high current density region over 10 mA/cm^2 in the range of 0.8-0.7 V_{RHE} with mass transport limitation stating 0.7 V_{RHE}. As due to consistency of Tafel slop for Pt/C in $HClO_4$ in high and low current density region, the mass transport effects are at a minimum level, the transition between high and low current density region occurs in the range of 0.75-0.8 V_{RHE}. As the same behaviour in the polarization curve, the Pt/C in H_2SO_4 with and without membrane was more prone to degradation. The sample without membrane achieved the Tafel slope of 59.24 mV/dec in the low current density region while 93.98 mV/dec in the high current density region with transport limitation started at 0.75 V_{RHE}. Pt/C with membrane achieved the Tafel slope of 60.06 mV/dec in low current density regions, and 86.48 mV/dec in high current density region transport limitation started at $\simeq$0.7 V_{RHE}.

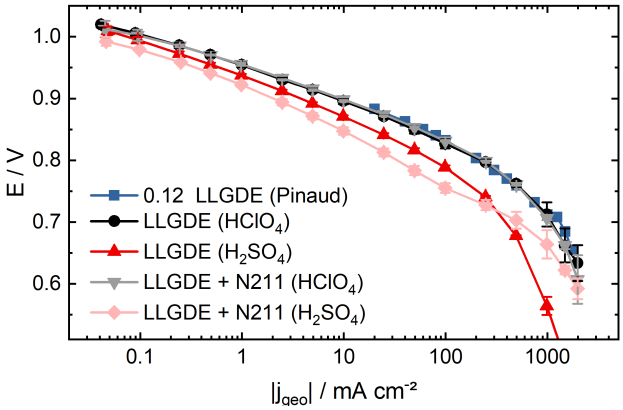

Figure 4.5: Tafel commercial Pt/C for ORR in O_2 obtained via SGEIS (current is normalize to geometric area)

The effect of the membrane cannot be neglected, the reason if the material of membrane, i.e. Nafion™, which belongs to the sulfonic acid group and chemical closer to sulfuric acid. It shows that there is a significant variation in results for different electrolytes.

The GDL without membrane showed better performance as compared to their counterpart with membrane because the resistivity of the membrane causing a thick barrier of produced water and not be able to push back to the bulk electrolyte as CVs were conducted without the gas purged from the cathode which limits the water management system in the cell. The samples in H_2SO_4 were not able to cope up to the $HClO_4$; the performance can relate in the variation of Tafel slope to overpotential. In the previous literature for Pt single catalyst performance in sulfuric acid, the crystal surface is more subject to high sulfate anion adsorption [235] which could be the reason for the less performance of directly interface Pt/C in H_2SO_4 without membrane. Another reason that can be perceived based on the observations that the absorbed anion species such as chlorine and sulfate ions from $HClO_4$ and H_2SO_4 can significantly impact the deterioration of catalyst stability which is more severe for sulfate ions. The kinetic effect of catalyst will enhance more peroxide production with the possibility of influence on membranes (especially perfluorinated membranes) which usually degrades in the presence of radical ions [236, 237]. Previous

kinetics studies of Pt and alloys showed that the activities in $HClO_4$ are higher than H_2SO_4 which also happens in our case [238]. Typically, it can be assumed that sulfate anions adsorption of Pt/C surface has detrimental effects; it inhibits the reduction of oxides by blocking the active sites. To some extent, the membranes are also prone to degradation has some positive effect by blocking the anions, and also it does not affect the reaction pathway. Moreover, single-crystal studies could be more helpful to analyze the effect, as it has been studied previously that different facets and geometry of Pt has a tendency to adsorb selective anions such as (100) is more active towards ORR in H_2SO_4 while tetrahedral (111) facts are more catalytic active for ORR in $HClO_4$. However, it is still challenging to understand the behaviour of chemisorb sulfate ions, causing detrimental effect, and yet several other advance studies can be done to investigate it thoroughly. GDE gives an estimate of ORR performance of catalyst layer with and without membrane and can give results nearly to same of fuel cell catalyst benchmarking methods.

4.1.3 ORR performance degradation in synthetic air back purged GDL in different electrolytes for PEMFC in GDE

During air purging for ORR performance instead of oxygen, the performance drops drastically and even reaches to mass transport losses. The same catalyst was not able to approach the current density of $\simeq$2 A/cm^2 as it has been seen before for ORR in oxygen in the previous section. The reason for the low performance is the less concentration of oxygen at the electrode-electrolyte interface.

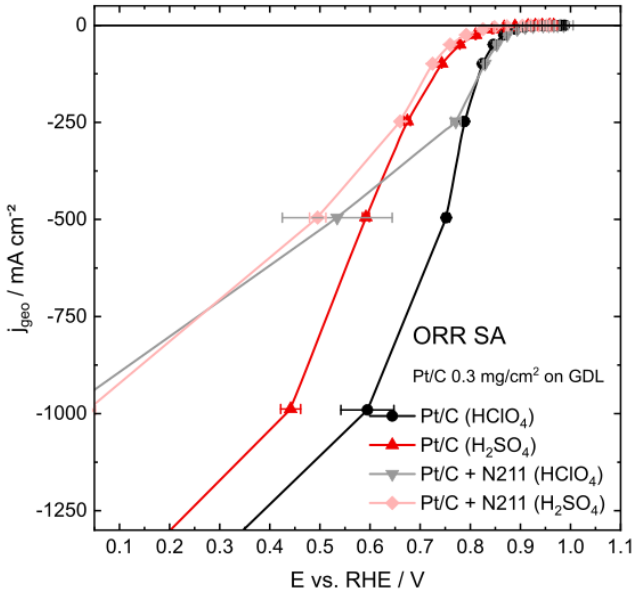

Figure 4.6: Polarization curve of commercial Pt/C in ORR for synthetic air

In comparison to ORR in H_2SO_4, the sample in $HClO_4$ with and without membrane showed similar performance till 0.7 V_{RHE} at 247 mA/cm^2 . Nevertheless, the performance difference exceeds to a

certain level that sample with membrane approached to mass transport limitation at ≃900 mA/cm^2 and sample without membrane approach to transport limitation at the current density of 1250 mA/cm^2 at 0.35 V_{RHE}. The activity of Pt/C in H_2SO_4 with/without a membrane is lower than $HClO_4$. The onset of Pt/C in H_2SO_4 is 0.84 V_{RHE} as compared to onset in $HClO_4$ which is 0.89 V_{RHE} showing that high activation energy is needed for Pt/C in H_2SO_4 to achieve high current density. The Pt/C without membrane approach to limiting mass transport at 0.2 V_{RHE} at 1.25 A/cm^2 with a difference of 15 mV and the difference is more or less similar in high current density region. The Pt/C with the membrane was impacted by severe mass transport limitation at ≃1.0 A/cm^2, and all the degradation that happened for all samples were in ohmic loss region. The transport limitation can also be seen in Tafel plot in Figure 4.7 where the current normalized to geometric area is plotted against potential , the OCV of Pt/C are nearly to ≃0.986 V_{RHE} for Pt/C (with and without membrane) in $HClO_4$ and ≃0.96 V_{RHE} in H_2SO_4 (withmembrane) which are lower than the literature CV values for PEMFC H_2/O_2 fuel cell(≃1.23 V_{RHE}) [239]. Near to theoretical value which is not approachable in a half cell as no external hydrogen provided and no possibility of platinum dissolution which usually observed to highest from OCV operation [240].

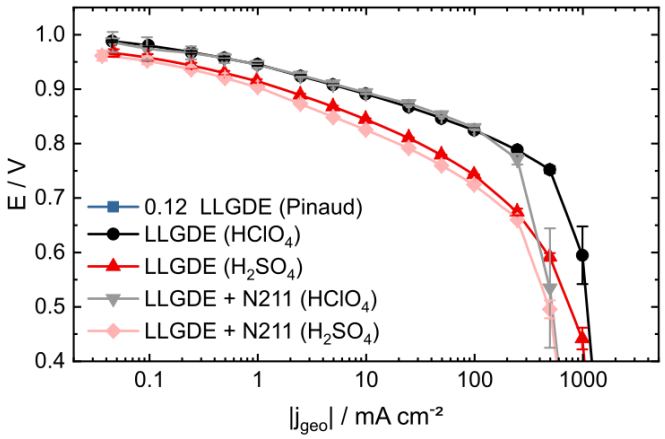

Figure 4.7: Tafel Plot commercial Pt/C in ORR for synthetic air

The Tafel slopes of same Pt/C catalyst in the different electrolyte is not similar, considering the Tafel plot of Pt/C in $HClO_4$ with a slope of 0.57 mV/dec in the range of 0.97-0.8 V_{RHE} in low current density region which is in agreement with Ehelebe et al. [241] for the same experiment done before in GDE half-cell. The comparability of both samples with/without a membrane is similar, but the mass transport limitation occurs at 0.77 V_{RHE} with Tafel slope of ≃152 mV/dec facing severe degradation inactivity for the sample with membrane. The Tafel slope of Pt/C in H_2SO_4 at low current density region from 0.97-0.8 V_{RHE} is 65.53 mV/dec which becomes higher (≃121 mV/dec) at high current density region from 0.75 V_{RHE}. In order to look deep into the difference in activities, several reasons could have a different impact

on performance. The first reason is the oxygen starvation as the concentration of oxygen in synthetic air is less than pure 99.99% O_2 which was used for ORR in O_2 previously and had better catalytic activity. Oxygen starvation is not a new phenomenon and widely studied before by other researchers for PEMFC [242–244]. It can lead to issues like voltage reversal, non-homogeneous degradation of fuel cell and current distribution [169, 242]. The most losses occur in this investigation are ohmic and slow gas diffusion cathode. In order to avoid the slow gas diffusion, when the air was an oxidant at the cathode, the flow rate of air was kept higher 375 ml/min as compared to oxygen 250 ml/min in GDE cell. The impedance at low current density also performed in this work which significantly showed fewer losses and stability in that region. However, in low current density region, the rate-determining process is charge transfer which is already known with a better understanding of mass transport limitations [245]. There are other parameters related to low performance such as the GDE works at high current densities as compared to RDE with humidified gases that can generate excess water at the cathode. Now, GDL, which is highly porous, can be affected by the water accumulated on the pores which would block the adequate pore size for gasses to pass through. It can be predicted that oxidant might not be enough to attain maximum current density till $\simeq$2 A/cm^2 that can lead the process of proton reduction to be taken place in the cathode outlet area resulting voltage loss to negative. This reversal phenomenon [246] can be controlled by adjusting the stoichiometric ratio of oxidants mainly air which can be related to high current density [**?**]. In order to improve the mass transfer at high current density, the high driving force will be needed, the optimization of GDE structural parameters will be helpful to mitigate the mass transport resistances along with the current distribution across cathode is sensitive to air stoichiometry [247]. The current distribution is heterogeneous for air as compared to pure oxygen which tends to be more homogeneous. With oxygen the current is distributed across the channel is dominated by oxygen gradient resulting in high current density at the inlet of cathode while for air, the oxygen concentration gradient is higher and resulting in more possibility of oxygen starvation. The performance of the catalyst with the membrane in each electrolyte was low, which shows the hindrances in mass transport. The GDE with membrane can be affected by the resistances in all regions of polarization (activation, ohmic and mass transport). This resistance is related to the electronic resistance imposing by a membrane that can affect the porous clusters of GDL and resulting in less diffusion of oxidant, which is already starved by air purging. Although the membranes are essential for effective water management, it requires cathode to be highly permeable with itself restricting gas permeability. If water management is poorly designed, which is affected by the low availability of reactants to the hydrophobicity of the electrode, there will be more gas diffusion losses. With all these results in the light of hypothesis and critical parameters, the understanding of gas diffusion layer and its behaviour to various oxidants in the fuel cell is still in question along with oxidant starvation and water accumulation issues.

4.1.4 Variation in ORR activity for forward and backward scan in oxygen purged cathode during polarization

The impedance spectroscopy was carried out with forwarding and backward scan, and most of the times, especially for ORR in SA, the resulting polarization of both scans are not similar. In the Figure 4.8, an example of Pt/C in SA ORR is given with the significant difference in polarization curves for both scans with hysteresis. This difference is assumed to be directly related to the humidification of gases and water management. Since it can be seen that a forward scan is leading to low current densities as compared to backward scan. As approaching to high current densities in the forward scan, the water is generated to a certain extent causing flooding at the cathode, but due to high humidification of the cathode at the back sweep, the more positive can be observed in back sweep [60].

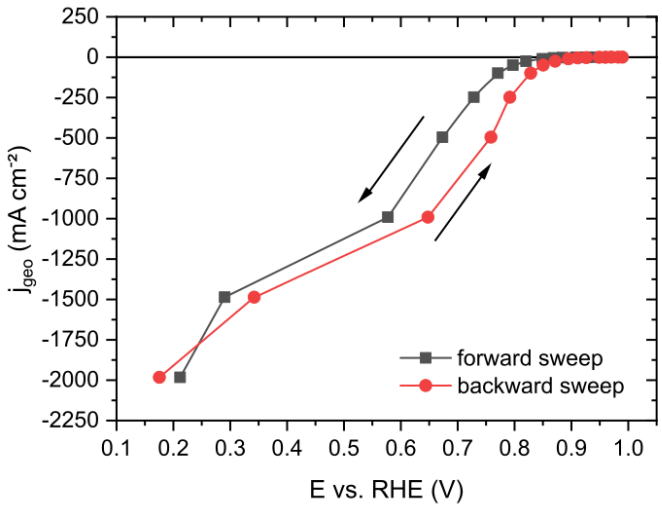

Figure 4.8: Impact of forward and backward scan on polarization

Despite of the difference, the concave of curves in both scan types is nearly similar at high current densities. There are some other explanations given for the difference in forward and reserves scan that the catalyst performance in both scans can differ due to reduction time on peroxide generation. At 100% relative humidity, the hydrogen peroxide generation will be higher if there is longer reduction time. Nevertheless, in all experiments, this is not the only factor that affects the performance at cathodic and anodic scans such as temperature, scan rate, humidity and rate of diffusion is also a complex function for reduction time [248]. However, it is believable that the intermediates produced during the forward sweep will be different from the backward sweep (typical scan direction) for voltammograms and impedance spectra [249]. As the potential waveform is similar, so both forward and reverse scan should be similar. The presence of oxygenated species covering the catalyst surface can block the active sites in forwarding scan leading to a deviation with the back scan polarization curve [60, 250]. This issue is still challenging

to minimize the difference between both scan rates by effective water management and improving the catalyst structural properties. However, the hysteresis of forward and backward is still unclear, and the difference is usually caused by rate-determining step, and the question remains that either the cathodic or anodic sweep are relatable. Therefore, in this work, the average value of cathodic and anodic sweeps was taken into account, but if there is a difference of more than 20 mV, the conventional back sweep polarization curve was preferred for consideration.

4.1.5 Activity of commercial Pt /C catalyst in alkaline media for AEMFC in GDE half-cell setup

Due to the corrosive nature of the acidic electrolyte, the alkaline and neutral electrolytes research is a widely investigated topic in past years. Alkaline electrolyte grabbed significant attention due to the beneficial properties of the stable environment while imposing the problems of membranes stability. In most of the cases, non PGM electrolyte was preferred for alkaline electrolyte research. Despite state-of-the-art Pt catalyst outstanding performance in the acid electrolyte, it is yet not well reported for the alkaline electrolyte. Although, acid electrolyte research was supported both theoretically and experimentally through Sabatier volcano relationships that describes that surface binding is the primary descriptor for the activity of electrocatalyst. Still, there is a gap for the descriptor of ORR performance in alkaline with platinum as an electrocatalyst. The CVs of platinum in alkaline Figure 4.9 gives different features as compared to CVs in acid (See Figure 4.3), especially in H*upd* region, the peaks of hydrogen adsorption occupy the different onset potential is approaching to a contracted double layer region.

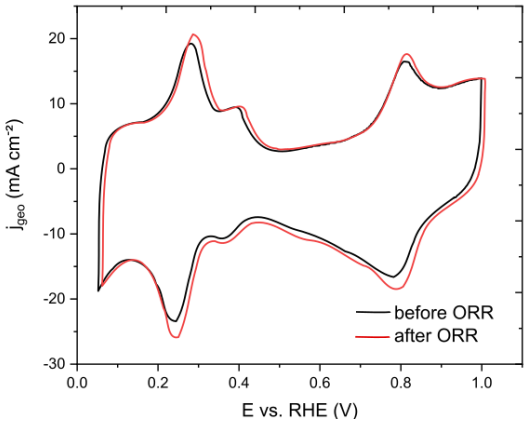

Figure 4.9: Pt/C Cyclic voltammogram before and after ORR in O_2 with no severe difference

The typical CVs of Pt/C in alkaline (KOH) agrees with the literature which comprises of three regions underpotential deposition, double layer region and Pt oxidation region [251]. The voltammograms were recorded at the scan rate of 100 mV/sec, and no significant degradation observed before and after ORR steps. In the underpotential deposition regions, the peaks between 0.25-0.4 V_{RHE} attributed to the in-

teractive sites of Pt(110) and Pt(100). It is a crucial region due to anions adsorption on the surface from the electrolyte. The position of peaks for their relative surface plane is similar to the single-crystal Pt in alkaline media, and due to the minor shift after ORR towards more positive onset, it can be assumed that some inhabitation effect occurred by blocked sites [252, 253]. By integrating the H*upd*, the determined ECSA was found to be 72 m^2/g_{pt} which is slightly higher than the available surface area in literature i.e. 62 m^2/g_{pt}.

The high surface area could be possible by some interference of Pt oxide reduction, which can be restricted by limiting the positive potential window. Similarly, the double-layer region also observed the similar high currents originated from the capacitive nature of highly porous and conductive catalyst support (Carbon). The Pt-oxide region in alkaline is very similar to that of acid electrolyte from 0.6 V_{RHE} to on-wards expecting the bulge in back sweep shifting to more positive potential than in acid. The KOH has the ability to absorb oxidized species in an irreversible way on the Pt surface which is usually dissolved in acid, but it is yet to explore more the relation of binding energy as a descriptor of performance in alkaline media for ORR.

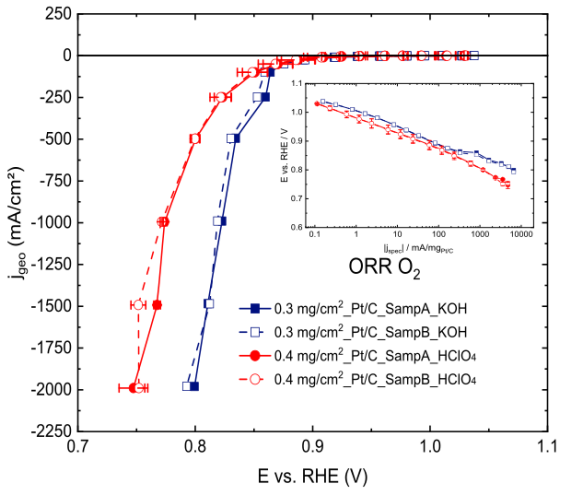

Figure 4.10: Pt/C polarization curve and Tafel plot for activity investigation in KOH electrolyte

The ORR conducted in $HClO_4$ and KOH with a similar catalyst is shown in Figure 4.10 and there is a significant comparison. It is well known that ORR in acid electrolyte for Pt/C catalyst with relatively high performance in Fe-N-C but ORR in alkaline electrolyte for Pt/C in AEMFC is still yet to explore fully. Due to the versatility of GDE, the commercial Pt/C HISPEC-4000 was investigated at high current densities. The catalyst in KOH exhibited very high activity of approaching to 2 A/cm^2 at 0.799 V_{RHE} with a high onset value of 0.88 V_{RHE}. In alkaline solution, the reaction needed less activation energy approaching to high current density. While approaching to 2 A/cm^2, the activity was changing linearly with a different of 10-20 mV from 500-2000 mA/cm^2. The same behaviour was observed in the second

sample; therefore, the reproducibility of GDE for this experiment can be observed.

In comparison to ORR in $HClO_4$, the catalyst exhibited lower activity in acid approaching to 2 A/cm^2 at 0.751 V_{RHE} with the similar onset and results in $HClO_4$ agree with previous literature. The activities deviation for ORR started at high current densities from 100 mA/cm^2 up to 2 A/cm^2 with an increasing difference of 20-40 mV. Even though the activity of Pt/C in alkaline is relatively high than the latest research approaching to 0.73 V_{RHE} at 2 A/cm^2, the results in GDE are not conclusive. In the Tafel plot Figure 4.10, it can be observed that the activation losses are shallow as compared to Pt/C in $HClO_4$ and no server mass transport limitation is observed. The difference in Tafel plots for $HClO_4$ and KOH can be due to the water management issue or overestimation of the date at high current density region.

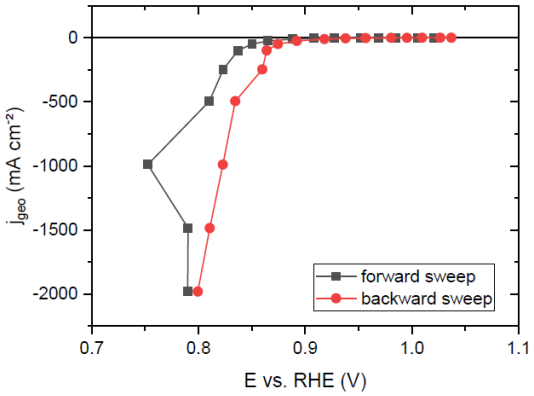

Figure 4.11: Backward and forward sweep defence in activity for Pt/C in alkaline that can lead to overestimated errors

It can be observed that there is a possibility of overestimation through data correction and processing or some unseen mass transport issues. This issue has been already addressed by Pinaud et al. [215] that over-correction can lead to overestimated results and this is more crucial due to two factors such as temperature variation causing changes in resistance and iR correction at high currents. Also, in previous research, it has been stated that the stability of Pt/C in alkaline is fragile and aggressive, resulting in low activity and loss of ECSA after several degradation cycles [254]. Therefore, the high performing results are due to overestimation and correction of Nyquist plot which can be studied further to optimize the protocol for Pt/C in alkaline.

Hypothetically, 1% of the error can deviate the polarization curve to 25 mV to a positive or negative direction. Also, it can be seen in the Figure 4.11, the difference in forward and backward scan is very uncertain, although the commercial catalyst usually contains Nafion™ which is proved to be valid for water management and transport issues [32], there is more information yet to explore. Significantly, most of the experiments for AEMFC were carried out with non PGM catalyst which is preferred over Pt/C due to more stability, low cost and versatile applications [196, 255].

4.2 Advanced Pt/HGS catalyst

The state-of-the-art platinum electrocatalyst usually supported on carbon for maximum exposure to active sites. However, due to the harsh conditions at the PEMFC cathode, the performance of electrocatalyst is unstable during fuel cell operations mainly due to degradation mechanism during cycling. Platinum is still considered as the state of the art electrocatalyst for PEMFC, the other factors that can influence the catalyst performance are the support of catalyst since the significant issues such as detachment, agglomeration, Ostwald ripening and support corrosion are related to surface. Therefore, the optimization of catalyst support is one of the critical targets for electrocatalyst to improve performance. Encapsulation of catalyst nanoparticles in mesoporous structures and nanostructure of support is a proven method to enhance the stability of the catalyst. Over the past years, the carbon support was studied for nanostructuring the carbon material into shells, nanotubes and templates having benefits of catalyst utilization, stability and durability. There are quite a few studies of the influence of fuel cell startup, accelerated cycling to the activity of the catalyst in nanostructured mesoporous support. In this work, an advanced Pt/C catalyst on hollow graphite spheres (HGS) developed by Galeano et al. [256] was studied that has particular mesoporous structure synthesized from graphitizing carbon with high conductivity and porosity. The HGS has unique features of high surface area (>1000 m^2/g), interconnected pores and high order of graphitization which plays a crucial role to tackle catalyst particles agglomeration and detachment issues in PEMFC cell [257]. The porous structure and cavities provide separation and trapping of catalyst nanoparticles with maximum accessibility. Due to the mesoporous network, the diffusion pathways are very selectable and short from the graphite sphere shells resulting from the voids. As the carbon corrosion is an issue for catalyst support, the carbon is graphitized to the support a 3D structural network with a high surface area that gives an advantage of inter-particle distance [256, 258, 259].

The distribution of Pt nanoparticles has a more considerable influence on performance which can be optimized during the synthesis stage by suppressing the degradation pathways for ORR (such as agglomeration and detachment) by changing the degree of graphitization. In order to achieve highly porous HGS structure and encapsulating the Pt nanoparticles, "Confined space allowing" which is an advanced version of impregnation-reduction proved to be newly developed technique that prevents the sintering of nanoparticles and makes it more viable at high-temperature [260]. The particles are separated in the mesoporous structure also helps in reducing the possibility of sintering. However, it is imperative to take control of temperature, as, during the synthesis, the high-temperature annealing increases the effect of the carbon layer covering the active sites by blocking the catalyst surface.

Due to the pore confinement approach through spatial distribution, the catalyst degradation pathways can be suppressed, such as agglomeration and particle detachments. The morphological changes of the mesoporous structure of HGS have been studied in RDE and single fuel cell [256, 261]. As the prepa-

ration of Pt/HGS requires high temperature, the confinement can impose different properties during electrochemical measurements due to surface morphology and exposure to the active site of encapsulated catalyst.

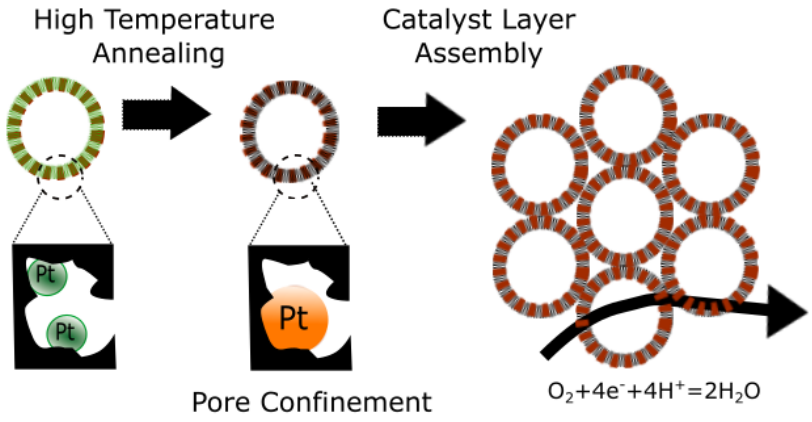

Figure 4.12: Pore confinement of Pt nanoparticles in hallow graphite spheres .Reprinted with permission from [256], Copyrights 2012 American Chemical Society

4.2.1 Impact of stress cycling on the activity enhancement of Pt/HGS

In this work, the effects of break-in procedure and AST cycles were carried out in GDE half-cell to investigate the highest possible activity of Pt/HGS in 1.0 M $HClO_4$. The approach is to get a state to achieve maximum activation through intense cycling by applying positive potential from 0.6-1.0 V_{RHE}. The cycling can help to detach the excess carbon layer covering the active sites of sintered Pt nanoparticles and helps in providing better accessibility for the reaction. The AST protocol was modified with the number of cycling for ECSA after specific degradation cycles at room temperature with a scan rate of 1.0 V/sec. In fuel cell, the testing for degradation that will last for several days is merely hard to achieve, which limits us to operate the cycling at faster scan rates for enduring and reliable assessment. The performance of catalyst activation through cycling was analyzed by H*upd* method in Ar saturated environment and the ECSA was determined before and after cycling for 2500, 5000, 1000 and 30000 potential cycles. Even though the periodic evaluation through H*upd* method could impose artefacts and more prone to degradation but at the end of life the electrocatalyst can be compared to the state of the art catalyst or more samples testing for reproducible results. The content of Pt is directly related to the surface area and more active sites exposure [262], so the loading of catalyst can also play an important which will be discussed later. However, GDE half-cell measurement is vital for catalyst layer evaluation and initial screening of catalyst, therefore, it is desirable to test all the catalyst at similar standard condi-

tions. The identical conditions will give a better understanding of the collection of kinetic data as well as durability studies. The performance in GDE half-cell can vary from the realistic fuel cell measurements due to degradation test at the standard temperature as the electrocatalyst performance can be provoked at high temperature [171]. Also, at higher scan rates, the performance can be overestimated by the number of platinum oxides formation [263]. In the lab investigations done previously (not published), it has been found that Pt/HGS requires ageing (10,000 cycles) to reach it maximum potential activity and it will show better performance in PEMFC due to high oxygen diffusion through the mesoporous structure. Most of the degradation and ageing test of platinum and carbon corrosion were carried out in MEA with simulated startup and break-in procedures. Under simulated load-cycling conditions, the main observed degradation mechanism changes to particle migration and coalescence and these stubble mechanisms cannot be adequately identified in MEA and therefore opens an area for GDE half-cell to investigate the most active state of Pt/HGS for PEMFC.

In order to understand the effect of ageing and the catalyst loading impact on the ORR performance, samples with loading 0.04 mg_{Pt}/cm^2 and 0.1 mg_{Pt}/cm^2 were prepared, and the test has been done twice to check the reproducibility of results. The samples were aged through cycling, and the polarization ORR curve and Tafel plot was constructed from the data of SGEIS. The non-activated samples demonstrate that the initial activity of Pt/HGS can be seen in Figure 4.13, where solid lines represent the sample with different loading, and dotted lines represent that additional testing for reproducible results.

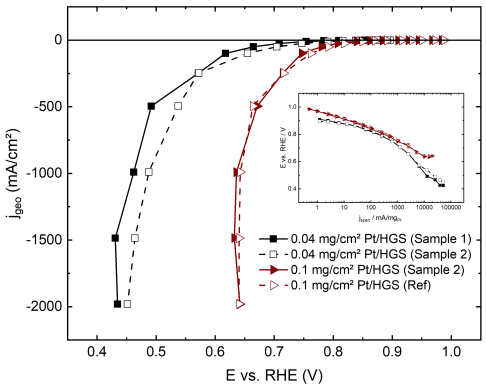

Figure 4.13: Polarization curve and Tafel plot showing ORR performance of non-activated samples in 1.0 M $HClO_4$ for Pt/HGS

The impact of loading of state-of-the-art Pt/C has been extensively studied by various researchers that showed that the ORR performance is also dependent on optimal catalyst loading. It can be seen in polarization curve Figure 4.13 that sample with higher loading of 0.1 mg_{Pt}/cm^2 approached the current density of 2 A/cm^2 at 0.65 V_{RHE} with almost the same half-wave potential and onset potential of 0.75 V_{RHE}. The second sample of the same loading exhibited the exactly similar trend. The sample with

low loading of 0.04 mg_{Pt}/cm^2 approached the limited current density of ≃0.45 V_{RHE} (average) at the limiting current density of 2A/cm^2. The onset potential of this sample was meagre compared to higher loading sample with E_{onset} ≃0.6 V_{RHE}. Therefore, low loading sample exhibited higher activation losses. The difference of activities in both samples is less at low current densities while it is broadening as the polarization approaches to limiting current density with a difference of ≃20 mV, the trend is also similar to the catalyst investigation for Pt/C catalyst in GDE half-cell. The OCV of higher and lower Pt loading ranges from ≃0.9-1.0 V_{RHE}. The OCV of lower loading is slightly lower than the practical OCV value of commercial fuel cell which can be possible through increasingly electrical conductivity across the catalyst layer or some losses in the circuit and kinetic loss at cathode due to low loading [264]. The different loadings exhibited different performances but with the reproducible results and the difference in the specific activity of the same catalyst could be affected by mass transport and flooding of voids in catalyst support. Although GDE method significantly investigate the catalyst performance, certain issues are still yet to be addressed, such as water transport mechanism. The Tafel plot for non-activated samples of low loading Pt/HGS (0.04 mg_{Pt}/cm^2), higher Tafel slope of 58.59 mV/dec in the potential range of 1.0-0.7 V_{RHE} was achieved in low current density region (2.446-24.7 mA/cm^2) and 152.15 mV/dec in high current density region with potential over 0.6 V_{RHE}. There is a gradient in the slope from mass transport region over 0.6V V_{RHE}, which shows that losses are higher for low loading Pt/HGS. The Tafel plot of higher loading Pt/HGS (0.1 mg_{Pt}/cm^2) can also be seen in Figure 4.13, Tafel slop 64.56 mV/dec has been found out in low current density region from 24.69-246.97 mA/cm^2 in the potential range of 1-0.7 V_{RHE}. However, the sample exhibit more or less similar activity with a Tafel slope of 93.65 mV/dec while there has not been much difference between both samples with reproducible results showing that higher same loading will exhibit better performance. The different loadings exhibited different performances but with the reproducible results and the difference in the specific activity of the same catalyst could be affected by mass transport and flooding of voids in catalyst support. Although GDE method significantly investigate the catalyst performance, certain issues are still yet to be addressed, such as water transport mechanism. The Tafel plot for non-activated samples is shown in Figure 4.13 for low loading Pt/HGS (0.04 mg_{Pt}/cm^2), higher Tafel slope of 58.59 mV/dec in the potential range of 1.0-0.7 V_{RHE} was achieved in low current density region (2.446-24.7 mA/cm^2) and 152.15 mV/dec in high current density region with potential over 0.6 V_{RHE}. There is a gradient in the slope from mass transport region over 0.6 V_{RHE}, which shows that losses are higher for low loading Pt/HGS. The Tafel plot of higher loading Pt/HGS (0.1 mg_{Pt}/cm^2) can also be seen in Figure 4.13 with slope of 64.56 mV/dec has been found out in low current density region from 24.69-246.97 mA/cm^2 in the potential range of 1-0.7 V_{RHE}. The sample exhibit more or less similar activity with a Tafel slope of 93.65 mV/dec; however, there is not much difference between both samples showing that higher loading exhibited better performance with reproducible results..

4.2.2 Validation of performance optimization by continuous potential cycling

The most active state of the Pt/HGS for ORR in O_2 was subjected to several break-in procedures and continuous potential cycles till 30,000 cycles with an interval at 10000^{th} cycle. The study confirms the most active state for Pt/HGS by samples provider which quoted that "Pt/HGS reaches to the most active state at 10,000 potential cycles". In the previous research, the idea was given that the surface area of catalyst increases by degradation cycles [257]. This indication gives an idea about the encapsulated structures are being blocked or restricted. The blocked voids can affect the entrapped catalyst nanoparticles, and therefore, the catalyst will require more activation. The main reason of blockage is the carbon as support which can also cover the catalyst surface. The activation can be achieved either by burning the carbon deposited over the catalyst surface through thermal treatments or to oxidize the carbon in the proximity of catalyst nanoparticle, which is blocking the pores. The burning approach is not appropriate; it will emit some byproducts such as CO and CO_2; thus, the oxidation in the electrochemical system is more appropriate and viable. The oxidation of deposited carbon over the Pt nanoparticles surface is done by potential sweeping which helps to improve accessibility and also wettability of channels in mesoporous structures eventually results in increasing access to the catalyst nanoparticles. In comparison to other catalyst support such as Vulcan for Pt nanoparticles, Pt/HGS demonstrated better stability with negligible losses and no agglomeration and even after degradation test, Vulcan support proved to be more vulnerable with particles loss of more than half of the original catalyst [256]. Most importantly, there are several limitations when it comes to the catalyst by design approach with new support that can sustain the minimum amount of catalyst within the complex 3D catalyst layer and absence of these 3D structures in RDE films can also lead to degradation mechanism with possibility of misleading interpretation [265].

To see the activity enhancement, the sample with loading 0.04 mg_{Pt}/cm^2 was investigated and it can be seen that sample is subjected for ORR at 10,000 and 30,000 cycles and compared with state of the Pt/C with loading 0.041 mg_{Pt}/cm^2 in GDE half-cell. There is a uniform trend with potential loss as approaching to high current density region. Initially, the Pt/HGS after catalyst cleaning cycles ($\simeq$50) before AST cycling, the sample approached to limiting current density of 2 A/cm^2 at the potential of 0.451 V_{RHE} and onset potential of 0.79 V_{RHE} (see Figure 4.14). The activation losses are higher as the OCV for Pt/HGS was 0.89 V_{RHE} which is lower than the standard OCV value for H_2/O_2 fuel cell. In comparison to state-of-the-art Pt/C, the difference in activity of catalyst with limiting current density of 2 A/cm^2 is 100 mV. However, this difference is lower than the activity difference at the half-wave potential value, which is 180 mV. During 10000 cycles, the activity of the catalyst was enhanced greatly from 0.45 V_{RHE} to 0.51 V_{RHE} at the current density of 2 A/cm^2. The OCV value was highest to 0.93 V_{RHE} approaching near to theoretical values.

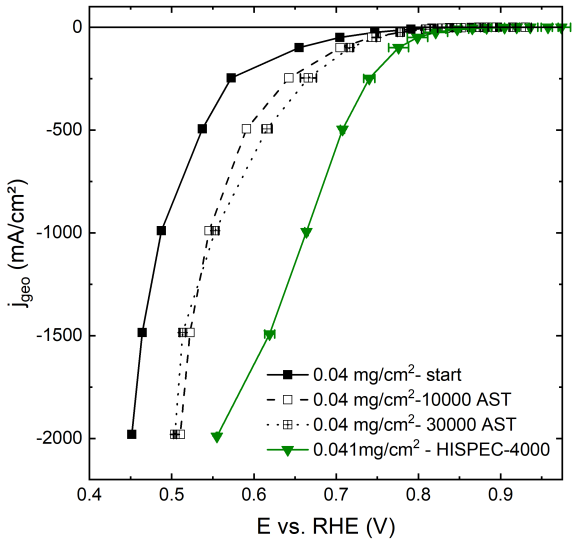

Figure 4.14: Low loading Pt/HGS performance enhancement by 10- 30k stress cycles in $HClO_4$

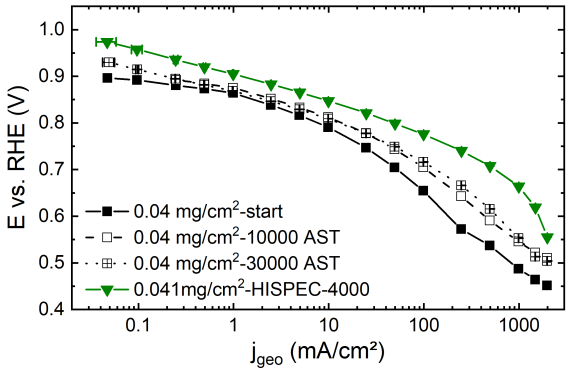

Figure 4.15: Tafel Plot of Pt/HGS with 0.04 mg_{Pt}/cm^2 loading in comparison with commercial HISPEC-4000 Pt/C

In comparison to the commercial state of the art Pt/C with almost similar loading 0.4 mg_{Pt}/cm^2, the catalytic performance of highly active Pt/HGS is still not approachable. However, in term of mass transport, it can be seen in the Figure 4.15, the losses are higher for the respective catalyst at the high current density region from 1 A/cm^2 to 2 A/cm^2 with almost 110 mV loss for commercial Pt/C and 50mV for Pt/HGS. Despite the less initial catalytic performance of Pt/HGS, it is much stable with good mass transport during the potential cycling of 10000 cycles. Researchers also confirm this stability of Pt/HGS during cycling that Pt/HGS is subjected to fewer losses during degradation cycles [257,266]. The catalyst is then subjected to a total of 30000 cycles and approached the 0.50 V_{RHE} at 2 A/cm^2. Initially, the ORR performance of catalyst at low current density region reduced to $\simeq$10-20 mV from the activity of 10000 cycles, but as it proceeds to high current density region, the performance improved with almost similar activity to the most active state. The sample initially exhibits a slope of 44 mV/dec at low current

density region (>0.6 V_{RHE}) in Figure 4.15, but as it approaches high current density region with a slope of 157.579 mV/dec, the catalytic performance degrades in the region <0.6 V_{RHE}. The specific activity of the most active state of catalyst at ≃0.89 VV_{RHE} is 0.49 mA/cm^2 which is comparable to literature(0.47 mA/cm^2 at 0.9 V_{RHE}) [256]. The support design approach of the catalyst by encapsulating into voids is beneficial for stabilizing and retaining the performance, but it requires prior activation. Due to the voids, the Pt nanoparticles do not suffer from the possible degradation mechanism such as detachment and agglomeration because of suppression of accessibility to catalyst particles. This indicates that support is affecting not only the activity of catalyst but also accessibility of electrolyte to the nanoparticles imposing no limitations despite the confined particles.

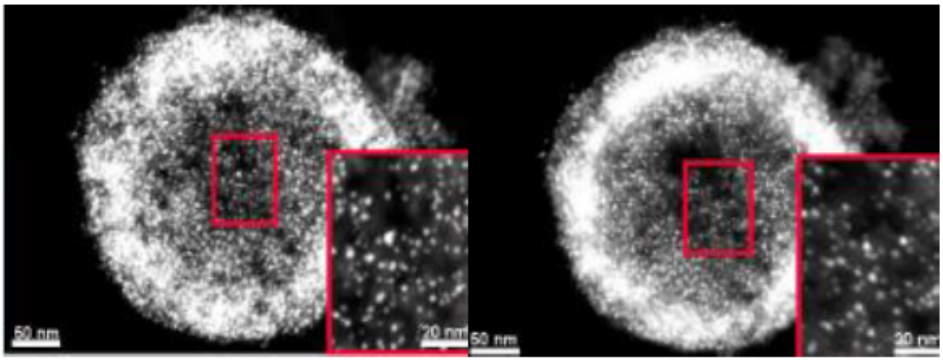

Figure 4.16: Pt/HGS surface morphology changes during cycling. Reprinted from [257]

The Pt/HGS prepared with high loading of 0.1 mg_{Pt}/cm^2 through spray coating was investigated for activation and compared with state of art Pt/C catalyst and low loading (0.04 mg_{Pt}/cm^2). The procedure for activation was similar, as described earlier. Initially, the catalyst without activation achieved the activity of 0.63 V_{RHE} at the current density of 2 A/cm^2. However, the onset of the polarization curve was approached to ≃0.8 V_{RHE} showing that high activation is required. In comparison to the state-of-the-art Pt/C, the difference in activity is 40 mV. It can also be seen from Figure 4.17 that at the half-wave potential, the activity of the non-activated catalyst is 10 mV higher than the potential at limiting current density. This shows that high loading sample is prone to little structural changes as thicker catalyst layer can impose the transport hindrance of gases and water within the catalyst layer. After subjecting to 10,000 cycles, the catalyst performance was enhanced a little in the region of 0.64-0.68 V_{RHE} but approaching to limiting current density of 2 A/cm^2, it remains nearly equal to the non-activated sample. However, after 30,000 cycles, the catalyst retained back to its initial activity of 0.6 V_{RHE} at 2 A/cm^2. In comparison to Pt/C, all activation state of catalyst approached to high activation losses and the difference of ≃ 30 mV at 2 A/cm^2. In the Tafel plot (Figure 4.18, all activation states exhibited similar activity with an almost same slope which means there are no limitations due to flooding.

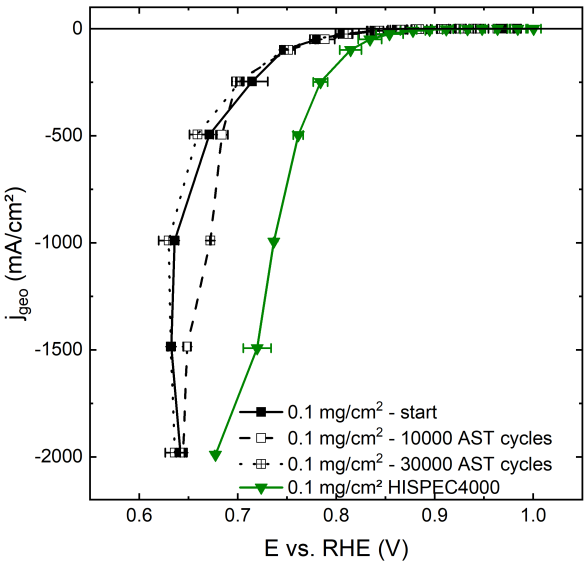

Figure 4.17: Polarization curve of Pt/HGS with high loading showing the performance enhancement by potential cycling

The OCV value lies around ≃0.97 V_{RHE} and is nearly comparable to the OCV of commercial platinum catalyst. In comparison to low loading catalyst, the ORR performance of 0.1 mg_{Pt}/cm^2 is almost ≃100 mV higher than the most active state of 0.04 mg_{Pt}/cm^2 (see Figure 4.14). The impact of high loading catalyst comparison to low loading catalyst, in our case, the GDL area is constant 2.01cm^2 and when depositing the Pt/HGS, the high loading will approach higher catalyst layer thickness on the constant surface area. The more the thickness of the catalyst layer, the more microporous structure will be affected. The particles tend to be more agglomerate in clusters rather than a uniform distribution over a defined area of cathode [267]. The effect of catalyst deposition technique can also influence the structural properties of catalyst coated GDL. The high loading provides a high mass activity and more active sites to catalyze the reaction. Therefore, the performance was better for 0.1 mg_{Pt}/cm^2. In comparison to the commercial HISPEC Pt/C catalyst, the Pt/HGS was not able to compete the performance (Figure 4.4). Now, if we look into consideration that both catalysts have the same nanoparticles but different supports which gives evidence that support also contributes to activity effect of catalyst. The pore confinement of Pt/HGS (each nanoparticle is separated physically in a mesoporous structure) is rigid but during graphitization and annealing the carbon layer deposits on the surface of the catalyst which can be removed by aggressive cycling. The impact of cycling on the activity performance of the catalyst is addressed before in this chapter. The nanoparticles are confined in pores due to the higher loading may be subjected to excessive filled concerning the capacity. Giving a higher loading will increase the activity but then also subjected to agglomeration and Ostwald ripening issues [257, 261].

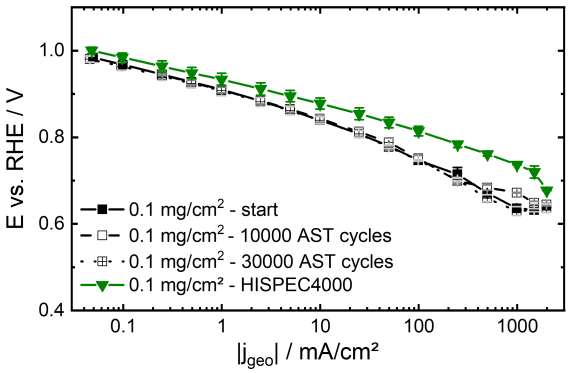

Figure 4.18: Tafel plot of high loading Pt/HGS with comparable stability to Pt/C

4.2.3 Complications during for ORR with EIS for Pt/HGS

During the determination of the kinetics of ORR for Pt/HGS by SGEIS techniques, the fluctuation of voltage at constant current step intervals (Figure 4.19) was observed throughout in most of the samples which lead to several potential sources of errors. These errors could be external or internal which are possible due to a particular geometry of catalyst and support, scan rates, impurities and not a well developed and tested protocol.

To our understanding, the main reason is the flooding of an electrode by ionomer, as HGS is completely porous support with the entrapped Pt nanoparticles. There could be the possibility of some pores completed filled with Nafion™while others are filled partially may interpret as the fluctuation of voltage through the time, the filled pores with Nafion block the active sites of nanoparticles. The other factor that can contribute to the flooding issue is the lack of oxygen and the instability of catalyst support. As there is not an effective water management system in GDE half cell because the GDL we used for Pt/HGS was without membranes, that can affect the transport function of water produced at the cathode of a fuel cell. Accumulated water works to increase the conductivity, but the excess water inside the cell on catalyst layer results in the high partial pressure of water vapour then achieving the saturation pressure for water condensation on GDL. The condensed water on GDL reduces the gas diffusivity and increase hindrances in the layer by limiting and blocking the flow paths for oxygen in the cathode [268, 269]. In Figure 4.19, it can be seen that voltage fluctuates with respect to the time and during the constant current provide for each step, the response was supposed to be constant. The hindrance to maintaining a constant potential is somehow unknown. The related Nyquist plot of the same system and catalyst in Figure 4.20 was not able to achieve a semicircle pathway. From the low-frequency region, it can be seen that the curve was attempting a semicircular pathway while the disturbance occurs when approaching to high-frequency region. During the investigation, several errors were generated, such as “Control amplifier overload” and “E−channel overflow” causing the disruption and failure mode, which is responsible for electrode material degradation. The degraded catalyst and porous support are affected by the hindrance

of water removal and diffusion of gases. It was also observed in some experiments that approaching amplifier overload leads to the dissolution of Pt/C catalyst. So, in this case, the proton conductivity is also affected by stress condition and decomposition of the catalyst material. Another impact that can be assumed is the corrosion of graphite spheres which could lead to uneven effect for surface area with loss of active sites. This corrosion can also result from the formation of carboxyl groups through changes in surface chemistry affecting the water management by flooding. As compared to RDE, GDE works at high current densities which can expel more water leading to potential drop, yet the disturbance and fluctuation of potential during ORR are still questionable and requires surface chemistry study. This issue can be addressed by combining the GDE cell with surface characterization tools.

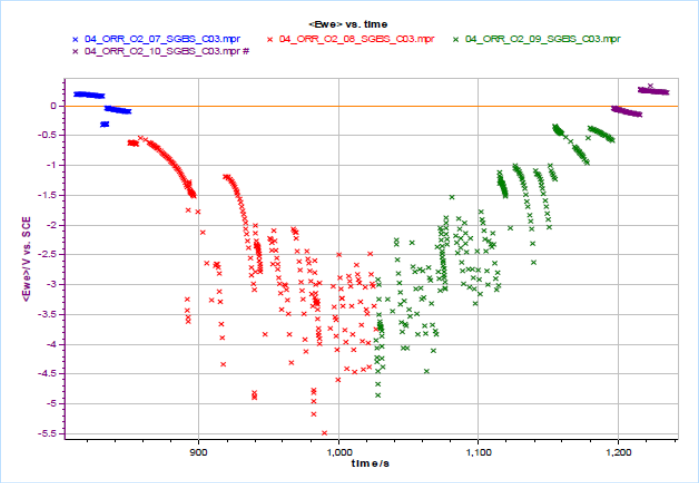

Figure 4.19: Voltage fluctuation with respect to time during SGEIS current range steps

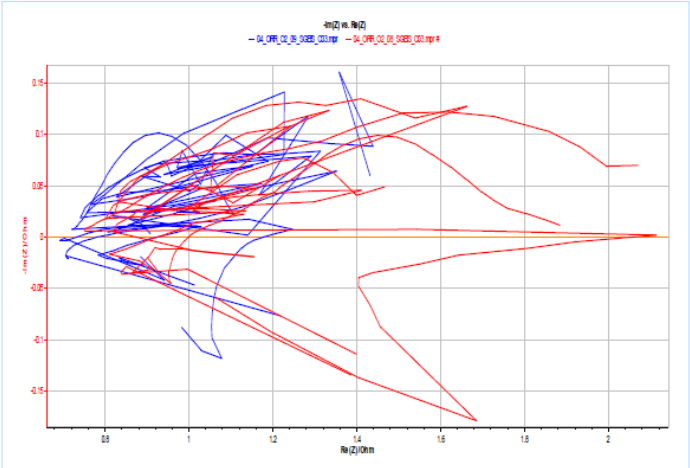

Figure 4.20: Disturbance in Nyquist plot with no observable semi-circle in high frequency region

4.2.4 ECSA determination and complications for Pt/HGS

Although, there are several methods to determine ECSA, the one we adopted for this study is H*upd* method by integrating the capacitance corrected charge in the range of 0.05-0.4 V_{RHE}. The technique used for this study to determine the ECSA was cyclic voltammetry for the estimation of adsorbed hydrogen monolayer on platinum. In this experiment, the CVs were conducted at 100mV/sec for three cycles from 0.05-1.2 V_{RHE}. The samples were not purged from the back of cathode as reported by Ehelebe et al. [15], which could lead to more positive potential by hydrogen evolution. It can be seen that the loading of Pt has an impact on the CVs, the capacitance current is higher for the sample with higher loading along with the peaks of hydrogen adsorption and desorption.

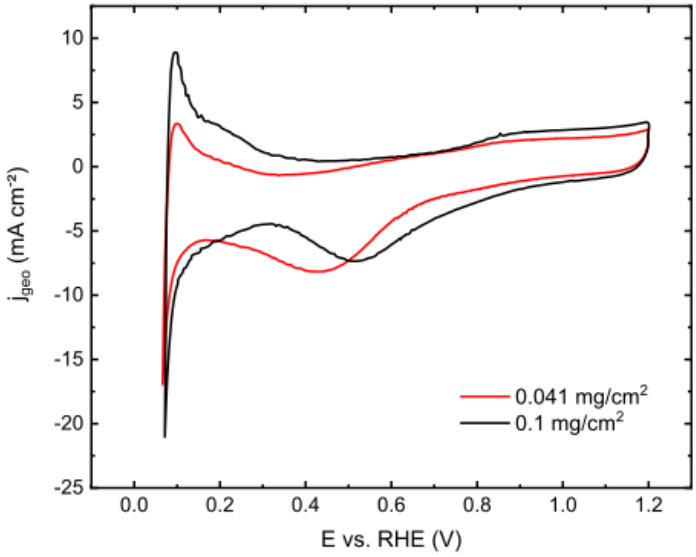

Figure 4.21: Cyclic voltammogram of Pt/HGS with high and loading GDL

In the H*upd* region, only one visible peak can be seen as compared to the commercial platinum catalyst, which means that not all facets of Pt are involved in Pt/HGS structure. The first visible peak comprehends to Pt(110) sites, the high current approaches to hydrogen oxidation and it can be seen that sample with lower loading (0.04 mg_{Pt}/cm^2) has a less integral area under the curve from 0.05-0.4 V_{RHE} as compared to sample with high loading 0.1 mg_{Pt}/cm^2. It will lead to high ECSA for higher loading sample, the primary effect can be observed in the H*upd* region from 0.05-0.4 V_{RHE} and the oxide region from 0.5-1.2 V_{RHE}. Due to the difference in loading the peak current density is higher for higher loading but both samples due to the same catalyst showed similar behaviour such as peak potential. The low oxidation current for the low loading sample can be due to adsorbed species from the electrolyte to the block the surface sites. It is stated before that the ECSA obtained from the hydrogen adsorption area must be equivalent to the hydrogen desorption area, which is not valid for our case. In the cathodic scan, the area

under the curve is less than the area for the anodic scan. This relates to the formation of a small amount of hydrogen formed near to the potential of 0.05 V_{RHE}. This molecular hydrogen will revolve around the Pt surface to the electrolyte for oxidation during an anodic scan. The current from hydrogen oxidation is then related to hydrogen desorption current and gives rise to desorption charge, which ultimately gives a high peak for higher ECSA. It was observed that the rise of peaks is due to current from hydrogen and thus the ECSA by H*upd* will not be able to cope with the exact values. Also, in the reverse anodic scan, the high amount of oxygen can be seen in a bulged curve in the region of 0.3-0.6 V_{RHE}, this down peak is more shifted to low positive potential for low loading catalyst. This is indifferent to the oxide reduction peak in Pt/C in $HClO_4$ [215] which lies in the regions of 0.6-0.8 V_{RHE} and shifted to lower potential 0.3-0.5 V_{RHE} in Pt/HGS showing that the amount of oxygen present in the system and the Pt oxides are reduced lately.

It can be seen in Figure 4.21 that the onset of hydrogen adsorption of low loading sample shifted to less positive potential as compared to high loading which is likely to be believed that low loading sample is not much catalytic active due to poisoning of Pt/HGS surface by impurities. The most common impurity that can be linked to this work is Cl- anions because $HClO_4$ was used as an electrolyte for this work [270]. The Cl- ions have devastated effects on Pt oxidation by poisoning the catalyst sites which could be used for hydrogen adsorption [233]. Other ECSA methods can be taken into considerations. However, up to now, this was the only way available for ECSA determination available during the investigation. Later CO stripping could be used for GDE in order to eliminate all those errors related to baseline correction and estimation of ECSA. The CO stripping is much more preferential method for ECSA estimation as it avoids the overestimation of peak current density, better baseline correction and oxidation charge higher than H*upd* [11, 271].

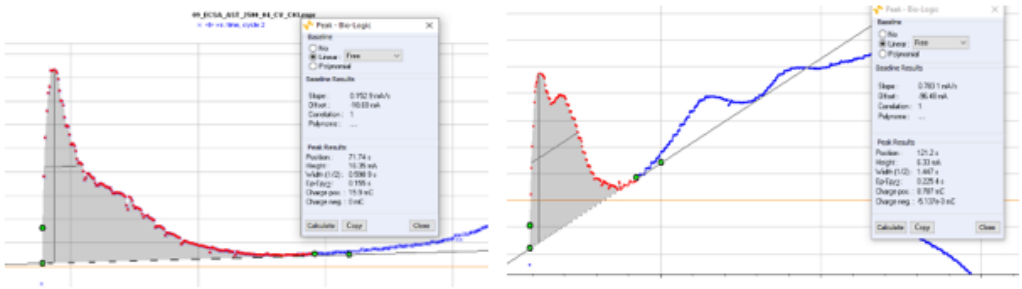

Figure 4.22: Baseline correction problem during integration and high peak current in hydrogen adsorption potential region leading to overestimation of ECSA

The H*upd* method have several complications for over/underestimation due to the baseline correction which can be seen in Figure 4.22 , some CVs are not suitable so due insignificant peak angle which makes it hard to draw a parallel baseline to the capacitive region.

The impact of activation can be seen during the intensive AST cycles affecting the surface area, which ultimately have an impact on catalyst utilization. In order to verify the statement from Pt/HGS manufacturers that the catalyst will achieve the maximum activity after subjecting to 10000 AST cycles, the catalyst in this research was subject to 30,000 AST cycles as standardized by DOE to see after-effects of 10K cycles. It is observable that the activation cycles can increase the electrochemically active surface area. In the beginning, before and after ORR cycling, the ECSA was found to be ≃50.84-52 m^2/g_{pt} which increased after 2500 cycles to 62 m^2/g_{pt} and then remain stable till 10k cycles with ECSA of 60 m^2/g_{pt}. Eventually, after 30,000 cycles, the ECSA reduced to lowest as 44.08 m^2/g_{pt} by not be able to retain its initial surface area. Although, it is challenging to subject catalyst to cyclic voltammetry cycles continuously, which requires stable cathode catalyst design to give reproducible results [272]. Initially, the ECSA was similar showing that the catalyst not subjected to particles agglomeration and growth, the chances of carbon corrosion is also negligible due to ECSA increases from 2500-10K cycles.

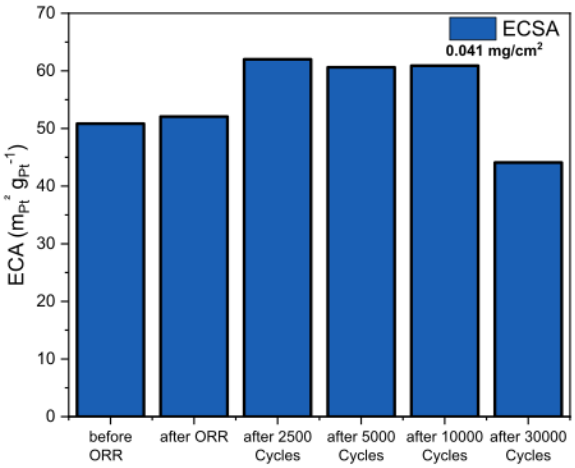

Figure 4.23: ECSA after several steps of stress cycling by integrating the H_{UPD} area for Pt/HGS

The high ECSA is possible due to the graphitized support, which reduces the possibility of carbon corrosion. A possible reason that could assume the pore filling nature of HGS support leading to pore flooding as it consists of cavities covering the Pt nanoparticles support. During the stress cycling, the degradation of ionomer, which is reasonable under cycling, could have reduced the flooding of pores which will result in more exposure to the catalyst surface. The ECSA decrease after 30K cycles relates to severe changes in the microstructure of catalyst and may be resulted in due to Pt dissolution and increase in interparticle distance. Due to the complex structure and small particle size of Pt/HGS, several further investigations would be needed which is out of the scope of this thesis such as Transmission electron microscopy (TEM) and Scanning electron microscope (SEM) descriptive analysis to see the structural changes within the catalyst support.

4.3 Non PGM Fe-N-C Catalyst Investigation for ORR in Alkaline Media

4.3.1 Degradation in AST Oxygen (O_2) and Argon (Ar)

The degradation of Fe-N-C influenced by oxygen is well understood for PEMFC due to production of Fenton reagent [273]. There is still a gap for degradation mechanism in AEMFC, which is addressed in this work. The impact of gases (O_2 and Ar) can impose different performance degradation behaviour during stress cycling. There is yet no other studies available for the performance degradation comparison in Ar and O_2 for AEMFC. Most of the AST protocols are designed in such a way that the data can be comparable and sufficient to give scale-up information. The AST protocol was used for Fe-N-C is based on the protocol developed by Ehelebe et al. [15] for Pt/C in an acid electrolyte. However, there is a need for extensive experiments to determine the proper AST protocol. The fuel cell performance must be diagnosed for various factors such as ionic resistance, activity degradation with proper series of experiments to propose a new accelerated protocol helping possibility to avoid failure mechanisms which could ultimately lead to unrealistic conditions [163]. During the continuous cycling with the potential sweep, the half-cell temperature can be increased due to the movement of electrons and radical ions. The temperature change can affect the degradation (mechanical and chemical) of ionomer. Also, the humidified oxygen was provided for AST, which would result in dimensional swelling of catalyst GDE and the possibility of flooding. The protocol used for this study to investigate the degradation mechanism of commercial non PGM catalyst (Fe-N-C Pajarito powder) is the modified version of Pt/C protocol for PEMFC in GDE half-cell. A break-in procedure was not carried out before degradation cycles as there is less possibility of carbon corrosion in alkaline media as compared to acid electrolyte [254]. The Fe-N-C catalyst was examined for degradation through AST by cycling continuously in the potential range of 0.6-1.0 V_{RHE} in Ar and O_2 for 5000 degradation cycles. Under certain specific conditions, the catalyst was subject to degradation by accelerating the cycles to 100 mV/sec leading to faster redox reaction. The deterioration effect for any changes in the catalytic activity can be subjected to particles detachments, leaching or flooding. The humidified gases are bubbled in the electrolyte and from the back of cathode at 50 mln in 1.0 M KOH.

Figure 4.24 and Figure 4.25 represents the polarization curve and Tafel plot, the ORR measurement has been carried out in a period of time before and after AST. In comparison to current density of 2 A/cm^2, the samples with Ar purged AST showed better performance after cycling with an increase in ORR activity from 0.49 V_{RHE} to 0.509 V_{RHE}. The better activity after ORR gives a clue that activation of the sample is necessary before the experiment; the study for activation is presented later in this section. However, the severe degradation of catalytic activity occurred for AST with O_2 from 0.49-0.233 V_{RHE}. It is interesting that catalyst was stable and showed similar ORR activity at high current density region

to that of Ar-AST samples. The conclusive investigation is yet remaining with more experiments and advanced tools.

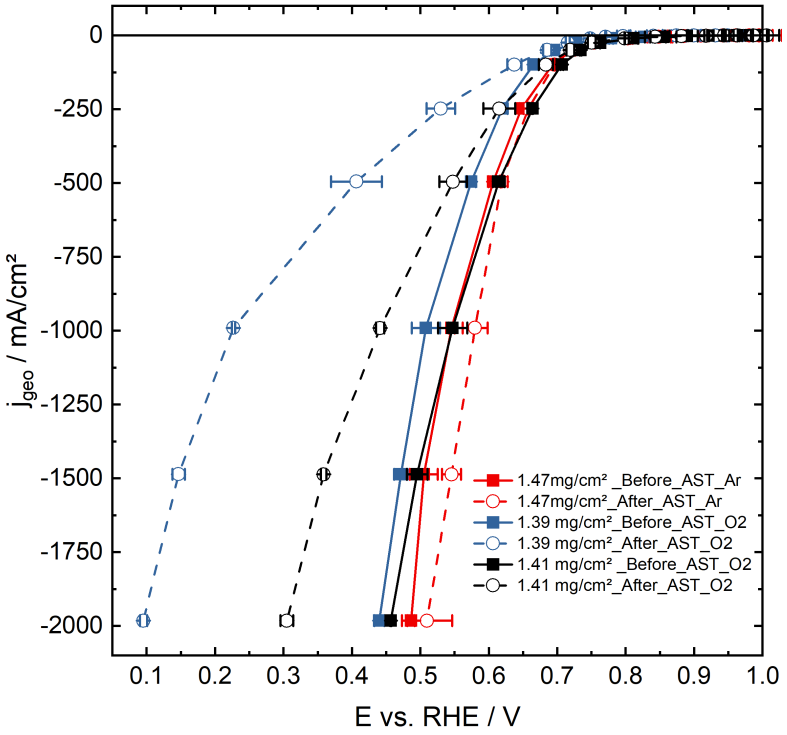

Figure 4.24: Polarization curve of Fe-N-C with average loading 1.5 mg_{Fe-N-C}/cm^2 facing degradation during ORR in $O_2$and Ar

In the beginning, in the low current densities region, all samples with an onset of 0.7-0.74 V_{RHE} exhibited similar performance, even though the activation losses are high, the ORR activity was affected after AST-O_2 samples in the mass transport region. The Ar-AST was stable throughout as the only reactive oxygen available was present in the electrolyte as dissolved oxygen. However, if AST-O_2 the catalyst was subjected to ORR with oxygen, and again the capacitive currents are also higher with oxygen. The observed onset for Fe-N-C before and after stress test is lower than commercial Pt/C catalyst. The losses in oxygen cycling after AST test were 145 mV and 257 mV respectively, since, the difference is not consistent. Therefore any general conclusion cannot be drawn. Although both samples followed the same trend in after O_2 AST, that catalytic activity of ORR started to decrease from the onset potential of 0.742 V_{RHE} and degrades while approaching to high current density region. The similar behaviour of polarization curve can be seen in the Tafel plot (Figure 4.25), the OCV of all samples in the presences of both gases is similar and comparable to Pt/C for PEMFC in the previous section.

The overall performance degradation can be seen in the high current density region of over 10 mA/cm^2

at 0.6 V_{RHE}, the Tafel slope of Ar was reduced after AST from 125.71 mV/dec to 102.61 mV/dec with activity enhancement while the slope of AST O_2 increased from 229.2 mV/dec to 304.49 mV/dec showing severe degradation. As the alkaline solution is very corrosive with the availability of dissolved water/O_2, it may be possible that Fe component of the catalyst was corroded, and the catalyst support is also susceptible of corrosion but to a negligible extent.

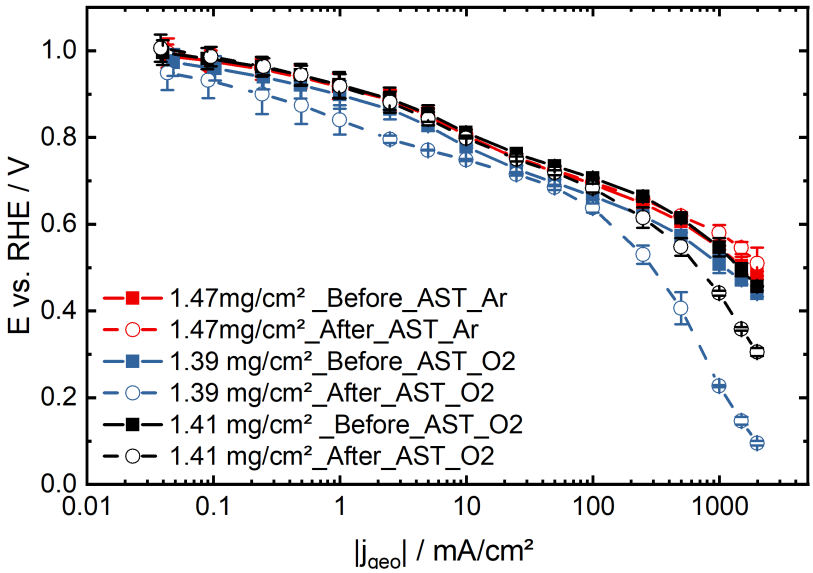

Figure 4.25: Tafel plot showing that severe degradation in high current density for ORR AST in O_2

In oxygen stress test, the catalyst performed less comparing to Ar stress test with its initial activity. The difference in activities for Fe-N-C catalyst after AST in alkaline could be due to high oxygen availability, and the electrolyte was thoroughly saturated with oxygen promoting 2 e^- reduction of O_2 to HO_2^-. The stability in Argon could be possible due to non-reactive gas which did not deteriorate the outer sphere mechanism which is usually promoted by the carbon support [223] since it has been already suggested that most unsafe conditions affecting catalyst performance are cathode side (oxygen supply). It is believed that the interatomic distance of Fe-C increases with the potential that can improve the OH adsorption through oxidation of Fe^{2+} [4]. During cycling with AST-O_2, much OH- radicals produced during 5000 cycles. It would lead to blocking the active sites of the catalyst. Another reason is the flooding of catalyst as if the water production rate is faster during the accelerated test with O_2 and the cathode side is not able to consume all the excessive water formed during cycling. Since oxygen tends to oxidize and corrode the Fe and carbon support, therefore it could be fatal for outer-sphere mechanisms [274]. The degradation of Fe-N-C in O_2 AST is visible clearly, and the same even worse trend could also be detected with synthesis air. The visible degradation has the main impact on mass transport region. Although, both samples of AST-O_2 were tested in a similar environment, but the difference in results could be

possible to not well-quantified degradation and more experiment study will give a decent approximation. Also, there was no cleaning cycles performance which could result in the activity of ORR after ECSA cleaning cycles in Ar and most of the degradation mechanism happened in the mass transport region. Since AEMFC suffers from poor water management, it can be concluded that the degradation happens in O_2 is due to the excess amount of water generated and less amount of water consumed at the cathode, since O_2 is responsible for liberating OH- ions. While, in Ar, the ORR activity is high due to less amount of water produced and consumed. The carbonation effect can also be taken into consideration that is generated by the mitigation of atmospheric CO_2 into the system. The other source of CO_2 for the GDE would be the feed gas (mainly air), but in this experiment, we used the pure O_2, which reduces the possibility of contamination. The CO_2 from the atmosphere is not negligible as even a minimum number of carbonates can cause overpotentials up to 400mV with 5000ppm concentration of CO_2 [275]. During AST cycles in O_2, there is more possibility of carbonation as O_2 is responsible for generating the OH- ions which react with CO_2 to form bicarbonates [276]. This is also one of the reasons that performance degradation was seen in O_2 as compared to AST in Ar with enhanced performance. However, it is not possible to give an exact evidence that supports the argument and further supplementary characterization methods can reveal more information.

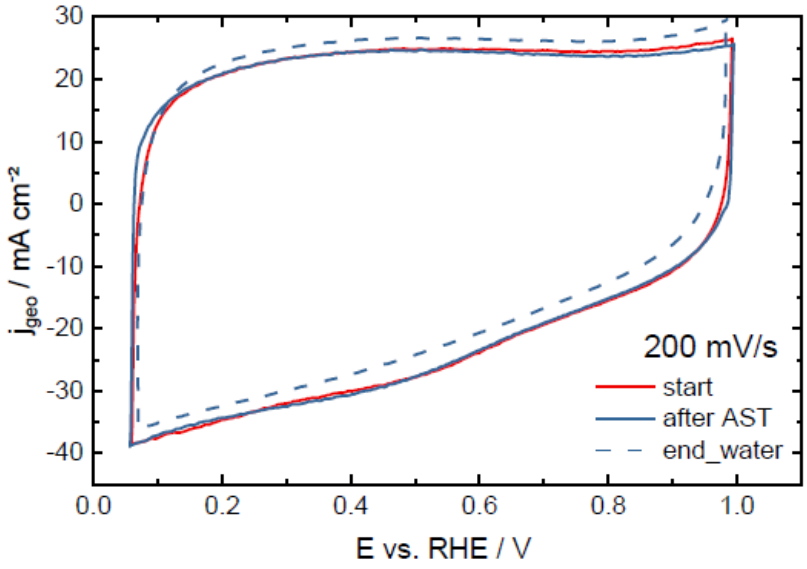

Figure 4.26: CVs of Fe-N-C before and after AST in Ar with no significant difference in capacitance

Despite the improvement in ORR activity of Fe-N-C in Ar saturated degradation test of 5000 cycles, there is significantly no noticeable change in the CVs, as shown in Figure 4.26. Due to similar double-layer capacitance, it can be assumed that the Fe sites were not subjected to dissolution, ripening, and leaching in a noble gas. As the N-C is not subjected to degradation in alkaline media, the total activity can be

associated with the iron sites. Over at the 0.3 V_{RHE}, there is no significant bulge/peak appears and CVs with minimal changes in the cathodic scan showing that no carbon oxidation occurs. The active sites are stable in Ar saturated degradation cycles in alkaline. However, the situation could differ for PEMFC where anions such as ClO^{-4}, HSO^{-4}, Cl^{-} can significantly poison the catalyst sites [277]. Although there is no graphical integrative method to determine the ECSA such as for Pt/C, the overall assumption can be withdrawn from the size of the capacitance area, which is proportional to ECSA. It is not very easy to quantify the active sites or leached Fe in the electrolyte except for high quantification methods such as a mass spectrometer. However, it is crucial to quantify the ECSA loss during cycling procedure

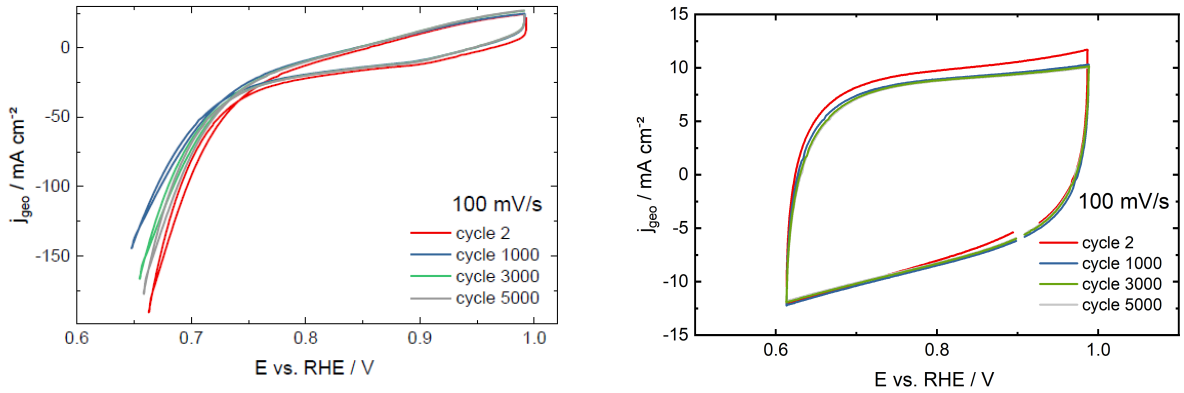

Figure 4.27: Fe-N-C AST for 5000 cycles in O_2 (left) and Ar (right) in the potential limit of 0.6-1.0 V_{RHE}

for an estimation of the catalyst layer active site structural changes. The ECSA determination criteria are available for PGM catalyst but not for non PGM catalyst, which can be possible by the estimation of catalyst dissolution and microscopic morphological change studies and it is beyond the scope of this studies but will be addressed later. There are mass transport issues during AST in Oxygen which can be regarded as OH- attack to the ionomer. In the degradation cycles Figure 4.27, it can be seen that the lower potential limit for degradation cycle was not achieved, i.e. 0.6 V_{RHE} with iR drop compensation and it is addressed before in this chapter that no significant standard protocol is available for Fe-N-C catalyst in AEMFC stability. Hence, when the catalyst was not able to achieve the lower potential limit, it can be referred to as difficulty in adapting protocol which can be improved by intensive series of experiments. In the beginning, the catalyst was able to achieve current density of 189 V_{RHE} at 0.66 V_{RHE} which has been reduced to 143 mA/cm^2 at 0.64 V_{RHE} after 1000 cycle. Later, as the number of cycles increased, we can see a gradual increase in activity, this shows that catalyst is subjected to activation due to non-uniform performance in degradation cycling.

4.3.2 Impact of Ion Exchange Capacity IEC

The Fe-N-C catalyst coated GDL was prepared with commercial Fe-N-C Pajarito powder and commercial ionomer Aemion™, both are optimized for AEMFC to operate without the use of PGM. The ionomer is classified into two categories with different ion exchange capacities (IEC), i.e. high ion exchange capacity ionomer (HIEC) and low ion exchange capacity ionomer (LIEC). In this section, the comparison and behaviour of Fe-N-C with different IEC is investigated. The main issue that affects the AEMFC performance is the degradation (chemical) of ion exchange material either ionomer or anion exchange membrane, which makes it unable to achieve the high activity as compared to Pt and its alloys in PEMFC. This degradation effect is caused by the nucleophilic attack and some elementary reactions between OH^- anions and functional groups of ion exchange material [278]. Due to the instability issue, the purpose of this work is to optimize the ionomer for better stability regardless of high performing activity. Despite the efforts made for optimizing and synthesizing the new functional group, the high current density and stability are yet to achieve [279]. The polarization curve of samples HIEC and LIEC with loading $\simeq 1.73 V_{RHE}$ is shown in Figure 4.28.

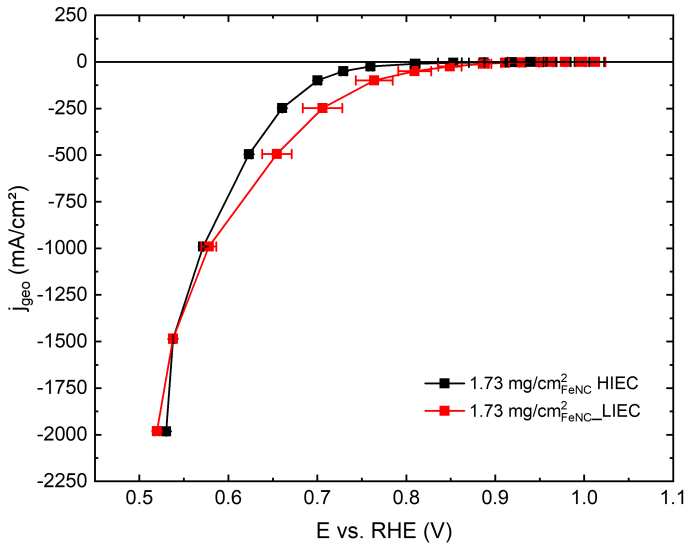

Figure 4.28: Polarization curve showing the performance difference for high and low anion exchange capacity ionomer

Both sample exhibited almost similar activity in O_2 ORR such as HIEC achieved 0.53 V_{RHE} at current density of $2 A/cm^2$ and LIEC with 0.51 V_{RHE} at 2 A/cm^2 . The activation required for both samples are different as HIEC with the onset of 0.8 V_{RHE} and LIEC with the onset of 0.88 V_{RHE}. It shows that high activation needed for the sample with high IEC. Interesting, as approaching to half-wave potential, the performance of LIEC was better, but the error bar shows that there is a difference in between forward

and a backward scan can be doubted for LIEC suffering from water imbalance issue. After achieving the half-wave potential, the HIEC performance-enhanced surpassing the LIEC activity that IEC content can impact the performance and stability at high current density.

Regarding IEC of ionomers, Aemion™ activity with higher efficiency and OH- conductivity is significantly better as compared to other ionomers with high IEC 1.3 meq/g [280]. The high IEC leads to high ionic conductivity, more water uptake, which results in more dimensional swelling. As at the beginning, HIEC requires more anions to activate, and it can be seen in the polarization curve that HIEC approached to the less positive onset and less activity till half-wave potential. On the other hand, fully activated and optimized LIEC performance slowed down at high current density due to loss of accessible sites and less water to unhindered produced bicarbonate conduction, a significant problem for AEMFC [281]. The swelling issue is also an essential factor that can limit the ORR activity for electrocatalyst to achieve high current density. The dimensional swelling is not just limited to water intake but also the type of electrolyte, and it has been studied before that in KOH, anion exchange polymer could be subjected to 80% of dimensional swelling even though it has highest conductivity [281].

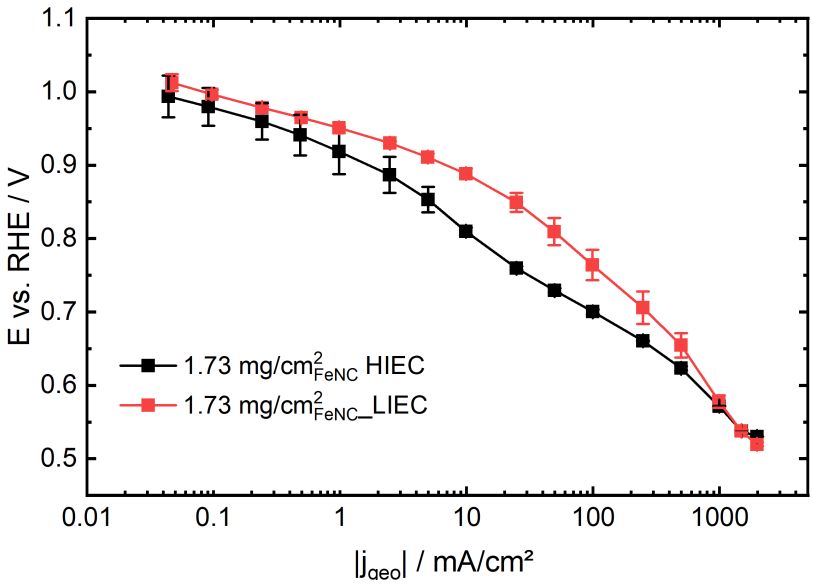

Figure 4.29: Tafel plot showing the difference of activity in low current density region for nearly similar catalyst loading with different exchange capacity

In the Tafel plot (Figure 4.29), the OCV of LIEC and HIEC Fe-N-C was found to be 0.99-1.01 V_{RHE} which is below thermodynamic value of H_2/O_2 fuel cell showing the activation losses. The LIEC Tafel slope of 51 mV/dec was achieved in the low current density region of 0.1-10 mA/cm^2 from 0.8-1.0 V_{RHE} and 181.94 mV/dec in the high current density region. This transition of the high slope of Tafel plot shows that catalyst was subjected to degradation from 0.8 V_{RHE}, which is high above the fuel cell limiting

degradation potential of 0.6 V_{RHE}. The HIEC Tafel slope of 99.89 mV/dec was achieved in low current density region of 0.1-10 mA/cm^2 from 0.7-0.95 V_{RHE} and 102.11 mV/dec in the high current density regions which shows that the performance degradation in the high current region for HIEC is not much bad as for LIEC. The cold start functioning of GDE (shut down, start-up and a sudden break in procedure) effect was also observed in for Fe-N-C IEC catalyst, and there is no significant performance degradation observed. It shows that the Fe-N-C was not able to achieve the feasible peak performance that it can be regarded as a replacement for Pt/C but due to its stable performance and not sudden degradation gives an advantage. However, more work can be done with different immobilized backbone ionomers having better IEC and durability that can be added to Pajarito powder. The extensive studies in GDE also showed that how quick and optimize the GDE method is, that it can help to quickly investigate and optimize the catalyst layer properties with the performance that can be relatable to fuel cell [241].

4.3.3 Catalyst layer optimization of Fe-N-C LIEC by Activation Procedure

The Fe-N-C catalyst coated GDL layers prepared by doctor blading were in the range of 1.5-1.7 mg/cm^2 and shown as an average in results which were immersed in KOH to achieve high conductivity [282]. Since there is not optimal predefined protocol for Fe-N-C testing in half cell, we used the protocol for PEMFC platinum catalyst for ORR evaluation [15]. The catalyst membrane with ionomer needs to be converted to OH- form to prevent hindered nucleophilic attack, which can affect the conductivity and ion exchange capacity [283]. The samples were preconditioned by immersing in KOH for several intervals (rinsing, 40 Min, 24, 48 and 72 hours) and then washed with degassed water thoroughly to remove the impurities. The GDL was then preserved in an airtight pack as it has been reported that upon exposure to atmospheric CO_2, the conductivity will reduce drastically to 60-70% in few hours due to rapid conversion of OH- to mixed carbonate/hydroxide form [65, 282, 284]. Several breaks in procedures were carried out in Ar saturated environment during cyclic voltammetry to initiate the activation.

The polarization curve and Tafel plot of all samples (averaged) in linear and logarithmic scale are demonstrated in Figure 4.30 and 4.31, the 48h sample exhibit the high onset and have less linear drop during activation losses. However, the sample with 72h loading has a rapid drop during activation losses and with much severe mass transport limitation as compared to other samples with different activation time. In comparison to activation losses, the sample with 48h activation exhibits the onset at 0.8 V_{RHE} (Figure 4.30), the activity of all samples reduced gradually in the kinetically controlled region (0.6-0.9 V_{RHE}).

the Tafel plot (Figure 4.31), 48h activation exhibited high performance while the 72h activation falls below the non-activated samples. Variation in the activity is due to loss of cationic active sites, ion dilution and swelling along with long term immersion of CCM in an electrolyte that increases the

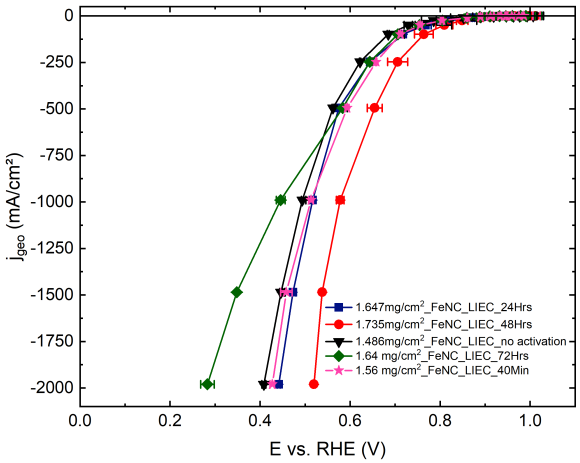

Figure 4.30: Fe-N-C LIEC ORR performance enhancement by immersion time-based activation procedure

impurity ions which needed to be removed accordingly [282,285]. The 72h immersion showed a significant low performance that would be possible due to two reason. One possibility is Fe-N-C catalyst or ionomer stability (resulting due to OH- attack at the C-2 position of Benzimidazolium ring) [286]. Another possibility for less activity in the high current density region is due dimensional swelling and water uptake for monovalent anion as reported in the literature that OH- ions can lead to more dimensional swelling as compared to Cl^- & I^- ions [281,285]. In the kinetic region (around 0.8 V_{RHE}), all the samples exhibited a similar performance.

The CV's for Fe-N-C catalyst, as shown in Figure 4.32 are quasi rectangular, which is due to the high surface area of carbon matter. The area within the curves gives information for double-layer capacitance. It can also be seen that in the CVs, as the activation time increases, the double-layer capacitance also increased, due to the exposure of active sites and high surface area during activation except for 72 hr sample as the high capacitance resulted due to reactive carbonate species from OH^- ions to atmospheric CO_2 [287]. We took the highly optimize sample (48hr activation) and performed degradation and break-in procedures, as shown in Figure 4.30. The load cycling protocol was used to investigate activity degradation after 5000 Cycles from 0.6-1.0 V_{RHE}. There is not a significant effect after 5000 degradation cycles since Fe-N-C is a stable catalyst even after several degradation procedures and another reason is that AST is performed at room temperature. As observed before that there is little morphology change for Fe-N-C catalyst, the difference can be observed on the change of capacitance current densities. The observed difference might be inconsistent due to geometric area coverage by particles detachment or as an average decrease of the number of electrons involved per O_2 molecule reduced(decreased selectivity toward water formation). Since the activity was not approached to a high level may be interpreted as the

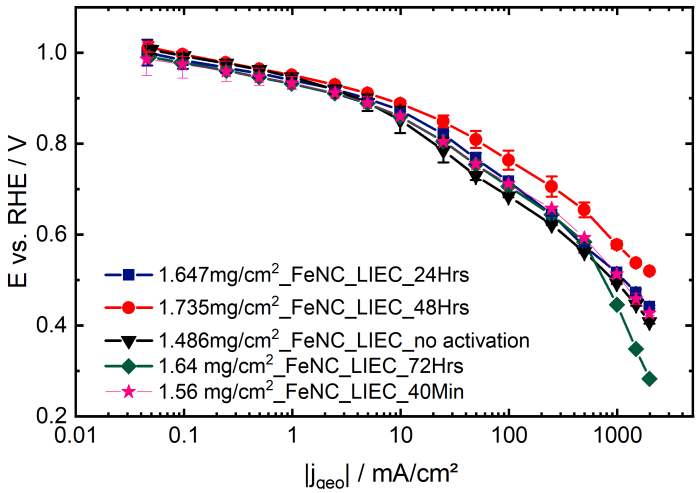

Figure 4.31: Tafel plot of Fe-N-C with LIEC optimization

loss and modification highly active sites with the less selective sites after AST, the catalyst detachment can be visualized from the minor change in CVs.

The CVs during AST underwent to negligible changes during the degradation cycles (5000) which shows the high stability of metal-free catalyst in the alkaline electrolyte because the attribution of Fe-N-C has a high stable 3D structure with high surface area and good conductivity [288, 289]. In a structural way, the commercial ionomer is optimized for the C2 position by benzimidazolium ring, which has the ability to shield the ionomer from OH^- attach eventually lead to high molecular stability during 48 hours of activation [281]. In comparison to the performance of previously synthesized Fe-N-C in the literature that the impact of ionomer has a drastic impact on the activity of the catalyst and the optimized ionomer has better performance than other Fe-N-C with ionomer (Tokuyama, ion exchange capacity 1.5 mmol/g) and the commercial Pt/C [198, 199, 201]. Our Fe-N-C with Aemion™ionomer considerably have better activity and with consistent activity in the kinetic region due to the high amount of surface oxide. The polarization curve demonstrates that Pt/C (in the previous section) performed better than in high potential region but less catalytic active and stable than Fe-N-C at high current densities.

The lower starting potential at OCV for Fe-N-C with 48 hrs activation at 1.01 V_{RHE} is quite like others which confirms that there is no problem of fuel cross over and mixed potential. Furthermore, in the literature, the optimisation has been done to analyse the impact of ionomer ratio to Fe-N-C ratio which approached the peak performance 35 wt.% ionomer approaching to 680 mA/cm^2 [201]. As the ionomer content increases, the conductivity of cathode also increases, which ultimately results for high performance. Nevertheless, the particular limitation is possible as more and more ionomer content increases, and there is a possibility of pores filling, which will block active suites and thus reducing activity. As compared to the platinum catalyst in alkaline, the Fe-N-C showed better performance in high poten-

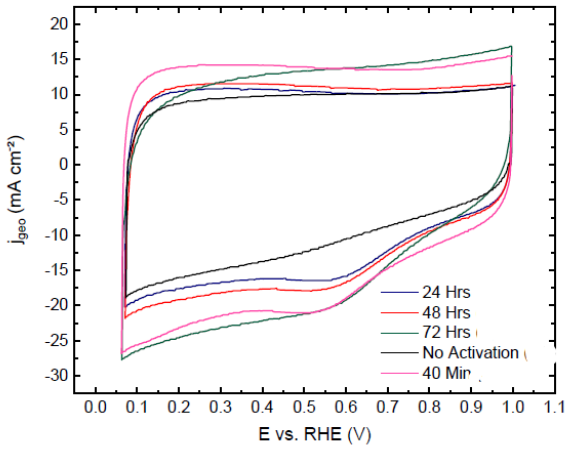

Figure 4.32: Fe-N-C LIEC CVs demonstrate the different capacitance during different activation time

tial regions and thus made it suitable for alkaline fuel cell. The results presented of this subsection is published in the "Electrochemistry Communications" journal [241].

4.3.4 Reproducibility Fe-N-C HIEC

To investigate the reproducibility of results, Fe-N-C HIEC GDLs were prepared with loading from 0.89-1.73 mg/cm^2 for ORR in O_2. The polarization curve in Figure 4.33 depicts the performance of Fe-N-C in comparison to commercial Pt/C to the current density of 2 A/cm^2. The impact of loading can be seen that as the catalyst loading increases, the activity gets better but to a certain extent.

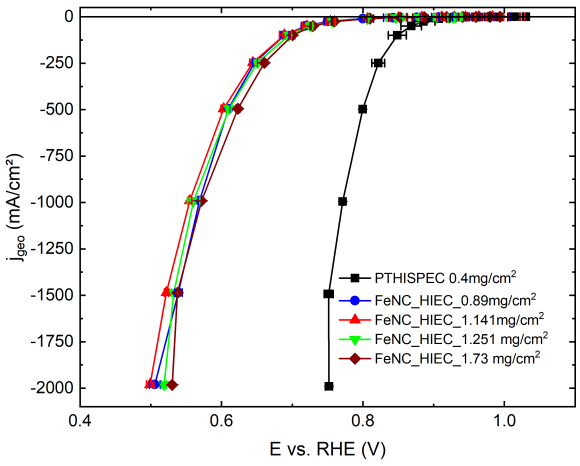

Figure 4.33: Fe-N-C HIEC Polarization curve showing the reproducibility of results

The Fe-N-C achieved the limiting current density of 2 A/cm^2 at 0.49-0.53 V_{RHE} with a higher onset of 0.80 V_{RHE} which agrees with our previous results. Unlike Pt/C which very high activity of 0.7 V_{RHE} at 2A/cm^2 in the acid electrolyte, the Fe-N-C perceived very high activation losses which are subjected to hydration level of anion exchange material. Despite the similar performance in polarization curve, all sample have different OCV without correlation to loading and the activity degradation starts at 0.8 V_{RHE} in the low current density region with an increasing slope in high current density region (Figure 4.34). The performance gap is vast between Pt/C and Fe-N-C HIEC which may require some more activation study to optimize the catalyst layer properties.

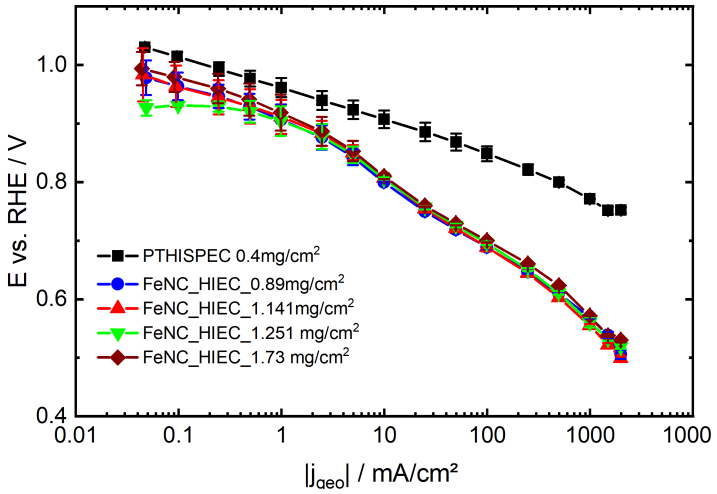

Figure 4.34: Tafel Plot of Fe-N-C LIEC in comparison with state-of-the-art Pt/C catalyst

4.3.5 Stability of Fe-N-C with HIEC Ionomer in ORR O_2

To address the stability of catalyst and ionomer in alkaline, the optimized Fe-N-C with anion conducting ionomer HIEC is subjected to ORR in O_2 before and after 5000 AST degradation cycles in Ar.

It is well known that the properties of anion exchange materials change concerning time in a high pH environment for a prolonged duration. Therefore, several methods can be used to optimize stability such as exploring high conducting ionomer, carbonates reduction technique.

With the use of high conductive ionomer Aemion™ HIEC, the Fe-N-C was able to achieve and maintain its performance at high current density. The performance of Fe-N-C is similar after subjecting to 5000 degradation cycles with the onset of 0.801 V_{RHE} and approached limiting current density of 2 A/cm^2 at 0.53 V_{RHE}. Similarly, the OCV value for measurements is similar $\simeq$1.0 V_{RHE} with a Tafel slope of 110.2 mV/dec in low current density region of 0.1 mA/cm^2 to 10 mA/cm^2 from 0.8-1.0 V_{RHE}. The Tafel slope then increased to 142.55 mV/dec at high current density region, and it can be seen in Figure

4.35 that the Tafel slope of both measurements is linear and almost similar which shows that not severe degradation occurs in the system. The high stability of Fe-N-C shows that with Aemion™ ionomer can cope the hydration level of the nucleophile. All the experiments conducted in 1.0 M KOH, high electrolyte concentration corresponds to less water content resulting in high viscosity. Therefore, it will be interesting to investigate the low concentration/less viscous electrolyte to observe the effect on stability [290]. As approaching to high current density, the cathode is subjected to water starvation which leads to severe hydration of anion exchange material and thus the catalyst will be acquiring high activation energy and overpotentials, which can be seen in the polarization curve.

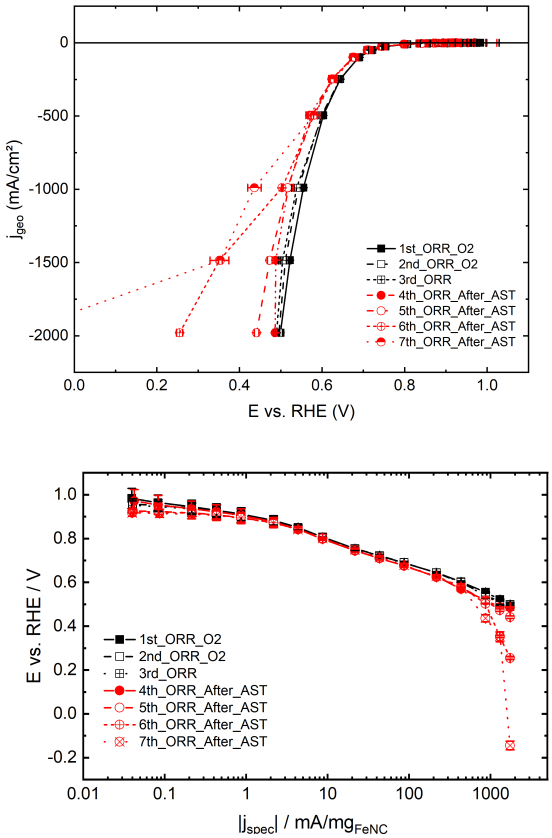

Figure 4.35: The stability of optimized Fe-N-C (1.18 mg/cm^2 with HIEC before and after ORR in Polarization curve (top) and Tafel curve(bottom)

4.3.6 Impact of non-Optimize Fe-N-C with H^+ Conducting Ionomer Nafion™in 1.0 M $HClO_4$

The Fe-N-C in the acid electrolyte has been studied in past years, but it still hasn't gained much attention due to low initial activity for ORR [14, 291–293]. To see the effect of type of ionomer, Nafion™is added to

Fe-N-C Pajarito Powder, and the effect can be seen in the polarization curve Figure 4.36. The catalyst was subjected to sequential ORR in O_2 to investigate any effect on the performance. The activity of catalyst degrades gradually with less positive onset and approach to mass transport limitation without reaching to the limiting current density of GDE i.e. 2 A/cm^2. In the first ORR measurement, the Fe-N-C approached to 930 mA/cm^2 at 0.1 V_{RHE} which reduced to 750 mA/cm^2 at 0.1 V_{RHE} for second and third (after 5000 degradation cycles) ORR measurement.

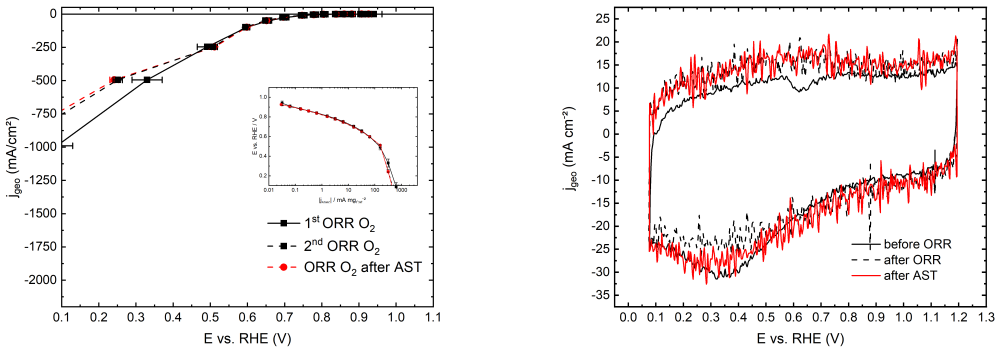

Figure 4.36: Severe degradation of Fe-N-C with proton conducting ionomer in acid electrolyte

Now, if we look in CVs Figure 4.36, the voltammogram is not stable with fluctuation in current density in both scans, and the pseudocapacitance is changing with increasing potential. The disturbance in the system yet not enabled GDE to investigate the catalyst layer properties as the problem is continuous since we have got reproducible results for this experiment. Now taking consideration of Fe-N-C, the catalyst is optimized for AEMFC alkaline solution, especially KOH electrolyte. The Nafion is mostly used for PGM catalyst as a binder in PEMFC, and the iron is most subjected to corrosion and dissolution in acid. Although Fe-N-C showed a suitable activity for ORR in acid, its combination with different electrocatalyst is a broad field of research. Now taking consideration of FeNC and Nafion™, the catalyst is not optimized for PEMFC. The Fe-N-C is subjected to degradation which can be suspected of different routes such as surface oxidation, carbon corrosion, protonation of N-group and demtallation [294]. The ORR selectivity and activity of Fe-N-C Pajarito Powder is higher in alkaline electrolyte KOH as reported in chapter 2 as compared to acid due to the more robust and more accessible binding to HO_2^- as these ions are predominant in KOH while the affinity is lower for H_2O_2. The condition can also be affected if the Fe-N-C with Nafion as we know that Nafion is mostly used in PEMFC due to its excellent conductivity (78 mS/cm) for H^+ ions transportation [295], which in case of AEMFC, the Nafion conductivity for ions transport is 2-20 mS/cm [296]. Nafion is also known for high water absorption ionomer which can significantly dry out the cathode if not subjected to highly humidified O_2 as the ionomer absorbed

water within its structure. If this is true for our system, then degradation by dry condition lead to Hofmann elimination resulting in loss of functional group in polymer. It has been found previously that the formation of H_2O_2 in the presence of Fe-N-C is pH-dependent as acidic pH range is more selective to H_2O_2 and Fe cations leading to reactive oxygen species formation [294]. However, there is not much research available for the proper understanding of the combination of Fe-N-C with Nafion degradation on a molecular level, and there is still a gap to identify the root cause of the problem either the problem lies in the conduction of ionomer or the water management issue causes the observable performance degradation.

5

Conclusion

Contents

5.1 Conclusions

To address the challenges of benchmarking the electrocatalyst for ORR, a novel optimized GDE half cell was used for this research to bridge the gap between fundamental and applied techniques such as RDE and MEA. In this research, the catalyst layers were optimized with GDE and investigated for the activity behaviour of ORR at high current density (2 A/cm^2) approaching to MEA and reproducible and reliable results similar to RDE. The novelty of GDE half cell is that the conditions can be created to mimic the fuel cell environment and can be used for PEMFC and AEMFC electrocatalyst investigation. This broadens the aspect of investigation and characterization of numerous types of catalysts such as PGM and non PGM to optimize their ORR performance by the effect of several procedures, i.e. break-in, stress cycling, ionomer activation and cold start. With all those benefits, there is still a gap to investigate the water management issues which flooding in case of PEMFC and low hydration level in case of AEMFC electrocatalyst. In this research, all research objectives were met to analyze the versatility of GDE half cell investigation. The electrolyte and membrane can affect the performance of ORR electrocatalyst as observed in the commercial Pt/C with and without membrane in a different acid electrolyte ($HClO_4$ and H_2SO_4). The type of electrolyte and addition of membrane have an effect on the ORR performance of Pt/C. The ECSA of Pt/C HISPEC 4000 in GDE was 66.59 m^2/g_{pt} in 1.0 M $HClO_4$, 61.55 m^2/g_{pt} in 1.0 M H_2SO_4 without membrane and 53.67 m^2/g_{pt} in 1.0 M $HClO_4$ with membrane and 25.49 m^2/g_{pt} in 1.0 M H_2SO_4 without membrane. The ECSA of samples with the membrane is near to the specified ECSA of HISPEC-4000 that is 60 m^2/g_{pt}. The addition of membrane reduced the ECSA due to the blockage of the active site, but the samples were more stable in $HClO_4 > H_2SO_4$. The gas purging from the back of electrode also influenced the ORR activity of commercial Pt/C, oxygen and synthetic air was compared, and the samples attain severe mass transport limitation in synthetic air due to low concentration of O_2 with a loss of activity of 1 A/cm^2. The radical chlorine and sulfate ions can poison the catalyst activity, and the probability of Pt dissolution is high due to uncertain events of amplifier overloading. It has been found that diprotic effect of H_2SO_4 can limit the activity of commercial Pt/C and the higher affinity to sulfate ions on catalyst layer can reduce the performance and subjected to high mass transport limitation, and it can be overcome with the introduction of ion-conducting Nafion™membrane. The Pt/C HISPEC 4000 with the loading of 0.3 mg/cm^2 approached to limiting current density of 2 A/cm^2 at 0.63V_{RHE} in 1.0 M $HClO_4$, the catalyst showed very high performance in KOH in contrast to the literature which shows the overestimation of performance, and it is considered as a drawback in GDE half cell measurements. The difference in sweeps mainly due to water management issue, can disturb the correct investigation of ORR activity. The advanced Pt/HGS was investigated in 1.0 M $HClO_4$ to validate the results from the producers that it can reach to maximum activity after subjecting to 10k degradation cycles. It is stated in past research that during the synthesis of Pt/HGS, the carbon that limits the non-particles performance deposited during high-temperature annealing can be reduced by continuous cycling which

is confirmed by this research the highest activity was achieved after 10k stress cycling AST. Pt/HGS approached to the high surface area of over 60 m^2/g_{pt}, similar to the commercial Pt/C-HISPEC but the activity was not comparable. The effect of loading showed an influence on ORR activity as Pt/HGS with 0.1 mg/cm^2 achieved the highest activation of 0.63 V_{RHE} in its most active state, and it has been found that pores flooding issue can influence the disturbance during ORR determination. However, it is not much compared to commercial Pt/C activity in literature and several issues regarding flooding of flooding and forward/backward scan difference was also addressed in this research. Finally, the GDE half-cell was conditioned to mimic the AEMFC for the optimization of non PGM electrocatalyst Fe-N-C (Pajarito powder) and high anion conducting ionomer Aemion™ with different ion exchange capacity. The catalyst layer was optimized by immersing the catalyst coated GDL in 1.0 M KOH for 48 hours demonstrating the best performance and the catalyst showed very high and uniform stability with 5000 AST cycles in the potential sweep of 0.6-1.0 V_{RHE}. However, the gap still exists to reach the performance of highly efficient Pt/C and alloys, Fe-N-C is a stable and cheap catalyst, but it is subjected to carbonation with atmospheric CO_2 in KOH and low activity. Several other investigations can be done in GDE such as ECSA determination by CO stripping to tackle the issues we faced during H_2 stripping and investigation of Pt-alloys for ORR in the half cell. Due to quick and fast track GDE methods, it is possible to investigate numerous catalysts in a short period of time quickly, but this investigation sometimes does not tell the full story such as catalyst morphological changes during cycling, the amount of catalyst dissolution, these properties investigation can be accommodated by combining GDE with other tools such as transmission electron microscopy TEM and scanning flow cell- Inductively coupled plasma ICP mass spectrometer for future work.

Bibliography

[1] IEA, "Renewables Information (2019 edition)," *IEA Statistics*, 2019.

[2] European Environmental Agency, "Greenhouse gas emissions from transport in Europe," Tech. Rep., 2019. [Online]. Available: https://www.eea.europa.eu/data-and-maps/indicators/transport-emissions-of-greenhouse-gases/transport-emissions-of-greenhouse-gases-12

[3] Adria Wilson, Gregory Kleen and D. Papageorgopoulos, "Fuel Cell System Cost -2017 DOE Hydrogen and Fuel Cells Program Record," Department of Energy USA, Tech. Rep., 2017. [Online]. Available: https://www.hydrogen.energy.gov/pdfs/17007_fuel_cell_system_cost_2017.pdf

[4] B. Pivovar, "Catalysts for fuel cell transportation and hydrogen related uses," *Nature Catalysis*, vol. 2, no. 7, pp. 562–565, jul 2019. [Online]. Available: http://www.nature.com/articles/s41929-019-0320-9

[5] X. X. Wang, M. T. Swihart, and G. Wu, "Achievements, challenges and perspectives on cathode catalysts in proton exchange membrane fuel cells for transportation," *Nature Catalysis*, vol. 2, no. 7, pp. 578–589, 2019. [Online]. Available: http://dx.doi.org/10.1038/s41929-019-0304-9

[6] B. N. Popov, J.-W. Lee, A. Kriston, and T. Kim, "Review—Development of Highly Active and Durable Hybrid Compressive Platinum Lattice Catalysts for Polymer Electrolyte Membrane Fuel Cells: Mathematical Modeling and Experimental Work," *Journal of The Electrochemical Society*, vol. 167, no. 5, p. 054512, feb 2020. [Online]. Available: https://iopscience.iop.org/article/10.1149/1945-7111/ab6bc6

[7] M. K. Debe, "Electrocatalyst approaches and challenges for automotive fuel cells," *Nature*, vol. 486, no. 7401, pp. 43–51, 2012. [Online]. Available: http://dx.doi.org/10.1038/nature11115

[8] S. Sui, X. Wang, X. Zhou, Y. Su, S. Riffat, and C.-j. Liu, "A comprehensive review of Pt electrocatalysts for the oxygen reduction reaction: Nanostructure, activity, mechanism and carbon support in PEM fuel cells," *Journal of Materials Chemistry A*, vol. 5, no. 5, pp. 1808–1825, 2017. [Online]. Available: http://xlink.rsc.org/?DOI=C6TA08580F

[9] Y. Li, X. Liu, L. Zheng, J. Shang, X. Wan, R. Hu, X. Guo, S. Hong, and J. Shui, "Preparation of Fe–N–C catalysts with FeN x (x = 1, 3, 4) active sites and comparison of their activities for the oxygen reduction reaction and performances in proton exchange membrane fuel cells," *Journal of Materials Chemistry A*, vol. 7, no. 45, pp. 26 147–26 153, 2019. [Online]. Available: http://xlink.rsc.org/?DOI=C9TA08532G

[10] S. Martens, L. Asen, G. Ercolano, F. Dionigi, C. Zalitis, A. Hawkins, A. Martinez, L. Seidl, A. C. Knoll, J. Sharman, P. Strasser, D. Jones, and O. Schneider, "A comparison of rotating disc electrode , fl oating electrode technique and membrane electrode assembly measurements for catalyst testing," *Journal of Power Sources*, vol. 392, no. January, pp. 274–284, 2018. [Online]. Available: https://doi.org/10.1016/j.jpowsour.2018.04.084

[11] K. Mayrhofer, D. Strmcnik, B. Blizanac, V. Stamenkovic, M. Arenz, and N. Markovic, "Measurement of oxygen reduction activities via the rotating disc electrode method: From Pt model surfaces to carbon-supported high surface area catalysts," *Electrochimica Acta*, vol. 53, no. 7, pp. 3181–3188, feb 2008. [Online]. Available: https://linkinghub.elsevier.com/retrieve/pii/S0013468607014272

[12] E. Pizzutilo, J. Knossalla, S. Geiger, J.-P. Grote, G. Polymeros, C. Baldizzone, S. Mezzavilla, M. Ledendecker, A. Mingers, S. Cherevko, F. Schüth, and K. J. J. Mayrhofer, "The Space Confinement Approach Using Hollow Graphitic Spheres to Unveil Activity and Stability of Pt-Co Nanocatalysts for PEMFC," *Advanced Energy Materials*, vol. 7, no. 20, p. 1700835, oct 2017. [Online]. Available: http://doi.wiley.com/10.1002/aenm.201700835

[13] R. Yang, J. Leisch, P. Strasser, and M. F. Toney, "Structure of Dealloyed PtCu 3 Thin Films and Catalytic Activity for Oxygen Reduction," *Chemistry of Materials*, vol. 22, no. 16, pp. 4712–4720, aug 2010. [Online]. Available: https://pubs.acs.org/doi/10.1021/cm101090p

[14] F. Jaouen, V. Goellner, M. Lefèvre, J. Herranz, E. Proietti, and J. Dodelet, "Oxygen reduction activities compared in rotating-disk electrode and proton exchange membrane fuel cells for highly active FeNC catalysts," *Electrochimica Acta*, vol. 87, pp. 619–628, jan 2013. [Online]. Available: https://linkinghub.elsevier.com/retrieve/pii/S0013468612015204

[15] K. Ehelebe, D. Seeberger, M. T. Y. Paul, S. Thiele, K. J. J. Mayrhofer, and S. Cherevko, "Evaluating Electrocatalysts at Relevant Currents in a Half-Cell: The Impact of Pt Loading on Oxygen Reduction Reaction," *Journal of The Electrochemical Society*, vol. 166, no. 16, pp. F1259–F1268, nov 2019. [Online]. Available: https://iopscience.iop.org/article/10.1149/2.0911915jes

[16] E4tech, J. Matthey, and U. G. Survey, "Platinum reserves applications, demand and statistics," 2020.

[17] F. Fuel Cell Technologies Office, "DOE Technical Targets for Polymer Electrolyte Membrane Fuel Cell Components," *Office of Energy Efficiency & Renewable Energy*, 2017.

[18] O. Z. Sharaf and M. F. Orhan, "An overview of fuel cell technology: Fundamentals and applications," *Renewable and Sustainable Energy Reviews*, vol. 32, pp. 810–853, apr 2014. [Online]. Available: https://linkinghub.elsevier.com/retrieve/pii/S1364032114000227

[19] M. K. Mahapatra and P. Singh, "Fuel Cells," in *Future Energy*. Elsevier, dec 2014, pp. 511–547. [Online]. Available: https://linkinghub.elsevier.com/retrieve/pii/B9780080994246000247

[20] C. L. Ludwig Mond, "V. A new form of gas battery," *Proceedings of the Royal Society of London*, vol. 46, no. 280-285, pp. 296–304, dec 1890. [Online]. Available: https://royalsocietypublishing.org/doi/10.1098/rspl.1889.0036

[21] U. Lucia, "Overview on fuel cells," *Renewable and Sustainable Energy Reviews*, vol. 30, pp. 164–169, feb 2014. [Online]. Available: https://linkinghub.elsevier.com/retrieve/pii/S1364032113006965

[22] A. Kirubakaran, S. Jain, and R. Nema, "A review on fuel cell technologies and power electronic interface," *Renewable and Sustainable Energy Reviews*, vol. 13, no. 9, pp. 2430–2440, dec 2009. [Online]. Available: https://linkinghub.elsevier.com/retrieve/pii/S1364032109000872

[23] F. de Bruijn, "The current status of fuel cell technology for mobile and stationary applications," *Green Chemistry*, vol. 7, no. 3, p. 132, 2005. [Online]. Available: http://xlink.rsc.org/?DOI=b415317k

[24] X. LI and I. SABIR, "Review of bipolar plates in PEM fuel cells: Flow-field designs," *International Journal of Hydrogen Energy*, vol. 30, no. 4, pp. 359–371, mar 2005. [Online]. Available: https://linkinghub.elsevier.com/retrieve/pii/S0360319904003453

[25] A. El-kharouf and B. G. Pollet, "Gas Diffusion Media and their Degradation," in *Polymer Electrolyte Fuel Cell Degradation*. Elsevier, 2012, pp. 215–247. [Online]. Available: https://linkinghub.elsevier.com/retrieve/pii/B9780123869364100041

[26] E. Passalacqua, F. Lufrano, G. Squadrito, A. Patti, and L. Giorgi, "Nafion content in the catalyst layer of polymer electrolyte fuel cells: effects on structure and performance," *Electrochimica Acta*, vol. 46, no. 6, pp. 799–805, jan 2001. [Online]. Available: https://linkinghub.elsevier.com/retrieve/pii/S0013468600006794

[27] T. A. Zawodzinski, "A Comparative Study of Water Uptake By and Transport Through Ionomeric Fuel Cell Membranes," *Journal of The Electrochemical Society*, vol. 140, no. 7, p. 1981, 1993. [Online]. Available: https://iopscience.iop.org/article/10.1149/1.2220749

[28] S. M. Haile, "Fuel cell materials and components, The Golden Jubilee Issue—Selected topics in Materials Science and Engineering: Past, Present and Future, edited by S. Suresh." *Acta Materialia*, vol. 51, no. 19, pp. 5981–6000, nov 2003. [Online]. Available: https://linkinghub.elsevier.com/retrieve/pii/S1359645403004737

[29] Q. He, "Development of novel anodic and cathodic materials applied in proton exchange membrane, direct methanol, alkaline and phosphoric acid fuel cells," Ph.D. dissertation, 2010. [Online]. Available: http://hdl.handle.net/2047/d20000290

[30] L. Carrette, K. A. Friedrich, and U. Stimming, "Fuel Cells - Fundamentals and Applications," *Fuel Cells*, vol. 1, no. 1, pp. 5–39, may 2001. [Online]. Available: https://doi.org/10.1002/1615-6854(200105)1:1⟨5::AID-FUCE5⟩3.0.CO;2-G

[31] S. Peighambardoust, S. Rowshanzamir, and M. Amjadi, "Review of the proton exchange membranes for fuel cell applications," *International Journal of Hydrogen Energy*, vol. 35, no. 17, pp. 9349–9384, sep 2010. [Online]. Available: https://linkinghub.elsevier.com/retrieve/pii/S0360319910009523

[32] J. Zhang, *PEM Fuel Cell Electrocatalysts and Catalyst Layers*, J. Zhang, Ed. London: Springer London, 2008. [Online]. Available: http://link.springer.com/10.1007/978-1-84800-936-3

[33] F. Barbir, *PEM Fuel Cells*. Elsevier, 2005. [Online]. Available: https://linkinghub.elsevier.com/retrieve/pii/B9780120781423X50009

[34] X.-Z. Yuan, C. Song, H. Wang, and J. Zhang, *Electrochemical Impedance Spectroscopy in PEM Fuel Cells*. London: Springer London, 2010. [Online]. Available: http://link.springer.com/10.1007/978-1-84882-846-9

[35] R. O'Hayre, S.-W. Cha, W. Colella, and F. B. Prinz, "Chapter 3: Fuel Cell Reaction Kinetics," in *Fuel Cell Fundamentals*. Hoboken, NJ, USA: John Wiley & Sons, Inc, apr 2016, pp. 77–116. [Online]. Available: http://doi.wiley.com/10.1002/9781119191766.ch3

[36] T. Yoshida and K. Kojima, "Toyota MIRAI Fuel Cell Vehicle and Progress Toward a Future Hydrogen Society," *Interface magazine*, vol. 24, no. 2, pp. 45–49, jan 2015. [Online]. Available: https://iopscience.iop.org/article/10.1149/2.F03152if

[37] N. M. Markovic, "Interfacing electrochemistry," *Nature Materials*, vol. 12, no. 2, pp. 101–102, feb 2013. [Online]. Available: http://www.nature.com/articles/nmat3554

[38] R. O'Hayre, S.-W. Cha, W. Colella, and F. B. Prinz, *Fuel Cell Fundamentals*. Hoboken, NJ, USA: John Wiley & Sons, Inc, may 2016. [Online]. Available: http://doi.wiley.com/10.1002/9781119191766

[39] L. R. F. Allen J. Bard, *Electrochemical Methods, Fundamental Applications*, 2000. [Online]. Available: https://www.wiley.com/en-ir/Electrochemical+Methods:+Fundamentals+and+Applications,+2nd+Edition-p-9780471043720

[40] H. Wang, X. Z. Yuan, and H. Li, *PEM fuel cell diagnostic tools*, 2011.

[41] H. A. Gasteiger, S. S. Kocha, B. Sompalli, and F. T. Wagner, "Activity benchmarks and requirements for Pt, Pt-alloy, and non-Pt oxygen reduction catalysts for PEMFCs," *Applied Catalysis B: Environmental*, vol. 56, no. 1-2, pp. 9–35, mar 2005. [Online]. Available: https://linkinghub.elsevier.com/retrieve/pii/S0926337304004941

[42] M. Warshay and P. R. Prokopius, "The fuel cell in space: yesterday, today and tomorrow," *Journal of Power Sources*, vol. 29, no. 1-2, pp. 193–200, jan 1990. [Online]. Available: https://linkinghub.elsevier.com/retrieve/pii/037877539080019A

[43] J. W. Patrick, "Handbook of fuel cells. Fundamentals technology and applications," *Fuel*, vol. 83, no. 4-5, p. 623, mar 2004. [Online]. Available: https://linkinghub.elsevier.com/retrieve/pii/S0016236103003296

[44] C. Song, Y. Tang, J. L. Zhang, J. Zhang, H. Wang, J. Shen, S. McDermid, J. Li, and P. Kozak, "PEM fuel cell reaction kinetics in the temperature range of 23–120°C," *Electrochimica Acta*, vol. 52, no. 7, pp. 2552–2561, feb 2007. [Online]. Available: https://linkinghub.elsevier.com/retrieve/pii/S0013468606009583

[45] M. E. Youssef, R. Amin, and K. El-Khatib, "Development and performance analysis of PEMFC stack based on bipolar plates fabricated employing different designs," *Arabian Journal of Chemistry*, vol. 11, no. 5, pp. 609–614, jul 2018. [Online]. Available: https://linkinghub.elsevier.com/retrieve/pii/S1878535215002208

[46] B. K. Kakati and V. Mohan, "Development of Low-Cost Advanced Composite Bipolar Plate for Proton Exchange Membrane Fuel Cell?" *Fuel Cells*, vol. 8, no. 1, pp. 45–51, feb 2008. [Online]. Available: http://doi.wiley.com/10.1002/fuce.200700008

[47] P. Lettenmeier, R. Wang, R. Abouatallah, B. Saruhan, O. Freitag, P. Gazdzicki, T. Morawietz, R. Hiesgen, A. S. Gago, and K. A. Friedrich, "Low-Cost and Durable Bipolar Plates for Proton Exchange Membrane Electrolyzers," *Scientific Reports*, vol. 7, no. 1, p. 44035, apr 2017. [Online]. Available: http://www.nature.com/articles/srep44035

[48] O. Alo, I. Otunniyi, H. Pienaar, and S. Iyuke, "Materials for Bipolar Plates in Polymer Electrolyte Membrane Fuel Cell: Performance Criteria and Current Benchmarks," *Procedia*

Manufacturing, vol. 7, pp. 395–401, 2017. [Online]. Available: https://linkinghub.elsevier.com/retrieve/pii/S2351978916301743

[49] L. Cindrella, A. Kannan, J. Lin, K. Saminathan, Y. Ho, C. Lin, and J. Wertz, "Gas diffusion layer for proton exchange membrane fuel cells—A review," *Journal of Power Sources*, vol. 194, no. 1, pp. 146–160, oct 2009. [Online]. Available: https://linkinghub.elsevier.com/retrieve/pii/S0378775309006399

[50] J. Chen, T. Matsuura, and M. Hori, "Novel gas diffusion layer with water management function for PEMFC," *Journal of Power Sources*, vol. 131, no. 1-2, pp. 155–161, may 2004. [Online]. Available: https://linkinghub.elsevier.com/retrieve/pii/S0378775304000345

[51] A. Nabovati, J. Hinebaugh, A. Bazylak, and C. H. Amon, "Effect of porosity heterogeneity on the permeability and tortuosity of gas diffusion layers in polymer electrolyte membrane fuel cells," *Journal of Power Sources*, vol. 248, pp. 83–90, feb 2014. [Online]. Available: https://linkinghub.elsevier.com/retrieve/pii/S0378775313015577

[52] G. Sasikumar, J. Ihm, and H. Ryu, "Dependence of optimum Nafion content in catalyst layer on platinum loading," *Journal of Power Sources*, vol. 132, no. 1-2, pp. 11–17, may 2004. [Online]. Available: https://linkinghub.elsevier.com/retrieve/pii/S0378775304001272

[53] W. Daud, R. Rosli, E. Majlan, S. Hamid, R. Mohamed, and T. Husaini, "PEM fuel cell system control: A review," *Renewable Energy*, vol. 113, pp. 620–638, dec 2017. [Online]. Available: https://linkinghub.elsevier.com/retrieve/pii/S0960148117305281

[54] N. F. Asri, T. Husaini, A. B. Sulong, E. H. Majlan, and W. R. W. Daud, "Coating of stainless steel and titanium bipolar plates for anticorrosion in PEMFC: A review," *International Journal of Hydrogen Energy*, vol. 42, no. 14, pp. 9135–9148, apr 2017. [Online]. Available: https://linkinghub.elsevier.com/retrieve/pii/S0360319915311708

[55] M. M. Whiston, I. L. Azevedo, S. Litster, K. S. Whitefoot, C. Samaras, and J. F. Whitacre, "Expert assessments of the cost and expected future performance of proton exchange membrane fuel cells for vehicles," *Proceedings of the National Academy of Sciences*, vol. 116, no. 11, pp. 4899–4904, mar 2019. [Online]. Available: http://www.pnas.org/lookup/doi/10.1073/pnas.1804221116

[56] J. Wang, H. Wang, and Y. Fan, "Techno-Economic Challenges of Fuel Cell Commercialization," *Engineering*, vol. 4, no. 3, pp. 352–360, jun 2018. [Online]. Available: https://linkinghub.elsevier.com/retrieve/pii/S2095809917307750

[57] R. T. White, S. H. Eberhardt, Y. Singh, T. Haddow, M. Dutta, F. P. Orfino, and E. Kjeang, "Four-dimensional joint visualization of electrode degradation and liquid water distribution inside

operating polymer electrolyte fuel cells," *Scientific Reports*, vol. 9, no. 1, p. 1843, dec 2019. [Online]. Available: http://www.nature.com/articles/s41598-018-38464-9

[58] J. Brunton, E. Coyle, D. Kennedy, H. Schmidt-Walter, H. J. Kohnke, G. Sauer, S. Schudt, and J. P. Hamilton, "Engineering of a Single Alkaline Fuel Cell Part I: Construction of a Test Bed," *i-manager's Journal on Electrical Engineering*, vol. 2, no. 3, pp. 8–17, mar 2009. [Online]. Available: http://www.imanagerpublications.com/article/253

[59] F. Bidault, D. Brett, P. Middleton, and N. Brandon, "Review of gas diffusion cathodes for alkaline fuel cells," *Journal of Power Sources*, vol. 187, no. 1, pp. 39–48, feb 2009. [Online]. Available: https://linkinghub.elsevier.com/retrieve/pii/S0378775308019897

[60] J. Garche, *Encyclopedia of Electrochemical Power Sources*. Elsevier, 2009. [Online]. Available: https://linkinghub.elsevier.com/retrieve/pii/C20091283584

[61] G. McLean, "An assessment of alkaline fuel cell technology," *International Journal of Hydrogen Energy*, vol. 27, no. 5, pp. 507–526, may 2002. [Online]. Available: https://linkinghub.elsevier.com/retrieve/pii/S0360319901001811

[62] V. M. Truong, N. B. Duong, C.-L. Wang, and H. Yang, "Effects of Cell Temperature and Reactant Humidification on Anion Exchange Membrane Fuel Cells," *Materials*, vol. 12, no. 13, p. 2048, jun 2019. [Online]. Available: https://www.mdpi.com/1996-1944/12/13/2048

[63] J. Larminie and A. Dicks, *Fuel Cell Systems Explained*. West Sussex, England: John Wiley & Sons, Ltd,., feb 2003. [Online]. Available: http://doi.wiley.com/10.1002/9781118878330

[64] F. Xu, Y. Su, and B. Lin, "Progress of Alkaline Anion Exchange Membranes for Fuel Cells: The Effects of Micro-Phase Separation," *Frontiers in Materials*, vol. 7, feb 2020. [Online]. Available: https://www.frontiersin.org/article/10.3389/fmats.2020.00004/full

[65] S. Suzuki, H. Muroyama, T. Matsui, and K. Eguchi, "Influence of CO2 dissolution into anion exchange membrane on fuel cell performance," *Electrochimica Acta*, vol. 88, pp. 552–558, jan 2013. [Online]. Available: https://linkinghub.elsevier.com/retrieve/pii/S0013468612017197

[66] G. Li, Y. Wang, J. Pan, J. Han, Q. Liu, X. Li, P. Li, C. Chen, L. Xiao, J. Lu, and L. Zhuang, "Carbonation effects on the performance of alkaline polymer electrolyte fuel cells," *International Journal of Hydrogen Energy*, vol. 40, no. 20, pp. 6655–6660, jun 2015. [Online]. Available: https://linkinghub.elsevier.com/retrieve/pii/S036031991500765X

[67] G. Merle, S. S. Hosseiny, M. Wessling, and K. Nijmeijer, "New cross-linked PVA based polymer electrolyte membranes for alkaline fuel cells," *Journal of Membrane Science*, vol.

409-410, pp. 191–199, aug 2012. [Online]. Available: https://linkinghub.elsevier.com/retrieve/pii/S0376738812002475

[68] J. Zhang, T. Zhou, J. Qiao, Y. Liu, and J. Zhang, "Hydroxyl anion conducting membranes poly(vinyl alcohol)/poly(diallyldimethylammonium chloride) for alkaline fuel cell applications: Effect of molecular weight," *Electrochimica Acta*, vol. 111, pp. 351–358, nov 2013. [Online]. Available: https://linkinghub.elsevier.com/retrieve/pii/S0013468613014667

[69] M. Tanaka, K. Fukasawa, E. Nishino, S. Yamaguchi, K. Yamada, H. Tanaka, B. Bae, K. Miyatake, and M. Watanabe, "Anion Conductive Block Poly(arylene ether)s: Synthesis, Properties, and Application in Alkaline Fuel Cells," *Journal of the American Chemical Society*, vol. 133, no. 27, pp. 10 646–10 654, jul 2011. [Online]. Available: https://pubs.acs.org/doi/10.1021/ja204166e

[70] Y. Zhao, H. Yu, D. Yang, J. Li, Z. Shao, and B. Yi, "High-performance alkaline fuel cells using crosslinked composite anion exchange membrane," *Journal of Power Sources*, vol. 221, pp. 247–251, jan 2013. [Online]. Available: https://linkinghub.elsevier.com/retrieve/pii/S0378775312013511

[71] X. Wang, M. Li, B. T. Golding, M. Sadeghi, Y. Cao, E. H. Yu, and K. Scott, "A polytetrafluoroethylene-quaternary 1,4-diazabicyclo-[2.2.2]-octane polysulfone composite membrane for alkaline anion exchange membrane fuel cells," *International Journal of Hydrogen Energy*, vol. 36, no. 16, pp. 10 022–10 026, aug 2011. [Online]. Available: https://linkinghub.elsevier.com/retrieve/pii/S0360319911012602

[72] Y. Zhao, J. Pan, H. Yu, D. Yang, J. Li, L. Zhuang, Z. Shao, and B. Yi, "Quaternary ammonia polysulfone-PTFE composite alkaline anion exchange membrane for fuel cells application," *International Journal of Hydrogen Energy*, vol. 38, no. 4, pp. 1983–1987, feb 2013. [Online]. Available: https://linkinghub.elsevier.com/retrieve/pii/S0360319912025013

[73] N. Li, Y. Leng, M. A. Hickner, and C.-Y. Wang, "Highly Stable, Anion Conductive, Comb-Shaped Copolymers for Alkaline Fuel Cells," *Journal of the American Chemical Society*, vol. 135, no. 27, pp. 10 124–10 133, jul 2013. [Online]. Available: https://pubs.acs.org/doi/10.1021/ja403671u

[74] X. Ren, S. C. Price, A. C. Jackson, N. Pomerantz, and F. L. Beyer, "Highly Conductive Anion Exchange Membrane for High Power Density Fuel-Cell Performance," *ACS Applied Materials & Interfaces*, vol. 6, no. 16, pp. 13 330–13 333, aug 2014. [Online]. Available: https://pubs.acs.org/doi/10.1021/am503870g

[75] F. Zhang, H. Zhang, and C. Qu, "Imidazolium functionalized polysulfone anion exchange membrane for fuel cell application," *Journal of Materials Chemistry*, 2011.

[76] J. Ran, L. Wu, J. R. Varcoe, A. L. Ong, S. D. Poynton, and T. Xu, "Development of imidazolium-type alkaline anion exchange membranes for fuel cell application," *Journal of Membrane Science*, vol. 415-416, pp. 242–249, oct 2012. [Online]. Available: https://linkinghub.elsevier.com/retrieve/pii/S0376738812003705

[77] Y. Oshiba, J. Hiura, Y. Suzuki, and T. Yamaguchi, "Improvement in the solid-state alkaline fuel cell performance through efficient water management strategies," *Journal of Power Sources*, vol. 345, pp. 221–226, mar 2017. [Online]. Available: https://linkinghub.elsevier.com/retrieve/pii/S0378775317301210

[78] N. Ramaswamy and S. Mukerjee, "Alkaline Anion-Exchange Membrane Fuel Cells: Challenges in Electrocatalysis and Interfacial Charge Transfer," *Chemical Reviews*, vol. 119, no. 23, pp. 11 945–11 979, dec 2019. [Online]. Available: https://pubs.acs.org/doi/abs/10.1021/acs.chemrev.9b00157

[79] M. Mamlouk, K. Scott, J. Horsfall, and C. Williams, "The effect of electrode parameters on the performance of anion exchange polymer membrane fuel cells," *International Journal of Hydrogen Energy*, vol. 36, no. 12, pp. 7191–7198, jun 2011. [Online]. Available: https://linkinghub.elsevier.com/retrieve/pii/S0360319911006641

[80] Z. Pan, L. An, T. Zhao, and Z. Tang, "Advances and challenges in alkaline anion exchange membrane fuel cells," *Progress in Energy and Combustion Science*, vol. 66, pp. 141–175, may 2018. [Online]. Available: https://linkinghub.elsevier.com/retrieve/pii/S0360128517301673

[81] L. An and T. Zhao, "Transport phenomena in alkaline direct ethanol fuel cells for sustainable energy production," *Journal of Power Sources*, vol. 341, pp. 199–211, feb 2017. [Online]. Available: https://linkinghub.elsevier.com/retrieve/pii/S0378775316316846

[82] Y. Leng, G. Chen, A. J. Mendoza, T. B. Tighe, M. A. Hickner, and C.-Y. Wang, "Solid-State Water Electrolysis with an Alkaline Membrane," *Journal of the American Chemical Society*, vol. 134, no. 22, pp. 9054–9057, jun 2012. [Online]. Available: https://pubs.acs.org/doi/10.1021/ja302439z

[83] X. Ge, A. Sumboja, D. Wuu, T. An, B. Li, F. W. T. Goh, T. S. A. Hor, Y. Zong, and Z. Liu, "Oxygen Reduction in Alkaline Media: From Mechanisms to Recent Advances of Catalysts," *ACS Catalysis*, vol. 5, no. 8, pp. 4643–4667, aug 2015. [Online]. Available: https://pubs.acs.org/doi/10.1021/acscatal.5b00524

[84] H. S. Wroblowa, Yen-Chi-Pan, and G. Razumney, "Electroreduction of oxygen," *Journal of Electroanalytical Chemistry and Interfacial Electrochemistry*, vol. 69, no. 2, pp. 195–201, apr 1976. [Online]. Available: https://linkinghub.elsevier.com/retrieve/pii/S0022072876802501

[85] A. Morozan, B. Jousselme, and S. Palacin, "Low-platinum and platinum-free catalysts for the oxygen reduction reaction at fuel cell cathodes," *Energy & Environmental Science*, vol. 4, no. 4, p. 1238, 2011. [Online]. Available: http://xlink.rsc.org/?DOI=c0ee00601g

[86] I. Katsounaros, W. B. Schneider, J. C. Meier, U. Benedikt, P. U. Biedermann, A. A. Auer, and K. J. J. Mayrhofer, "Hydrogen peroxide electrochemistry on platinum: towards understanding the oxygen reduction reaction mechanism," *Physical Chemistry Chemical Physics*, vol. 14, no. 20, p. 7384, 2012. [Online]. Available: http://xlink.rsc.org/?DOI=c2cp40616k

[87] S. Siahrostami, A. Verdaguer-Casadevall, M. Karamad, D. Deiana, P. Malacrida, B. Wickman, M. Escudero-Escribano, E. A. Paoli, R. Frydendal, T. W. Hansen, I. Chorkendorff, I. E. L. Stephens, and J. Rossmeisl, "Enabling direct H2O2 production through rational electrocatalyst design," *Nature Materials*, vol. 12, no. 12, pp. 1137–1143, dec 2013. [Online]. Available: http://www.nature.com/articles/nmat3795

[88] M. Busch, N. B. Halck, U. I. Kramm, S. Siahrostami, P. Krtil, and J. Rossmeisl, "Beyond the top of the volcano? – A unified approach to electrocatalytic oxygen reduction and oxygen evolution," *Nano Energy*, vol. 29, pp. 126–135, nov 2016. [Online]. Available: https://linkinghub.elsevier.com/retrieve/pii/S2211285516300581

[89] S. Cheong, J. D. Watt, and R. D. Tilley, "Shape control of platinum and palladium nanoparticles for catalysis," *Nanoscale*, vol. 2, no. 10, p. 2045, 2010. [Online]. Available: http://xlink.rsc.org/?DOI=c0nr00276c

[90] N. M. Markovic, H. A. Gasteiger, and P. N. Ross, "Oxygen Reduction on Platinum Low-Index Single-Crystal Surfaces in Sulfuric Acid Solution: Rotating Ring-Pt(hkl) Disk Studies," *The Journal of Physical Chemistry*, vol. 99, no. 11, pp. 3411–3415, mar 1995. [Online]. Available: https://pubs.acs.org/doi/abs/10.1021/j100011a001

[91] H. Yano, M. Kataoka, H. Yamashita, H. Uchida, and M. Watanabe, "Oxygen Reduction Activity of Carbon-Supported Pt−M (M = V, Ni, Cr, Co, and Fe) Alloys Prepared by Nanocapsule Method," *Langmuir*, vol. 23, no. 11, pp. 6438–6445, may 2007. [Online]. Available: https://pubs.acs.org/doi/10.1021/la070078u

[92] M. Shao, A. Peles, and K. Shoemaker, "Electrocatalysis on Platinum Nanoparticles: Particle Size Effect on Oxygen Reduction Reaction Activity," *Nano Letters*, vol. 11, no. 9, pp. 3714–3719, sep 2011. [Online]. Available: https://pubs.acs.org/doi/10.1021/nl2017459

[93] W. Wang, Z. Wang, M. Yang, C.-J. Zhong, and C.-J. Liu, "Highly active and stable Pt (111) catalysts synthesized by peptide assisted room temperature electron reduction for

oxygen reduction reaction," *Nano Energy*, vol. 25, pp. 26–33, jul 2016. [Online]. Available: https://linkinghub.elsevier.com/retrieve/pii/S2211285516300775

[94] S. Sui, X. Wang, X. Zhou, Y. Su, S. Riffat, and C.-j. Liu, "A comprehensive review of Pt electrocatalysts for the oxygen reduction reaction: Nanostructure, activity, mechanism and carbon support in PEM fuel cells," *Journal of Materials Chemistry A*, vol. 5, no. 5, pp. 1808–1825, 2017. [Online]. Available: http://xlink.rsc.org/?DOI=C6TA08580F

[95] P. T. Yu, W. Gu, J. Zhang, R. Makharia, F. T. Wagner, and H. A. Gasteiger, "Carbon-Support Requirements for Highly Durable Fuel Cell Operation," in *Polymer Electrolyte Fuel Cell Durability*. New York, NY: Springer New York, 2009, pp. 29–53. [Online]. Available: http://link.springer.com/10.1007/978-0-387-85536-3{_}3

[96] X. Ren, Q. Lv, L. Liu, B. Liu, Y. Wang, A. Liu, and G. Wu, "Current progress of Pt and Pt-based electrocatalysts used for fuel cells," *Sustainable Energy & Fuels*, vol. 4, no. 1, pp. 15–30, 2020. [Online]. Available: http://xlink.rsc.org/?DOI=C9SE00460B

[97] S. Samad, K. S. Loh, W. Y. Wong, T. K. Lee, J. Sunarso, S. T. Chong, and W. R. Wan Daud, "Carbon and non-carbon support materials for platinum-based catalysts in fuel cells," *International Journal of Hydrogen Energy*, vol. 43, no. 16, pp. 7823–7854, apr 2018. [Online]. Available: https://linkinghub.elsevier.com/retrieve/pii/S0360319918306578

[98] J. Greeley, I. E. L. Stephens, A. S. Bondarenko, T. P. Johansson, H. A. Hansen, T. F. Jaramillo, J. Rossmeisl, I. Chorkendorff, and J. K. Nørskov, "Alloys of platinum and early transition metals as oxygen reduction electrocatalysts," *Nature Chemistry*, vol. 1, no. 7, pp. 552–556, oct 2009. [Online]. Available: http://www.nature.com/articles/nchem.367

[99] B. Gurau, R. Viswanathan, R. Liu, T. J. Lafrenz, K. L. Ley, E. S. Smotkin, E. Reddington, A. Sapienza, B. C. Chan, T. E. Mallouk, and S. Sarangapani, "Structural and Electrochemical Characterization of Binary, Ternary, and Quaternary Platinum Alloy Catalysts for Methanol Electro-oxidation 1," *The Journal of Physical Chemistry B*, vol. 102, no. 49, pp. 9997–10 003, dec 1998. [Online]. Available: https://pubs.acs.org/doi/10.1021/jp982887f

[100] K. Kusada, D. Wu, and H. Kitagawa, "New Aspects of Platinum Group Metal[U+2010]Based Solid[U+2010]Solution Alloy Nanoparticles: Binary to High[U+2010]Entropy Alloys," *Chemistry – A European Journal*, vol. 26, no. 23, pp. 5105–5130, apr 2020. [Online]. Available: https://onlinelibrary.wiley.com/doi/abs/10.1002/chem.201903928

[101] V. Jalan, "Importance of Interatomic Spacing in Catalytic Reduction of Oxygen in Phosphoric Acid," *Journal of The Electrochemical Society*, vol. 130, no. 11, p. 2299, 1983. [Online]. Available: https://iopscience.iop.org/article/10.1149/1.2119574

[102] B. A. Kakade, H. Wang, T. Tamaki, H. Ohashi, and T. Yamaguchi, "Enhanced oxygen reduction reaction by bimetallic CoPt and PdPt nanocrystals," *RSC Advances*, vol. 3, no. 26, p. 10487, 2013. [Online]. Available: http://xlink.rsc.org/?DOI=c3ra40920a

[103] Q. Jia, W. Liang, M. K. Bates, P. Mani, W. Lee, and S. Mukerjee, "Activity Descriptor Identification for Oxygen Reduction on Platinum-Based Bimetallic Nanoparticles: In Situ Observation of the Linear Composition–Strain–Activity Relationship," *ACS Nano*, vol. 9, no. 1, pp. 387–400, jan 2015. [Online]. Available: https://pubs.acs.org/doi/10.1021/nn506721f

[104] D. Kaewsai and M. Hunsom, "Comparative Study of the ORR Activity and Stability of Pt and PtM (M = Ni, Co, Cr, Pd) Supported on Polyaniline/Carbon Nanotubes in a PEM Fuel Cell," *Nanomaterials*, vol. 8, no. 5, p. 299, may 2018. [Online]. Available: http://www.mdpi.com/2079-4991/8/5/299

[105] X.-Y. Lang, G.-F. Han, B.-B. Xiao, L. Gu, Z.-Z. Yang, Z. Wen, Y.-F. Zhu, M. Zhao, J.-C. Li, and Q. Jiang, "Mesostructured Intermetallic Compounds of Platinum and Non-Transition Metals for Enhanced Electrocatalysis of Oxygen Reduction Reaction," *Advanced Functional Materials*, vol. 25, no. 2, pp. 230–237, jan 2015. [Online]. Available: http://doi.wiley.com/10.1002/adfm.201401868

[106] M. Ammam and E. B. Easton, "Oxygen reduction activity of binary PtMn/C, ternary PtMnX/C (X = Fe, Co, Ni, Cu, Mo and, Sn) and quaternary PtMnCuX/C (X = Fe, Co, Ni, and Sn) and PtMnMoX/C (X = Fe, Co, Ni, Cu and Sn) alloy catalysts," *Journal of Power Sources*, vol. 236, pp. 311–320, aug 2013. [Online]. Available: https://linkinghub.elsevier.com/retrieve/pii/S0378775313002942

[107] Y.-Y. Feng, G.-R. Zhang, J.-H. Ma, G. Liu, and B.-Q. Xu, "Carbon-supported Pt[U+2041]Ag nanostructures as cathode catalysts for oxygen reduction reaction," *Physical Chemistry Chemical Physics*, vol. 13, no. 9, p. 3863, 2011. [Online]. Available: http://xlink.rsc.org/?DOI=c0cp01612h

[108] S. Mukerjee and S. Srinivasan, "Enhanced electrocatalysis of oxygen reduction on platinum alloys in proton exchange membrane fuel cells," *Journal of Electroanalytical Chemistry*, vol. 357, no. 1-2, pp. 201–224, oct 1993. [Online]. Available: https://linkinghub.elsevier.com/retrieve/pii/002207289380380Z

[109] E. J. Coleman, M. H. Chowdhury, and A. C. Co, "Insights Into the Oxygen Reduction Reaction Activity of Pt/C and PtCu/C Catalysts," *ACS Catalysis*, vol. 5, no. 2, pp. 1245–1253, feb 2015. [Online]. Available: https://pubs.acs.org/doi/10.1021/cs501762g

[110] V. R. Stamenkovic, B. S. Mun, M. Arenz, K. J. J. Mayrhofer, C. A. Lucas, G. Wang, P. N. Ross, and N. M. Markovic, "Trends in electrocatalysis on extended and nanoscale Pt-bimetallic

alloy surfaces," *Nature Materials*, vol. 6, no. 3, pp. 241–247, mar 2007. [Online]. Available: http://www.nature.com/articles/nmat1840

[111] S. Zhang, X. Zhang, G. Jiang, H. Zhu, S. Guo, D. Su, G. Lu, and S. Sun, "Tuning Nanoparticle Structure and Surface Strain for Catalysis Optimization," *Journal of the American Chemical Society*, vol. 136, no. 21, pp. 7734–7739, may 2014. [Online]. Available: https://pubs.acs.org/doi/10.1021/ja5030172

[112] V. R. Stamenkovic, B. S. Mun, K. J. J. Mayrhofer, P. N. Ross, and N. M. Markovic, "Effect of Surface Composition on Electronic Structure, Stability, and Electrocatalytic Properties of Pt-Transition Metal Alloys: Pt-Skin versus Pt-Skeleton Surfaces," *Journal of the American Chemical Society*, vol. 128, no. 27, pp. 8813–8819, jul 2006. [Online]. Available: https://pubs.acs.org/doi/10.1021/ja0600476

[113] J. Wu and H. Yang, "Synthesis and electrocatalytic oxygen reduction properties of truncated octahedral Pt3Ni nanoparticles," *Nano Research*, vol. 4, no. 1, pp. 72–82, jan 2011. [Online]. Available: http://link.springer.com/10.1007/s12274-010-0049-x

[114] J. Wu, J. Zhang, Z. Peng, S. Yang, F. T. Wagner, and H. Yang, "Truncated Octahedral Pt 3 Ni Oxygen Reduction Reaction Electrocatalysts," *Journal of the American Chemical Society*, vol. 132, no. 14, pp. 4984–4985, apr 2010. [Online]. Available: https://pubs.acs.org/doi/10.1021/ja100571h

[115] H. Wang, S. Yin, Y. Xu, X. Li, A. A. Alshehri, Y. Yamauchi, H. Xue, Y. V. Kaneti, and L. Wang, "Direct fabrication of tri-metallic PtPdCu tripods with branched exteriors for the oxygen reduction reaction," *Journal of Materials Chemistry A*, vol. 6, no. 18, pp. 8662–8668, 2018. [Online]. Available: http://xlink.rsc.org/?DOI=C8TA01698D

[116] M. Escudero-Escribano, K. D. Jensen, and A. W. Jensen, "Recent advances in bimetallic electrocatalysts for oxygen reduction: design principles, structure-function relations and active phase elucidation," *Current Opinion in Electrochemistry*, vol. 8, pp. 135–146, mar 2018. [Online]. Available: https://linkinghub.elsevier.com/retrieve/pii/S2451910317301667

[117] J. Greeley and J. Nørskov, "Electrochemical dissolution of surface alloys in acids: Thermodynamic trends from first-principles calculations," *Electrochimica Acta*, vol. 52, no. 19, pp. 5829–5836, may 2007. [Online]. Available: https://linkinghub.elsevier.com/retrieve/pii/S0013468607003556

[118] M. Pourbaix, *Atlas of electrochemical equilibria in aqueous solutions*, 1974.

[119] I. E. L. Stephens, A. S. Bondarenko, U. Grønbjerg, J. Rossmeisl, and I. Chorkendorff, "Understanding the electrocatalysis of oxygen reduction on platinum and its alloys,"

Energy & Environmental Science, vol. 5, no. 5, p. 6744, 2012. [Online]. Available: http://xlink.rsc.org/?DOI=c2ee03590a

[120] M. Chen, S. Hwang, J. Li, S. Karakalos, K. Chen, Y. He, S. Mukherjee, D. Su, and G. Wu, "Pt alloy nanoparticles decorated on large-size nitrogen-doped graphene tubes for highly stable oxygen-reduction catalysts," *Nanoscale*, vol. 10, no. 36, pp. 17 318–17 326, 2018. [Online]. Available: http://xlink.rsc.org/?DOI=C8NR05888A

[121] M. Shao, Q. Chang, J.-P. Dodelet, and R. Chenitz, "Recent Advances in Electrocatalysts for Oxygen Reduction Reaction," *Chemical Reviews*, vol. 116, no. 6, pp. 3594–3657, mar 2016. [Online]. Available: https://pubs.acs.org/doi/10.1021/acs.chemrev.5b00462

[122] J. Zhang, F. H. B. Lima, M. H. Shao, K. Sasaki, J. X. Wang, J. Hanson, and R. R. Adzic, "Platinum Monolayer on Nonnoble Metal−Noble Metal Core−Shell Nanoparticle Electrocatalysts for O 2 Reduction," *The Journal of Physical Chemistry B*, vol. 109, no. 48, pp. 22 701–22 704, dec 2005. [Online]. Available: https://pubs.acs.org/doi/10.1021/jp055634c

[123] P. Mani, R. Srivastava, and P. Strasser, "Dealloyed Pt−Cu Core−Shell Nanoparticle Electrocatalysts for Use in PEM Fuel Cell Cathodes," *The Journal of Physical Chemistry C*, vol. 112, no. 7, pp. 2770–2778, feb 2008. [Online]. Available: https://pubs.acs.org/doi/10.1021/jp0776412

[124] K. A. Kuttiyiel, K. Sasaki, Y. Choi, D. Su, P. Liu, and R. R. Adzic, "Bimetallic IrNi core platinum monolayer shell electrocatalysts for the oxygen reduction reaction," *Energy Environ. Sci.*, vol. 5, no. 1, pp. 5297–5304, 2012. [Online]. Available: http://xlink.rsc.org/?DOI=C1EE02067F

[125] V. Mazumder, M. Chi, K. L. More, and S. Sun, "Core/Shell Pd/FePt Nanoparticles as an Active and Durable Catalyst for the Oxygen Reduction Reaction," *Journal of the American Chemical Society*, vol. 132, no. 23, pp. 7848–7849, jun 2010. [Online]. Available: https://pubs.acs.org/doi/10.1021/ja1024436

[126] M. Oezaslan, F. Hasché, and P. Strasser, "Pt-Based Core–Shell Catalyst Architectures for Oxygen Fuel Cell Electrodes," *The Journal of Physical Chemistry Letters*, vol. 4, no. 19, pp. 3273–3291, oct 2013. [Online]. Available: https://pubs.acs.org/doi/10.1021/jz4014135

[127] J. R. Kitchin, J. K. Nørskov, M. A. Barteau, and J. G. Chen, "Role of Strain and Ligand Effects in the Modification of the Electronic and Chemical Properties of Bimetallic Surfaces," *Physical Review Letters*, vol. 93, no. 15, p. 156801, oct 2004. [Online]. Available: https://link.aps.org/doi/10.1103/PhysRevLett.93.156801

[128] B. Corona, M. Howard, L. Zhang, and G. Henkelman, "Computational screening of core@shell nanoparticles for the hydrogen evolution and oxygen reduction reactions," *The*

Journal of Chemical Physics, vol. 145, no. 24, p. 244708, dec 2016. [Online]. Available: http://aip.scitation.org/doi/10.1063/1.4972579

[129] M. Shao, B. H. Smith, S. Guerrero, L. Protsailo, D. Su, K. Kaneko, J. H. Odell, M. P. Humbert, K. Sasaki, J. Marzullo, and R. M. Darling, "Core–shell catalysts consisting of nanoporous cores for oxygen reduction reaction," *Physical Chemistry Chemical Physics*, vol. 15, no. 36, p. 15078, 2013. [Online]. Available: http://xlink.rsc.org/?DOI=c3cp52252k

[130] X. Wang, B. He, Z. Hu, Z. Zeng, and S. Han, "Current advances in precious metal core–shell catalyst design," *Science and Technology of Advanced Materials*, vol. 15, no. 4, p. 043502, aug 2014. [Online]. Available: http://www.tandfonline.com/doi/full/10.1088/1468-6996/15/4/043502

[131] J. S. Walker, N. V. Rees, and P. M. Mendes, "Progress towards the ideal core@shell nanoparticle for fuel cell electrocatalysis," *Journal of Experimental Nanoscience*, vol. 13, no. 1, pp. 258–271, jan 2018. [Online]. Available: https://www.tandfonline.com/doi/full/10.1080/17458080.2018.1509383

[132] J. Zhang, Y. Mo, M. B. Vukmirovic, R. Klie, K. Sasaki, and R. R. Adzic, "Platinum Monolayer Electrocatalysts for O 2 Reduction: Pt Monolayer on Pd(111) and on Carbon-Supported Pd Nanoparticles," *The Journal of Physical Chemistry B*, vol. 108, no. 30, pp. 10 955–10 964, jul 2004. [Online]. Available: https://pubs.acs.org/doi/10.1021/jp0379953

[133] G. Gupta, P. Iqbal, F. Yin, J. Liu, R. E. Palmer, S. Sharma, K. C.-F. Leung, and P. M. Mendes, "Pt Diffusion Dynamics for the Formation Cr–Pt Core–Shell Nanoparticles," *Langmuir*, vol. 31, no. 24, pp. 6917–6923, jun 2015. [Online]. Available: https://pubs.acs.org/doi/10.1021/acs.langmuir.5b01410

[134] L. Osmieri, "Transition Metal–Nitrogen–Carbon (M–N–C) Catalysts for Oxygen Reduction Reaction. Insights on Synthesis and Performance in Polymer Electrolyte Fuel Cells," *ChemEngineering*, vol. 3, no. 1, p. 16, feb 2019. [Online]. Available: http://www.mdpi.com/2305-7084/3/1/16

[135] K. Strickland, E. Miner, Q. Jia, U. Tylus, N. Ramaswamy, W. Liang, M.-T. Sougrati, F. Jaouen, and S. Mukerjee, "Highly active oxygen reduction non-platinum group metal electrocatalyst without direct metal–nitrogen coordination," *Nature Communications*, vol. 6, no. 1, p. 7343, nov 2015. [Online]. Available: http://www.nature.com/articles/ncomms8343

[136] S. Stariha, K. Artyushkova, A. Serov, and P. Atanassov, "Non-PGM membrane electrode assemblies: Optimization for performance," *International Journal of Hydrogen Energy*, vol. 40, no. 42, pp. 14 676–14 682, nov 2015. [Online]. Available: https://linkinghub.elsevier.com/retrieve/pii/S0360319915014500

[137] Y. Pan, F. Zhang, K. Wu, Z. Lu, Y. Chen, Y. Zhou, Y. Tang, and T. Lu, "Carbon supported Palladium–Iron nanoparticles with uniform alloy structure as methanol-tolerant electrocatalyst for oxygen reduction reaction," *International Journal of Hydrogen Energy*, vol. 37, no. 4, pp. 2993–3000, feb 2012. [Online]. Available: https://linkinghub.elsevier.com/retrieve/pii/S0360319911025407

[138] L. Zeng, X. Cui, L. Chen, T. Ye, W. Huang, R. Ma, X. Zhang, and J. Shi, "Non-noble bimetallic alloy encased in nitrogen-doped nanotubes as a highly active and durable electrocatalyst for oxygen reduction reaction," *Carbon*, vol. 114, pp. 347–355, apr 2017. [Online]. Available: https://linkinghub.elsevier.com/retrieve/pii/S0008622316310958

[139] J. Masa, W. Xia, M. Muhler, and W. Schuhmann, "On the Role of Metals in Nitrogen-Doped Carbon Electrocatalysts for Oxygen Reduction," *Angewandte Chemie International Edition*, vol. 54, no. 35, pp. 10 102–10 120, aug 2015. [Online]. Available: http://doi.wiley.com/10.1002/anie.201500569

[140] Z. Chen, D. Higgins, A. Yu, L. Zhang, and J. Zhang, "A review on non-precious metal electrocatalysts for PEM fuel cells," *Energy & Environmental Science*, vol. 4, no. 9, p. 3167, 2011. [Online]. Available: http://xlink.rsc.org/?DOI=c0ee00558d

[141] T. C. Nagaiah, A. Bordoloi, M. D. Sánchez, M. Muhler, and W. Schuhmann, "Mesoporous Nitrogen-Rich Carbon Materials as Catalysts for the Oxygen Reduction Reaction in Alkaline Solution," *ChemSusChem*, vol. 5, no. 4, pp. 637–641, apr 2012. [Online]. Available: http://doi.wiley.com/10.1002/cssc.201100284

[142] M. P. Karthikayini, G. Wang, P. A. Bhobe, A. Sheelam, V. K. Ramani, K. R. Priolkar, and R. K. Raman, "Effect of Protonated Amine Molecules on the Oxygen Reduction Reaction on Metal-Nitrogen-Carbon-Based Catalysts," *Electrocatalysis*, vol. 8, no. 1, pp. 74–85, jan 2017. [Online]. Available: http://link.springer.com/10.1007/s12678-016-0341-y

[143] C. Zhu, Q. Shi, B. Z. Xu, S. Fu, G. Wan, C. Yang, S. Yao, J. Song, H. Zhou, D. Du, S. P. Beckman, D. Su, and Y. Lin, "Hierarchically Porous M-N-C (M = Co and Fe) Single-Atom Electrocatalysts with Robust MN x Active Moieties Enable Enhanced ORR Performance," *Advanced Energy Materials*, vol. 8, no. 29, p. 1801956, oct 2018. [Online]. Available: http://doi.wiley.com/10.1002/aenm.201801956

[144] Y. Mun, M. J. Kim, S.-A. Park, E. Lee, Y. Ye, S. Lee, Y.-T. Kim, S. Kim, O.-H. Kim, Y.-H. Cho, Y.-E. Sung, and J. Lee, "Soft-template synthesis of mesoporous non-precious metal catalyst with Fe-N x /C active sites for oxygen reduction reaction in fuel cells," *Applied Catalysis B: Environmental*, vol. 222, pp. 191–199, mar 2018. [Online]. Available: https://linkinghub.elsevier.com/retrieve/pii/S092633731730927X

[145] F. Luo, C. H. Choi, M. J. Primbs, W. Ju, S. Li, N. D. Leonard, A. Thomas, F. Jaouen, and P. Strasser, "Accurate Evaluation of Active-Site Density (SD) and Turnover Frequency (TOF) of PGM-Free Metal–Nitrogen-Doped Carbon (MNC) Electrocatalysts using CO Cryo Adsorption," *ACS Catalysis*, vol. 9, no. 6, pp. 4841–4852, jun 2019. [Online]. Available: https://pubs.acs.org/doi/10.1021/acscatal.9b00588

[146] J. Liu, E. Li, M. Ruan, P. Song, and W. Xu, "Recent Progress on Fe/N/C Electrocatalysts for the Oxygen Reduction Reaction in Fuel Cells," *Catalysts*, vol. 5, no. 3, pp. 1167–1192, jul 2015. [Online]. Available: http://www.mdpi.com/2073-4344/5/3/1167

[147] U. I. Kramm, I. Herrmann-Geppert, P. Bogdanoff, and S. Fiechter, "Effect of an Ammonia Treatment on Structure, Composition, and Oxygen Reduction Reaction Activity of Fe–N–C Catalysts," *The Journal of Physical Chemistry C*, vol. 115, no. 47, pp. 23 417–23 427, dec 2011. [Online]. Available: https://pubs.acs.org/doi/10.1021/jp207417y

[148] J. Barek and J. Zima, "Eighty Years of Polarography - History and Future," *Electroanalysis*, vol. 15, no. 5-6, pp. 467–472, apr 2003. [Online]. Available: http://doi.wiley.com/10.1002/elan.200390055

[149] N. Elgrishi, K. J. Rountree, B. D. McCarthy, E. S. Rountree, T. T. Eisenhart, and J. L. Dempsey, "A Practical Beginner's Guide to Cyclic Voltammetry," *Journal of Chemical Education*, vol. 95, no. 2, pp. 197–206, feb 2018. [Online]. Available: https://pubs.acs.org/doi/10.1021/acs.jchemed.7b00361

[150] G. A. Mabbott, "An introduction to cyclic voltammetry," *Journal of Chemical Education*, vol. 60, no. 9, p. 697, sep 1983. [Online]. Available: https://pubs.acs.org/doi/abs/10.1021/ed060p697

[151] D. W. Kumsa, N. Bhadra, E. M. Hudak, S. C. Kelley, D. F. Untereker, and J. T. Mortimer, "Electron transfer processes occurring on platinum neural stimulating electrodes: a tutorial on the i (V e) profile," *Journal of Neural Engineering*, vol. 13, no. 5, p. 052001, oct 2016. [Online]. Available: https://iopscience.iop.org/article/10.1088/1741-2560/13/5/052001

[152] O. Diaz-Morales, T. J. P. Hersbach, C. Badan, A. C. Garcia, and M. T. Koper, "Hydrogen adsorption on nano-structured platinum electrodes," *Faraday Discussions*, vol. 210, pp. 301–315, 2018. [Online]. Available: http://xlink.rsc.org/?DOI=C8FD00062J

[153] J. Zhang, *PEM Fuel Cell Electrocatalysts and Catalyst Layers*, J. Zhang, Ed. London: Springer London, 2008. [Online]. Available: http://link.springer.com/10.1007/978-1-84800-936-3

[154] D. J. L. Brett, S. Atkins, N. P. Brandon, V. Vesovic, N. Vasileiadis, and A. Kucernak, "Localized Impedance Measurements along a Single Channel of a Solid Polymer Fuel Cell," *Electrochemical and Solid-State Letters*, vol. 6, no. 4, p. A63, 2003. [Online]. Available: https://iopscience.iop.org/article/10.1149/1.1557034

[155] A. Kulikovsky and M. Eikerling, "Analytical solutions for impedance of the cathode catalyst layer in PEM fuel cell: Layer parameters from impedance spectrum without fitting," *Journal of Electroanalytical Chemistry*, vol. 691, pp. 13–17, feb 2013. [Online]. Available: https://linkinghub.elsevier.com/retrieve/pii/S1572665712005140

[156] X. YUAN, H. WANG, J. COLINSUN, and J. ZHANG, "AC impedance technique in PEM fuel cell diagnosis—A review," *International Journal of Hydrogen Energy*, vol. 32, no. 17, pp. 4365–4380, dec 2007. [Online]. Available: https://linkinghub.elsevier.com/retrieve/pii/S036031990700328X

[157] V. V. Nikonenko and A. E. Kozmai, "Electrical equivalent circuit of an ion-exchange membrane system," *Electrochimica Acta*, vol. 56, no. 3, pp. 1262–1269, jan 2011. [Online]. Available: https://linkinghub.elsevier.com/retrieve/pii/S0013468610015057

[158] F.-M. Wang and J. Rick, "Synergy of Nyquist and Bode electrochemical impedance spectroscopy studies to commercial type lithium ion batteries," *Solid State Ionics*, vol. 268, pp. 31–34, dec 2014. [Online]. Available: https://linkinghub.elsevier.com/retrieve/pii/S0167273814003890

[159] P. M. Gomadam and J. W. Weidner, "Analysis of electrochemical impedance spectroscopy in proton exchange membrane fuel cells," *International Journal of Energy Research*, vol. 29, no. 12, pp. 1133–1151, oct 2005. [Online]. Available: http://doi.wiley.com/10.1002/er.1144

[160] G. Walter, "A review of impedance plot methods used for corrosion performance analysis of painted metals," *Corrosion Science*, vol. 26, no. 9, pp. 681–703, jan 1986. [Online]. Available: https://linkinghub.elsevier.com/retrieve/pii/0010938X86900338

[161] M. E. Orazem and B. Tribollet, *Electrochemical Impedance Spectroscopy*. Hoboken, NJ, USA: John Wiley & Sons, Inc., aug 2008. [Online]. Available: http://doi.wiley.com/10.1002/9780470381588

[162] N. Garland, T. Benjamin, and J. Kopasz, "DOE Fuel Cell Program: Durability Technical Targets and Testing Protocols," in *ECS Transactions*, vol. 11. ECS, 2007, pp. 923–931. [Online]. Available: http://ecst.ecsdl.org/cgi/doi/10.1149/1.2781004

[163] J. Wu, X. Z. Yuan, J. J. Martin, H. Wang, J. Zhang, J. Shen, S. Wu, and W. Merida, "A review of PEM fuel cell durability: Degradation mechanisms and mitigation strategies," *Journal of Power Sources*, vol. 184, no. 1, pp. 104–119, sep 2008. [Online]. Available: https://linkinghub.elsevier.com/retrieve/pii/S0378775308011968

[164] R. Borup, J. Meyers, B. Pivovar, Y. S. Kim, R. Mukundan, N. Garland, D. Myers, M. Wilson, F. Garzon, D. Wood, P. Zelenay, K. More, K. Stroh, T. Zawodzinski, J. Boncella, J. E. McGrath, M. Inaba, K. Miyatake, M. Hori, K. Ota, Z. Ogumi, S. Miyata, A. Nishikata, Z. Siroma, Y. Uchimoto, K. Yasuda, K.-i. Kimijima, and N. Iwashita, "Scientific Aspects of

Polymer Electrolyte Fuel Cell Durability and Degradation," *Chemical Reviews*, vol. 107, no. 10, pp. 3904–3951, oct 2007. [Online]. Available: https://pubs.acs.org/doi/10.1021/cr0501821

[165] J. J. Baschuk and X. Li, "Carbon monoxide poisoning of proton exchange membrane fuel cells," *International Journal of Energy Research*, vol. 25, no. 8, pp. 695–713, jun 2001. [Online]. Available: http://doi.wiley.com/10.1002/er.713

[166] A. Kongkanand and M. F. Mathias, "The Priority and Challenge of High-Power Performance of Low-Platinum Proton-Exchange Membrane Fuel Cells," *The Journal of Physical Chemistry Letters*, vol. 7, no. 7, pp. 1127–1137, apr 2016. [Online]. Available: https://pubs.acs.org/doi/10.1021/acs.jpclett.6b00216

[167] S. F. Burlatsky, V. Atrazhev, N. Cipollini, D. Condit, and N. Erikhman, "Aspects of PEMFC Degradation," in *ECS Transactions*, vol. 1. ECS, 2006, pp. 239–246. [Online]. Available: http://ecst.ecsdl.org/cgi/doi/10.1149/1.2214557

[168] E. Antolini, "Carbon supports for low-temperature fuel cell catalysts," *Applied Catalysis B: Environmental*, vol. 88, no. 1-2, pp. 1–24, apr 2009. [Online]. Available: https://linkinghub.elsevier.com/retrieve/pii/S0926337308003809

[169] A. TANIGUCHI, T. AKITA, K. YASUDA, and Y. MIYAZAKI, "Analysis of degradation in PEMFC caused by cell reversal during air starvation," *International Journal of Hydrogen Energy*, vol. 33, no. 9, pp. 2323–2329, may 2008. [Online]. Available: https://linkinghub.elsevier.com/retrieve/pii/S0360319908002267

[170] Y. Shao, G. Yin, and Y. Gao, "Understanding and approaches for the durability issues of Pt-based catalysts for PEM fuel cell," *Journal of Power Sources*, vol. 171, no. 2, pp. 558–566, sep 2007. [Online]. Available: https://linkinghub.elsevier.com/retrieve/pii/S0378775307014814

[171] D. Stevens and J. Dahn, "Thermal degradation of the support in carbon-supported platinum electrocatalysts for PEM fuel cells," *Carbon*, vol. 43, no. 1, pp. 179–188, 2005. [Online]. Available: https://linkinghub.elsevier.com/retrieve/pii/S0008622304005366

[172] C. Lee and W. Mérida, "Gas diffusion layer durability under steady-state and freezing conditions," *Journal of Power Sources*, vol. 164, no. 1, pp. 141–153, jan 2007. [Online]. Available: https://linkinghub.elsevier.com/retrieve/pii/S0378775306021318

[173] U. Pasaogullari and C.-Y. Wang, "Two-phase transport and the role of micro-porous layer in polymer electrolyte fuel cells," *Electrochimica Acta*, vol. 49, no. 25, pp. 4359–4369, oct 2004. [Online]. Available: https://linkinghub.elsevier.com/retrieve/pii/S0013468604003846

[174] S. Park, J.-W. Lee, and B. N. Popov, "A review of gas diffusion layer in PEM fuel cells: Materials and designs," *International Journal of Hydrogen Energy*, vol. 37, no. 7, pp. 5850–5865, apr 2012. [Online]. Available: https://linkinghub.elsevier.com/retrieve/pii/S0360319911028825

[175] M. F. Mathias, R. Makharia, H. A. Gasteiger, J. J. Conley, T. J. Fuller, C. J. Gittleman, S. S. Kocha, D. P. Miller, C. K. Mittelsteadt, T. Xie, S. G. Van, and P. T. Yu, "Two fuel cell cars in every garage?" 2005. [Online]. Available: https://www.electrochem.org/dl/interface/fal/fal05/IF8-05{_}Pg24-35.pdf

[176] M. Mathias, H. Gasteiger, R. Makharia, S. Kocha, T. Fuller, T. Xie, and J. Pisco, "Can available membranes and catalysts meet automotive polymer electrolyte fuel cell requirements?" in *ACS Division of Fuel Chemistry, Preprints*, 2004. [Online]. Available: http://web.anl.gov/PCS/acsfuel/preprint{%}20archive/Files/49_2_Philadelphia_10\protect\discretionary{\char\hyphenchar\font}{}{}04_1010.pdf.

[177] U. D. F. C. T. Team, "FCTT AST and Polarization Curve Protocols for PEMFCs - U.S. DRIVE Fuel Cell Tech Team Cell Component Accelerated Stress Test and Polarization Curve Protocols for PEM Fuel Cells," Tech. Rep., 2013. [Online]. Available: https://www.energy.gov/sites/prod/files/2015/08/f25/fcto{_}dwg{_}usdrive{_}fctt{_}accelerated{_}stress{_}tests{_}jan2013.pdf

[178] T. Omasta, L. Wang, X. Peng, C. Lewis, J. Varcoe, and W. Mustain, "Importance of balancing membrane and electrode water in anion exchange membrane fuel cells," *Journal of Power Sources*, vol. 375, pp. 205–213, jan 2018. [Online]. Available: https://linkinghub.elsevier.com/retrieve/pii/S0378775317306274

[179] T. J. Omasta, A. M. Park, J. M. LaManna, Y. Zhang, X. Peng, L. Wang, D. L. Jacobson, J. R. Varcoe, D. S. Hussey, B. S. Pivovar, and W. E. Mustain, "Beyond catalysis and membranes: visualizing and solving the challenge of electrode water accumulation and flooding in AEMFCs," *Energy & Environmental Science*, vol. 11, no. 3, pp. 551–558, 2018. [Online]. Available: http://xlink.rsc.org/?DOI=C8EE00122G

[180] M. Mandal, G. Huang, N. U. Hassan, X. Peng, T. Gu, A. H. Brooks-Starks, B. Bahar, W. E. Mustain, and P. A. Kohl, "The Importance of Water Transport in High Conductivity and High-Power Alkaline Fuel Cells," *Journal of The Electrochemical Society*, vol. 167, no. 5, p. 054501, oct 2020. [Online]. Available: https://iopscience.iop.org/article/10.1149/2.0022005JES

[181] G. Huang, M. Mandal, X. Peng, A. C. Yang-Neyerlin, B. S. Pivovar, W. E. Mustain, and P. A. Kohl, "Composite Poly(norbornene) Anion Conducting Membranes for Achieving Durability, Water Management and High Power (3.4 W/cm 2) in Hydrogen/Oxygen Alkaline Fuel Cells,"

Journal of The Electrochemical Society, vol. 166, no. 10, pp. F637–F644, jun 2019. [Online]. Available: https://iopscience.iop.org/article/10.1149/2.1301910jes

[182] M. Karuppannan, J. E. Park, H. E. Bae, Y.-H. Cho, and O. J. Kwon, "A nitrogen and fluorine enriched Fe/Fe 3 C@C oxygen reduction reaction electrocatalyst for anion/proton exchange membrane fuel cells," *Nanoscale*, vol. 12, no. 4, pp. 2542–2554, 2020. [Online]. Available: http://xlink.rsc.org/?DOI=C9NR08631E

[183] W. Yang, X. Liu, X. Yue, J. Jia, and S. Guo, "Bamboo-like Carbon Nanotube/Fe 3 C Nanoparticle Hybrids and Their Highly Efficient Catalysis for Oxygen Reduction," *Journal of the American Chemical Society*, vol. 137, no. 4, pp. 1436–1439, feb 2015. [Online]. Available: https://pubs.acs.org/doi/10.1021/ja5129132

[184] J. H. Kim, Y. J. Sa, H. Y. Jeong, and S. H. Joo, "Roles of Fe−N x and Fe−Fe 3 C@C Species in Fe−N/C Electrocatalysts for Oxygen Reduction Reaction," *ACS Applied Materials & Interfaces*, vol. 9, no. 11, pp. 9567–9575, mar 2017. [Online]. Available: https://pubs.acs.org/doi/10.1021/acsami.6b13417

[185] F.-L. Meng, Z.-L. Wang, H.-X. Zhong, J. Wang, J.-M. Yan, and X.-B. Zhang, "Reactive Multifunctional Template-Induced Preparation of Fe-N-Doped Mesoporous Carbon Microspheres Towards Highly Efficient Electrocatalysts for Oxygen Reduction," *Advanced Materials*, vol. 28, no. 36, pp. 7948–7955, sep 2016. [Online]. Available: http://doi.wiley.com/10.1002/adma.201602490

[186] L. Wang, X. Peng, W. E. Mustain, and J. R. Varcoe, "Radiation-grafted anion-exchange membranes: the switch from low- to high-density polyethylene leads to remarkably enhanced fuel cell performance," *Energy & Environmental Science*, vol. 12, no. 5, pp. 1575–1579, 2019. [Online]. Available: http://xlink.rsc.org/?DOI=C9EE00331B

[187] L. Wang, J. J. Brink, and J. R. Varcoe, "The first anion-exchange membrane fuel cell to exceed 1 W cm −2 at 70 °C with a non-Pt-group (O 2) cathode," *Chem. Commun.*, vol. 53, no. 86, pp. 11 771–11 773, 2017. [Online]. Available: http://xlink.rsc.org/?DOI=C7CC06392J

[188] T. J. Omasta, X. Peng, H. A. Miller, F. Vizza, L. Wang, J. R. Varcoe, D. R. Dekel, and W. E. Mustain, "Beyond 1.0 W cm −2 Performance without Platinum: The Beginning of a New Era in Anion Exchange Membrane Fuel Cells," *Journal of The Electrochemical Society*, vol. 165, no. 15, pp. J3039–J3044, sep 2018. [Online]. Available: https://iopscience.iop.org/article/10.1149/2.0071815jes

[189] H. A. Miller, A. Lavacchi, F. Vizza, M. Marelli, F. Di Benedetto, F. D'Acapito, Y. Paska, M. Page, and D. R. Dekel, "A Pd/C-CeO 2 Anode Catalyst for High-Performance Platinum-Free

Anion Exchange Membrane Fuel Cells," *Angewandte Chemie International Edition*, vol. 55, no. 20, pp. 6004–6007, may 2016. [Online]. Available: http://doi.wiley.com/10.1002/anie.201600647

[190] S. ZHANG, X. YUAN, H. WANG, W. MERIDA, H. ZHU, J. SHEN, S. WU, and J. ZHANG, "A review of accelerated stress tests of MEA durability in PEM fuel cells," *International Journal of Hydrogen Energy*, vol. 34, no. 1, pp. 388–404, jan 2009. [Online]. Available: https://linkinghub.elsevier.com/retrieve/pii/S0360319908013591

[191] J. Park, H. Oh, T. Ha, Y. I. Lee, and K. Min, "A review of the gas diffusion layer in proton exchange membrane fuel cells: Durability and degradation," *Applied Energy*, vol. 155, pp. 866–880, oct 2015. [Online]. Available: https://linkinghub.elsevier.com/retrieve/pii/S0306261915008260

[192] A. Riese, D. Banham, S. Ye, and X. Sun, "Accelerated Stress Testing by Rotating Disk Electrode for Carbon Corrosion in Fuel Cell Catalyst Supports," *Journal of The Electrochemical Society*, vol. 162, no. 7, pp. F783–F788, apr 2015. [Online]. Available: https://iopscience.iop.org/article/10.1149/2.0911507jes

[193] R. Borup, J. Davey, F. Garzon, D. Wood, P. Welch, and K. More, "PEM Fuel Cell Durability With Transportation Transient Operation," in *ECS Transactions*, vol. 3. ECS, 2006, pp. 879–886. [Online]. Available: http://ecst.ecsdl.org/cgi/doi/10.1149/1.2356206

[194] M. Schulze, N. Wagner, T. Kaz, and K. Friedrich, "Combined electrochemical and surface analysis investigation of degradation processes in polymer electrolyte membrane fuel cells," *Electrochimica Acta*, vol. 52, no. 6, pp. 2328–2336, jan 2007. [Online]. Available: https://linkinghub.elsevier.com/retrieve/pii/S0013468606008267

[195] D. Wood, J. Davey, P. Atanassov, and R. Borup, "PEMFC Component Characterization and Its Relationship to Mass-Transport Overpotentials during Long-Term Testing," in *ECS Transactions*, vol. 3. ECS, 2006, pp. 753–763. [Online]. Available: http://ecst.ecsdl.org/cgi/doi/10.1149/1.2356195

[196] H. A. Firouzjaie and W. E. Mustain, "Catalytic Advantages, Challenges, and Priorities in Alkaline Membrane Fuel Cells," *ACS Catalysis*, vol. 10, no. 1, pp. 225–234, jan 2020. [Online]. Available: https://pubs.acs.org/doi/10.1021/acscatal.9b03892

[197] L. Wang, J. J. Brink, and J. R. Varcoe, "The first anion-exchange membrane fuel cell to exceed 1 W cm −2 at 70 °C with a non-Pt-group (O 2) cathode," *Chem. Commun.*, vol. 53, no. 86, pp. 11 771–11 773, 2017. [Online]. Available: http://xlink.rsc.org/?DOI=C7CC06392J

[198] G. A. Ferrero, K. Preuss, A. Marinovic, A. B. Jorge, N. Mansor, D. J. L. Brett, A. B. Fuertes, M. Sevilla, and M.-M. Titirici, "Fe–N-Doped Carbon Capsules with Outstanding

Electrochemical Performance and Stability for the Oxygen Reduction Reaction in Both Acid and Alkaline Conditions," *ACS Nano*, vol. 10, no. 6, pp. 5922–5932, jun 2016. [Online]. Available: https://pubs.acs.org/doi/10.1021/acsnano.6b01247

[199] H. Ren, Y. Wang, Y. Yang, X. Tang, Y. Peng, H. Peng, L. Xiao, J. Lu, H. D. Abruña, and L. Zhuang, "Fe/N/C Nanotubes with Atomic Fe Sites: A Highly Active Cathode Catalyst for Alkaline Polymer Electrolyte Fuel Cells," *ACS Catalysis*, vol. 7, no. 10, pp. 6485–6492, oct 2017. [Online]. Available: https://pubs.acs.org/doi/10.1021/acscatal.7b02340

[200] C. Chen, X.-D. Yang, Z.-Y. Zhou, Y.-J. Lai, M. Rauf, Y. Wang, J. Pan, L. Zhuang, Q. Wang, Y.-C. Wang, N. Tian, X.-S. Zhang, and S.-G. Sun, "Aminothiazole-derived N,S,Fe-doped graphene nanosheets as high performance electrocatalysts for oxygen reduction," *Chemical Communications*, vol. 51, no. 96, pp. 17 092–17 095, 2015. [Online]. Available: http://xlink.rsc.org/?DOI=C5CC06562C

[201] M. M. Hossen, K. Artyushkova, P. Atanassov, and A. Serov, "Synthesis and characterization of high performing Fe-N-C catalyst for oxygen reduction reaction (ORR) in Alkaline Exchange Membrane Fuel Cells," *Journal of Power Sources*, vol. 375, pp. 214–221, jan 2018. [Online]. Available: https://doi.org/10.1016/j.jpowsour.2017.08.036

[202] E. Proietti, F. Jaouen, M. Lefèvre, N. Larouche, J. Tian, J. Herranz, and J.-P. Dodelet, "Iron-based cathode catalyst with enhanced power density in polymer electrolyte membrane fuel cells," *Nature Communications*, vol. 2, no. 1, p. 416, sep 2011. [Online]. Available: http://www.nature.com/articles/ncomms1427

[203] J. Shui, C. Chen, L. Grabstanowicz, D. Zhao, and D.-J. Liu, "Highly efficient nonprecious metal catalyst prepared with metal–organic framework in a continuous carbon nanofibrous network," *Proceedings of the National Academy of Sciences*, vol. 112, no. 34, pp. 10 629–10 634, aug 2015. [Online]. Available: http://www.pnas.org/lookup/doi/10.1073/pnas.1507159112

[204] A. Serov, M. J. Workman, K. Artyushkova, P. Atanassov, G. McCool, S. McKinney, H. Romero, B. Halevi, and T. Stephenson, "Highly stable precious metal-free cathode catalyst for fuel cell application," *Journal of Power Sources*, vol. 327, pp. 557–564, sep 2016. [Online]. Available: http://dx.doi.org/10.1016/j.jpowsour.2016.07.087https://linkinghub.elsevier.com/retrieve/pii/S0378775316309624

[205] S. Stariha, K. Artyushkova, M. J. Workman, A. Serov, S. Mckinney, B. Halevi, and P. Atanassov, "PGM-free Fe-N-C catalysts for oxygen reduction reaction: Catalyst layer design," *Journal of Power Sources*, vol. 326, pp. 43–49, sep 2016. [Online]. Available: http://dx.doi.org/10.1016/j.jpowsour.2016.06.098https://linkinghub.elsevier.com/retrieve/pii/S0378775316308102

[206] H. Zhang, H. T. Chung, D. A. Cullen, S. Wagner, U. I. Kramm, K. L. More, P. Zelenay, and G. Wu, "High-performance fuel cell cathodes exclusively containing atomically dispersed iron active sites," *Energy & Environmental Science*, vol. 12, no. 8, pp. 2548–2558, 2019. [Online]. Available: http://xlink.rsc.org/?DOI=C9EE00877B

[207] A. Serov, A. D. Shum, X. Xiao, V. De Andrade, K. Artyushkova, I. V. Zenyuk, and P. Atanassov, "Nano-structured platinum group metal-free catalysts and their integration in fuel cell electrode architectures," *Applied Catalysis B: Environmental*, vol. 237, no. May 2017, pp. 1139–1147, dec 2018. [Online]. Available: https://doi.org/10.1016/j.apcatb.2017.08.067https://linkinghub.elsevier.com/retrieve/pii/S0926337317308032

[208] I. Takahashi and S. S. Kocha, "Examination of the activity and durability of PEMFC catalysts in liquid electrolytes," *Journal of Power Sources*, vol. 195, no. 19, pp. 6312–6322, oct 2010. [Online]. Available: https://linkinghub.elsevier.com/retrieve/pii/S0378775310006877

[209] G. P. Keeley, S. Cherevko, and K. J. J. Mayrhofer, "The Stability Challenge on the Pathway to Low and Ultra-Low Platinum Loading for Oxygen Reduction in Fuel Cells," *ChemElectroChem*, vol. 3, no. 1, pp. 51–54, jan 2016. [Online]. Available: http://doi.wiley.com/10.1002/celc.201500425

[210] K. Shinozaki, J. W. Zack, S. Pylypenko, R. M. Richards, B. S. Pivovar, and S. S. Kocha, "Benchmarking the oxygen reduction reaction activity of Pt-based catalysts using standardized rotating disk electrode methods," *International Journal of Hydrogen Energy*, vol. 40, no. 46, pp. 16 820–16 830, dec 2015. [Online]. Available: https://linkinghub.elsevier.com/retrieve/pii/S0360319915020996

[211] R. L. Borup, A. Kusoglu, K. C. Neyerlin, R. Mukundan, R. K. Ahluwalia, D. A. Cullen, K. L. More, A. Z. Weber, and D. J. Myers, "Recent developments in catalyst-related PEM fuel cell durability," *Current Opinion in Electrochemistry*, vol. 21, pp. 192–200, jun 2020. [Online]. Available: https://linkinghub.elsevier.com/retrieve/pii/S2451910320300326

[212] M. J. Fleige, G. K. H. Wiberg, and M. Arenz, "Rotating disk electrode system for elevated pressures and temperatures," *Review of Scientific Instruments*, vol. 86, no. 6, p. 064101, jun 2015. [Online]. Available: http://aip.scitation.org/doi/10.1063/1.4922382

[213] C. M. Zalitis, D. Kramer, and A. R. Kucernak, "Electrocatalytic performance of fuel cell reactions at low catalyst loading and high mass transport," *Physical Chemistry Chemical Physics*, vol. 15, no. 12, p. 4329, 2013. [Online]. Available: http://xlink.rsc.org/?DOI=c3cp44431g

[214] N. Jia, R. B. Martin, Z. Qi, M. C. Lefebvre, and P. G. Pickup, "Modification of carbon supported catalysts to improve performance in gas diffusion electrodes," *Electrochimica Acta*, vol. 46,

no. 18, pp. 2863–2869, may 2001. [Online]. Available: https://linkinghub.elsevier.com/retrieve/pii/S0013468601005114

[215] B. A. Pinaud, A. Bonakdarpour, L. Daniel, J. Sharman, and D. P. Wilkinson, "Key Considerations for High Current Fuel Cell Catalyst Testing in an Electrochemical Half-Cell," *Journal of The Electrochemical Society*, vol. 164, no. 4, pp. F321–F327, feb 2017. [Online]. Available: https://iopscience.iop.org/article/10.1149/2.0891704jes

[216] M. Inaba, A. W. Jensen, G. W. Sievers, M. Escudero-Escribano, A. Zana, and M. Arenz, "Benchmarking high surface area electrocatalysts in a gas diffusion electrode: measurement of oxygen reduction activities under realistic conditions," *Energy & Environmental Science*, vol. 11, no. 4, pp. 988–994, 2018. [Online]. Available: http://xlink.rsc.org/?DOI=C8EE00019K

[217] S. V. Gangal and P. D. Brothers, "Perfluorinated Polymers, Polytetrafluoroethylene," in *Encyclopedia of Polymer Science and Technology*. Wiley, jun 2010. [Online]. Available: https://onlinelibrary.wiley.com/doi/abs/10.1002/0471440264.pst233.pub2

[218] P. L. Andresen and M. E. Indig, "Effects of Impurities and Supporting Electrolytes On SCC of 304 Stainless Steel in High Temperature Aqueous Environments," *CORROSION*, vol. 38, no. 10, pp. 531–541, oct 1982. [Online]. Available: http://corrosionjournal.org/doi/10.5006/1.3593856

[219] K. Shinozaki, J. W. Zack, R. M. Richards, B. S. Pivovar, and S. S. Kocha, "Oxygen Reduction Reaction Measurements on Platinum Electrocatalysts Utilizing Rotating Disk Electrode Technique," *Journal of The Electrochemical Society*, vol. 162, no. 10, pp. F1144–F1158, 2015. [Online]. Available: https://iopscience.iop.org/article/10.1149/2.1071509jes

[220] I. Schneider, D. Kramer, A. Wokaun, and G. Scherer, "Effect of inert gas flow on hydrogen underpotential deposition measurements in polymer electrolyte fuel cells," *Electrochemistry Communications*, vol. 9, no. 7, pp. 1607–1612, jul 2007. [Online]. Available: https://linkinghub.elsevier.com/retrieve/pii/S1388248107001014

[221] E. Lam and J. H. Luong, "Carbon Materials as Catalyst Supports and Catalysts in the Transformation of Biomass to Fuels and Chemicals," *ACS Catalysis*, vol. 4, no. 10, pp. 3393–3410, oct 2014. [Online]. Available: https://pubs.acs.org/doi/10.1021/cs5008393

[222] E. Auer, A. Freund, J. Pietsch, and T. Tacke, "Carbons as supports for industrial precious metal catalysts," *Applied Catalysis A: General*, vol. 173, no. 2, pp. 259–271, oct 1998. [Online]. Available: https://linkinghub.elsevier.com/retrieve/pii/S0926860X98001847

[223] O. Brown, "Carbon—Electrochemical and Physicochemical Properties," *Electrochimica Acta*, vol. 34, no. 4, p. 593, apr 1989. [Online]. Available: https://linkinghub.elsevier.com/retrieve/pii/0013468689870665

[224] I. Savych, S. Subianto, Y. Nabil, S. Cavaliere, D. Jones, and J. Rozière, "Negligible degradation upon in situ voltage cycling of a PEMFC using an electrospun niobium-doped tin oxide supported Pt cathode," *Physical Chemistry Chemical Physics*, vol. 17, no. 26, pp. 16 970–16 976, 2015. [Online]. Available: http://xlink.rsc.org/?DOI=C5CP01542A

[225] E. Pizzutilo, S. Geiger, J.-P. Grote, A. Mingers, K. J. J. Mayrhofer, M. Arenz, and S. Cherevko, "On the Need of Improved Accelerated Degradation Protocols (ADPs): Examination of Platinum Dissolution and Carbon Corrosion in Half-Cell Tests," *Journal of The Electrochemical Society*, vol. 163, no. 14, pp. F1510–F1514, 2016. [Online]. Available: https://iopscience.iop.org/article/10.1149/2.0731614jes

[226] K. Kinoshita, J. Lundquist, and P. Stonehart, "Potential cycling effects on platinum electrocatalyst surfaces," *Journal of Electroanalytical Chemistry and Interfacial Electrochemistry*, vol. 48, no. 2, pp. 157–166, nov 1973. [Online]. Available: https://linkinghub.elsevier.com/retrieve/pii/S0022072873802578

[227] S. Cherevko, G. P. Keeley, S. Geiger, A. R. Zeradjanin, N. Hodnik, N. Kulyk, and K. J. J. Mayrhofer, "Dissolution of Platinum in the Operational Range of Fuel Cells," *ChemElectroChem*, vol. 2, no. 10, pp. 1471–1478, oct 2015. [Online]. Available: http://doi.wiley.com/10.1002/celc.201500098

[228] P. Daubinger, J. Kieninger, T. Unmüssig, and G. A. Urban, "Electrochemical characteristics of nanostructured platinum electrodes a cyclic voltammetry study," *Phys. Chem. Chem. Phys.*, vol. 16, no. 18, pp. 8392–8399, 2014. [Online]. Available: http://xlink.rsc.org/?DOI=C4CP00342J

[229] K. Ehelebe, D. Seeberger, M. T. Y. Paul, S. Thiele, K. J. J. Mayrhofer, and S. Cherevko, "Evaluating Electrocatalysts at Relevant Currents in a Half-Cell: The Impact of Pt Loading on Oxygen Reduction Reaction," *Journal of The Electrochemical Society*, vol. 166, no. 16, pp. F1259–F1268, nov 2019. [Online]. Available: https://iopscience.iop.org/article/10.1149/2.0911915jes

[230] S. Alinejad, M. Inaba, J. Schröder, J. Du, J. Quinson, A. Zana, and M. Arenz, "Testing fuel cell catalysts under more realistic reaction conditions: accelerated stress tests in a gas diffusion electrode setup," *Journal of Physics: Energy*, vol. 2, no. 2, p. 024003, feb 2020. [Online]. Available: https://iopscience.iop.org/article/10.1088/2515-7655/ab67e2

[231] S. Thomas, Y.-E. Sung, H. S. Kim, and A. Wieckowski, "Specific Adsorption of a Bisulfate Anion on a Pt(111) Electrode. Ultrahigh Vacuum Spectroscopic and Cyclic Voltammetric Study," *The*

Journal of Physical Chemistry, vol. 100, no. 28, pp. 11 726–11 735, jan 1996. [Online]. Available: https://pubs.acs.org/doi/10.1021/jp9606321

[232] Y. Furuya, T. Mashio, A. Ohma, M. Tian, F. Kaveh, D. Beauchemin, and G. Jerkiewicz, "Influence of Electrolyte Composition and pH on Platinum Electrochemical and/or Chemical Dissolution in Aqueous Acidic Media," *ACS Catalysis*, vol. 5, no. 4, pp. 2605–2614, apr 2015. [Online]. Available: https://pubs.acs.org/doi/10.1021/cs5016035

[233] T. Schmidt, U. Paulus, H. Gasteiger, and R. Behm, "The oxygen reduction reaction on a Pt/carbon fuel cell catalyst in the presence of chloride anions," *Journal of Electroanalytical Chemistry*, vol. 508, no. 1-2, pp. 41–47, jul 2001. [Online]. Available: https://linkinghub.elsevier.com/retrieve/pii/S0022072801004995

[234] K. Shinozaki, J. W. Zack, R. M. Richards, B. S. Pivovar, and S. S. Kocha, "Oxygen Reduction Reaction Measurements on Platinum Electrocatalysts Utilizing Rotating Disk Electrode Technique," *Journal of The Electrochemical Society*, vol. 162, no. 10, pp. F1144–F1158, 2015. [Online]. Available: https://iopscience.iop.org/article/10.1149/2.1071509jes

[235] N. Markovic, "Kinetics of Oxygen Reduction on Pt(hkl) Electrodes: Implications for the Crystallite Size Effect with Supported Pt Electrocatalysts," *Journal of The Electrochemical Society*, vol. 144, no. 5, p. 1591, 1997. [Online]. Available: https://iopscience.iop.org/article/10.1149/1.1837646

[236] P. Frühwirt, A. Kregar, J. T. Törring, T. Katrašnik, and G. Gescheidt, "Holistic approach to chemical degradation of Nafion membranes in fuel cells: modelling and predictions," *Physical Chemistry Chemical Physics*, vol. 22, no. 10, pp. 5647–5666, 2020. [Online]. Available: http://xlink.rsc.org/?DOI=C9CP04986J

[237] T. H. Yu, Y. Sha, W.-G. Liu, B. V. Merinov, P. Shirvanian, and W. A. Goddard, "Mechanism for Degradation of Nafion in PEM Fuel Cells from Quantum Mechanics Calculations," *Journal of the American Chemical Society*, vol. 133, no. 49, pp. 19 857–19 863, dec 2011. [Online]. Available: https://pubs.acs.org/doi/10.1021/ja2074642

[238] V. Stamenković, T. J. Schmidt, P. N. Ross, and N. M. Marković, "Surface Composition Effects in Electrocatalysis: Kinetics of Oxygen Reduction on Well-Defined Pt 3 Ni and Pt 3 Co Alloy Surfaces," *The Journal of Physical Chemistry B*, vol. 106, no. 46, pp. 11 970–11 979, nov 2002. [Online]. Available: https://pubs.acs.org/doi/10.1021/jp021182h

[239] J. Zhang, Y. Tang, C. Song, J. Zhang, and H. Wang, "PEM fuel cell open circuit voltage (OCV) in the temperature range of 23°C to 120°C," *Journal of Power Sources*, vol. 163, no. 1, pp. 532–537, dec 2006. [Online]. Available: https://linkinghub.elsevier.com/retrieve/pii/S0378775306018301

[240] M. Mayur, M. Gerard, P. Schott, and W. Bessler, "Lifetime Prediction of a Polymer Electrolyte Membrane Fuel Cell under Automotive Load Cycling Using a Physically-Based Catalyst Degradation Model," *Energies*, vol. 11, no. 8, p. 2054, aug 2018. [Online]. Available: http://www.mdpi.com/1996-1073/11/8/2054

[241] K. Ehelebe, T. Ashraf, S. Hager, D. Seeberger, S. Thiele, and S. Cherevko, "Fuel cell catalyst layer evaluation using a gas diffusion electrode half-cell: Oxygen reduction reaction on Fe-N-C in alkaline media," *Electrochemistry Communications*, vol. 116, no. May, p. 106761, jul 2020. [Online]. Available: https://linkinghub.elsevier.com/retrieve/pii/S1388248120301120

[242] Z. Liu, L. Yang, Z. Mao, W. Zhuge, Y. Zhang, and L. Wang, "Behavior of PEMFC in starvation," *Journal of Power Sources*, vol. 157, no. 1, pp. 166–176, jun 2006. [Online]. Available: https://linkinghub.elsevier.com/retrieve/pii/S037877530501089X

[243] S. Qu, X. Li, M. Hou, Z. Shao, and B. Yi, "The effect of air stoichiometry change on the dynamic behavior of a proton exchange membrane fuel cell," *Journal of Power Sources*, vol. 185, no. 1, pp. 302–310, oct 2008. [Online]. Available: https://linkinghub.elsevier.com/retrieve/pii/S0378775308013505

[244] L. He, Z. Han, Y. Liu, Z. Niu, and Z. Liu, "Effects of gas starvation on performance of a single PEMFC," in *2017 IEEE Transportation Electrification Conference and Expo, Asia-Pacific (ITEC Asia-Pacific)*. IEEE, aug 2017, pp. 1–5. [Online]. Available: http://ieeexplore.ieee.org/document/8080857/

[245] V. Paganin, C. Oliveira, E. Ticianelli, T. Springer, and E. Gonzalez, "Modelisticinterpretation of the impedance response of a polymer electrolyte fuel cell," *Electrochimica Acta*, vol. 43, no. 24, pp. 3761–3766, aug 1998. [Online]. Available: https://linkinghub.elsevier.com/retrieve/pii/S0013468698001352

[246] C. Qin, J. Wang, D. Yang, B. Li, and C. Zhang, "Proton Exchange Membrane Fuel Cell Reversal: A Review," *Catalysts*, vol. 6, no. 12, p. 197, dec 2016. [Online]. Available: http://www.mdpi.com/2073-4344/6/12/197

[247] H. Chen, S. Xu, P. Pei, B. Qu, and T. Zhang, "Mechanism analysis of starvation in PEMFC based on external characteristics," *International Journal of Hydrogen Energy*, vol. 44, no. 11, pp. 5437–5446, feb 2019. [Online]. Available: https://linkinghub.elsevier.com/retrieve/pii/S0360319918337406

[248] K. Wandelt, "Encyclopedia of Interfacial Chemistry: Surface Science and Electrochemistry," *Focus on Catalysts*, vol. 2018, no. 3, p. 7, mar 2018. [Online]. Available: https://linkinghub.elsevier.com/retrieve/pii/S1351418018300965

[249] D. Y. Chung, K.-J. Lee, and Y.-E. Sung, "Methanol Electro-Oxidation on the Pt Surface: Revisiting the Cyclic Voltammetry Interpretation," *The Journal of Physical Chemistry C*, vol. 120, no. 17, pp. 9028–9035, may 2016. [Online]. Available: https://pubs.acs.org/doi/10.1021/acs.jpcc.5b12303

[250] H. Beyenal and J. Babauta, *Biofilms in Bioelectrochemical Systems*. Hoboken, NJ, USA: John Wiley & Sons, Inc, sep 2015. [Online]. Available: http://doi.wiley.com/10.1002/9781119097426

[251] W. Sheng, H. A. Gasteiger, and Y. Shao-Horn, "Hydrogen Oxidation and Evolution Reaction Kinetics on Platinum: Acid vs Alkaline Electrolytes," *Journal of The Electrochemical Society*, 2010.

[252] T. J. Schmidt, V. Stamenkovic, P. N. Ross, Jr., and N. M. Markovic, "Temperature dependent surface electrochemistry on Pt single crystals in alkaline electrolyte," *Physical Chemistry Chemical Physics*, vol. 5, no. 2, pp. 400–406, jan 2003. [Online]. Available: http://xlink.rsc.org/?DOI=b208322a

[253] N. M. Marković, S. T. Sarraf, H. A. Gasteiger, and P. N. Ross, "Hydrogen electrochemistry on platinum low-index single-crystal surfaces in alkaline solution," *J. Chem. Soc., Faraday Trans.*, vol. 92, no. 20, pp. 3719–3725, 1996. [Online]. Available: http://xlink.rsc.org/?DOI=FT9969203719

[254] A. Zadick, L. Dubau, N. Sergent, G. Berthomé, and M. Chatenet, "Huge Instability of Pt/C Catalysts in Alkaline Medium," *ACS Catalysis*, vol. 5, no. 8, pp. 4819–4824, aug 2015. [Online]. Available: https://pubs.acs.org/doi/10.1021/acscatal.5b01037

[255] X. Peng, V. Kashyap, B. Ng, S. Kurungot, L. Wang, J. Varcoe, and W. Mustain, "High-Performing PGM-Free AEMFC Cathodes from Carbon-Supported Cobalt Ferrite Nanoparticles," *Catalysts*, vol. 9, no. 3, p. 264, mar 2019. [Online]. Available: https://www.mdpi.com/2073-4344/9/3/264

[256] C. Galeano, J. C. Meier, V. Peinecke, H. Bongard, I. Katsounaros, A. A. Topalov, A. Lu, K. J. J. Mayrhofer, and F. Schüth, "Toward Highly Stable Electrocatalysts via Nanoparticle Pore Confinement," *Journal of the American Chemical Society*, vol. 134, no. 50, pp. 20 457–20 465, dec 2012. [Online]. Available: https://pubs.acs.org/doi/10.1021/ja308570c

[257] J. C. Meier, C. Galeano, I. Katsounaros, J. Witte, H. J. Bongard, A. A. Topalov, C. Baldizzone, S. Mezzavilla, F. Schüth, and K. J. J. Mayrhofer, "Design criteria for stable Pt/C fuel cell catalysts," *Beilstein Journal of Nanotechnology*, vol. 5, pp. 44–67, jan 2014. [Online]. Available: https://www.beilstein-journals.org/bjnano/articles/5/5

[258] H.-S. Oh, K. H. Lim, B. Roh, I. Hwang, and H. Kim, "Corrosion resistance and sintering effect of carbon supports in polymer electrolyte membrane fuel cells," *Electrochimica Acta*, vol. 54,

no. 26, pp. 6515–6521, nov 2009. [Online]. Available: https://linkinghub.elsevier.com/retrieve/pii/S0013468609008366

[259] A. Ramos, I. Cameán, and A. B. García, "Graphitization thermal treatment of carbon nanofibers," *Carbon*, vol. 59, pp. 2–32, aug 2013. [Online]. Available: https://linkinghub.elsevier.com/retrieve/pii/S0008622313002509

[260] C. Song, S. R. Hui, and J. Zhang, "High-temperature PEM Fuel Cell Catalysts and Catalyst Layers," in *PEM Fuel Cell Electrocatalysts and Catalyst Layers*. London: Springer London, 2008, pp. 861–888. [Online]. Available: http://link.springer.com/10.1007/978-1-84800-936-3{_}18

[261] C. Baldizzone, S. Mezzavilla, N. Hodnik, A. R. Zeradjanin, A. Kostka, F. Schüth, and K. J. J. Mayrhofer, "Activation of carbon-supported catalysts by ozonized acidic solutions for the direct implementation in (electro-)chemical reactors," *Chemical Communications*, vol. 51, no. 7, pp. 1226–1229, 2015. [Online]. Available: http://xlink.rsc.org/?DOI=C4CC08480B

[262] H. Berg, "Electrochemical Oxygen Technology," *Bioelectrochemistry and Bioenergetics*, vol. 32, no. 2, p. 200, nov 1993. [Online]. Available: https://linkinghub.elsevier.com/retrieve/pii/030245989380043T

[263] M. JAKSIC, B. JOHANSEN, and R. TUNOLD, "Electrochemical behaviour of platinum in alkaline and acidic solutions of heavy and regular water[U+2606]," *International Journal of Hydrogen Energy*, vol. 18, no. 10, pp. 817–837, oct 1993. [Online]. Available: https://linkinghub.elsevier.com/retrieve/pii/036031999390136X

[264] R. Zeis, A. Mathur, G. Fritz, J. Lee, and J. Erlebacher, "Platinum-plated nanoporous gold: An efficient, low Pt loading electrocatalyst for PEM fuel cells," *Journal of Power Sources*, vol. 165, no. 1, pp. 65–72, feb 2007. [Online]. Available: https://linkinghub.elsevier.com/retrieve/pii/S0378775306025250

[265] N. Hodnik, M. Zorko, B. Jozinović, M. Bele, G. Dražič, S. Hočevar, and M. Gaberšček, "Severe accelerated degradation of PEMFC platinum catalyst: A thin film IL-SEM study," *Electrochemistry Communications*, vol. 30, pp. 75–78, may 2013. [Online]. Available: https://linkinghub.elsevier.com/retrieve/pii/S1388248113000611

[266] J. Knossalla, P. Paciok, D. Göhl, D. Jalalpoor, E. Pizzutilo, A. M. Mingers, M. Heggen, R. E. Dunin-Borkowski, K. J. Mayrhofer, F. Schüth, and M. Ledendecker, "Shape-Controlled Nanoparticles in Pore-Confined Space," *Journal of the American Chemical Society*, vol. 140, no. 46, pp. 15 684–15 689, 2018.

[267] S. Martin, P. Garcia-Ybarra, and J. Castillo, "High platinum utilization in ultra-low Pt loaded PEM fuel cell cathodes prepared by electrospraying," *International Journal of Hydrogen Energy*, vol. 35, no. 19, pp. 10 446–10 451, oct 2010. [Online]. Available: https://linkinghub.elsevier.com/retrieve/pii/S0360319910014072

[268] S. I. Kim, K. D. Baik, B. J. Kim, N. W. Lee, and M. S. Kim, "Experimental study on mitigating the cathode flooding at low temperature by adding hydrogen to the cathode reactant gas in PEM fuel cell," *International Journal of Hydrogen Energy*, vol. 38, no. 3, pp. 1544–1552, feb 2013. [Online]. Available: https://linkinghub.elsevier.com/retrieve/pii/S0360319912025001

[269] A. Polak, G. Grzeczka, and T. Piłat, "Influence of cathode stoichiometry on operation of PEM fuel cells' stack supplied with pure oxygen," *Journal of Marine Engineering & Technology*, vol. 16, no. 4, pp. 283–290, feb 2017. [Online]. Available: https://www.tandfonline.com/doi/full/10.1080/20464177.2017.1381061

[270] K. Shinozaki, J. W. Zack, R. M. Richards, B. S. Pivovar, and S. S. Kocha, "Oxygen reduction reaction measurements on platinum electrocatalysts utilizing rotating disk electrode technique: I. Impact of impurities, measurement protocols and applied corrections," *Journal of the Electrochemical Society*, 2015.

[271] D. Z. Mezalira and M. Bron, "High stability of low Pt loading high surface area electrocatalysts supported on functionalized carbon nanotubes," *Journal of Power Sources*, vol. 231, pp. 113–121, jun 2013. [Online]. Available: https://linkinghub.elsevier.com/retrieve/pii/S037877531201871X

[272] J. Durst, A. Lamibrac, F. Charlot, J. Dillet, L. F. Castanheira, G. Maranzana, L. Dubau, F. Maillard, M. Chatenet, and O. Lottin, "Degradation heterogeneities induced by repetitive start/stop events in proton exchange membrane fuel cell: Inlet vs. outlet and channel vs. land," *Applied Catalysis B: Environmental*, vol. 138-139, pp. 416–426, jul 2013. [Online]. Available: https://linkinghub.elsevier.com/retrieve/pii/S092633731300180X

[273] V. Mittal, R. Kunz, and J. Fenton, "H 2 O 2 Formation Mechanism in PEMFC," *ECS Transactions*, vol. 1, no. 8, pp. 295–301, dec 2019. [Online]. Available: https://iopscience.iop.org/article/10.1149/1.2214562

[274] N. Ramaswamy and S. Mukerjee, "Fundamental Mechanistic Understanding of Electrocatalysis of Oxygen Reduction on Pt and Non-Pt Surfaces: Acid versus Alkaline Media," *Advances in Physical Chemistry*, vol. 2012, pp. 1–17, mar 2012. [Online]. Available: https://www.hindawi.com/archive/2012/491604/

[275] N. Ziv, W. E. Mustain, and D. R. Dekel, "The Effect of Ambient Carbon Dioxide on Anion-Exchange Membrane Fuel Cells," *ChemSusChem*, vol. 11, no. 7, pp. 1136–1150, apr 2018. [Online]. Available: http://doi.wiley.com/10.1002/cssc.201702330

[276] Y. Zheng, T. J. Omasta, X. Peng, L. Wang, J. R. Varcoe, B. S. Pivovar, and W. E. Mustain, "Quantifying and elucidating the effect of CO 2 on the thermodynamics, kinetics and charge transport of AEMFCs," *Energy & Environmental Science*, vol. 12, no. 9, pp. 2806–2819, 2019. [Online]. Available: http://xlink.rsc.org/?DOI=C9EE01334B

[277] Y. Hu, J. O. Jensen, C. Pan, L. N. Cleemann, I. Shypunov, and Q. Li, "Immunity of the Fe-N-C catalysts to electrolyte adsorption: Phosphate but not perchloric anions," *Applied Catalysis B: Environmental*, vol. 234, pp. 357–364, oct 2018. [Online]. Available: https://linkinghub.elsevier.com/retrieve/pii/S0926337318302558

[278] S. Gottesfeld, D. R. Dekel, M. Page, C. Bae, Y. Yan, P. Zelenay, and Y. S. Kim, "Anion exchange membrane fuel cells: Current status and remaining challenges," *Journal of Power Sources*, vol. 375, pp. 170–184, jan 2018. [Online]. Available: https://linkinghub.elsevier.com/retrieve/pii/S0378775317310340

[279] D. R. Dekel, "Review of cell performance in anion exchange membrane fuel cells," *Journal of Power Sources*, 2018.

[280] L. Sun, J. Guo, J. Zhou, Q. Xu, D. Chu, and R. Chen, "Novel nanostructured high-performance anion exchange ionomers for anion exchange membrane fuel cells," *Journal of Power Sources*, vol. 202, pp. 70–77, mar 2012. [Online]. Available: https://linkinghub.elsevier.com/retrieve/pii/S0378775311022142

[281] A. G. Wright, J. Fan, B. Britton, T. Weissbach, H.-F. Lee, E. A. Kitching, T. J. Peckham, and S. Holdcroft, "Hexamethyl-p-terphenyl poly(benzimidazolium): a universal hydroxide-conducting polymer for energy conversion devices," *Energy & Environmental Science*, vol. 9, no. 6, pp. 2130–2142, 2016. [Online]. Available: http://xlink.rsc.org/?DOI=C6EE00656F

[282] N. Ziv and D. R. Dekel, "A practical method for measuring the true hydroxide conductivity of anion exchange membranes," *Electrochemistry Communications*, vol. 88, pp. 109–113, mar 2018. [Online]. Available: https://linkinghub.elsevier.com/retrieve/pii/S1388248118300286

[283] J. Fan, A. G. Wright, B. Britton, T. Weissbach, T. J. G. Skalski, J. Ward, T. J. Peckham, and S. Holdcroft, "Cationic Polyelectrolytes, Stable in 10 M KOH aq at 100 °C," *ACS Macro Letters*, vol. 6, no. 10, pp. 1089–1093, oct 2017. [Online]. Available: https://pubs.acs.org/doi/10.1021/acsmacrolett.7b00679

[284] H. Yanagi and K. Fukuta, "Anion Exchange Membrane and Ionomer for Alkaline Membrane Fuel Cells (AMFCs)," in *ECS Transactions*, vol. 16. ECS, 2008, pp. 257–262. [Online]. Available: http://ecst.ecsdl.org/cgi/doi/10.1149/1.2981860

[285] C. G. Arges and L. Zhang, "Anion Exchange Membranes' Evolution toward High Hydroxide Ion Conductivity and Alkaline Resiliency," *ACS Applied Energy Materials*, vol. 1, no. 7, pp. 2991–3012, jul 2018. [Online]. Available: https://pubs.acs.org/doi/10.1021/acsaem.8b00387

[286] O. D. Thomas, K. J. Soo, T. J. Peckham, M. P. Kulkarni, and S. Holdcroft, "A stable hydroxide-conducting polymer," *Journal of the American Chemical Society*, 2012.

[287] J. Parrondo, C. G. Arges, M. Niedzwiecki, E. B. Anderson, K. E. Ayers, and V. Ramani, "Degradation of anion exchange membranes used for hydrogen production by ultrapure water electrolysis," *RSC Advances*, vol. 4, no. 19, p. 9875, 2014. [Online]. Available: http://xlink.rsc.org/?DOI=c3ra46630b

[288] Z. Shao, L. Tong, Y. Qian, R. Dun, and W. Li, "A new 3D crosslinked polymer strategy for highly efficient oxygen reduction Fe–N x /C catalysts," *RSC Advances*, vol. 7, no. 62, pp. 39 178–39 184, 2017. [Online]. Available: http://xlink.rsc.org/?DOI=C7RA06352K

[289] Y.-Z. Wang, W.-Y. Huang, T.-H. Hsieh, L.-C. Jheng, K.-S. Ho, S.-W. Huang, and L. Chao, "FeNxC Based Catalysts Prepared by the Calcination of Iron-Ethylenediamine@Polyaniline as the Cathode-Catalyst of Proton Exchange Membrane Fuel Cell," *Polymers*, vol. 11, no. 8, p. 1368, aug 2019. [Online]. Available: https://www.mdpi.com/2073-4360/11/8/1368

[290] K. F. L. Hagesteijn, S. Jiang, and B. P. Ladewig, "A review of the synthesis and characterization of anion exchange membranes," *Journal of Materials Science*, vol. 53, no. 16, pp. 11 131–11 150, aug 2018. [Online]. Available: http://link.springer.com/10.1007/s10853-018-2409-y

[291] D. Singh, J. Tian, K. Mamtani, J. King, J. T. Miller, and U. S. Ozkan, "A comparison of N-containing carbon nanostructures (CN) and N-coordinated iron–carbon catalysts (FeNC) for the oxygen reduction reaction in acidic media," *Journal of Catalysis*, vol. 317, pp. 30–43, aug 2014. [Online]. Available: https://linkinghub.elsevier.com/retrieve/pii/S0021951714001468

[292] K. Mamtani, D. Singh, J. Tian, J.-M. M. Millet, J. T. Miller, A. C. Co, and U. S. Ozkan, "Evolution of N-Coordinated Iron–Carbon (FeNC) Catalysts and Their Oxygen Reduction (ORR) Performance in Acidic Media at Various Stages of Catalyst Synthesis: An Attempt at Benchmarking," *Catalysis Letters*, vol. 146, no. 9, pp. 1749–1770, sep 2016. [Online]. Available: http://link.springer.com/10.1007/s10562-016-1800-z

[293] U. I. Kramm, A. Zana, T. Vosch, S. Fiechter, M. Arenz, and D. Schmeißer, "On the structural composition and stability of Fe–N–C catalysts prepared by an intermediate acid leaching," *Journal of Solid State Electrochemistry*, vol. 20, no. 4, pp. 969–981, apr 2016. [Online]. Available: http://link.springer.com/10.1007/s10008-015-3060-z

[294] C. H. Choi, H.-K. Lim, M. W. Chung, G. Chon, N. Ranjbar Sahraie, A. Altin, M.-T. Sougrati, L. Stievano, H. S. Oh, E. S. Park, F. Luo, P. Strasser, G. Dražić, K. J. J. Mayrhofer, H. Kim, and F. Jaouen, "The Achilles' heel of iron-based catalysts during oxygen reduction in an acidic medium," *Energy & Environmental Science*, vol. 11, no. 11, pp. 3176–3182, 2018. [Online]. Available: http://xlink.rsc.org/?DOI=C8EE01855C

[295] Y. Sone, "Proton Conductivity of Nafion 117 as Measured by a Four-Electrode AC Impedance Method," *Journal of The Electrochemical Society*, vol. 143, no. 4, p. 1254, 1996. [Online]. Available: https://iopscience.iop.org/article/10.1149/1.1836625

[296] G. Merle, M. Wessling, and K. Nijmeijer, "Anion exchange membranes for alkaline fuel cells: A review," *Journal of Membrane Science*, vol. 377, no. 1-2, pp. 1–35, jul 2011. [Online]. Available: https://linkinghub.elsevier.com/retrieve/pii/S0376738811003085

6

Extended Investigation for Errors and Problem Estimation and Reproducible Results

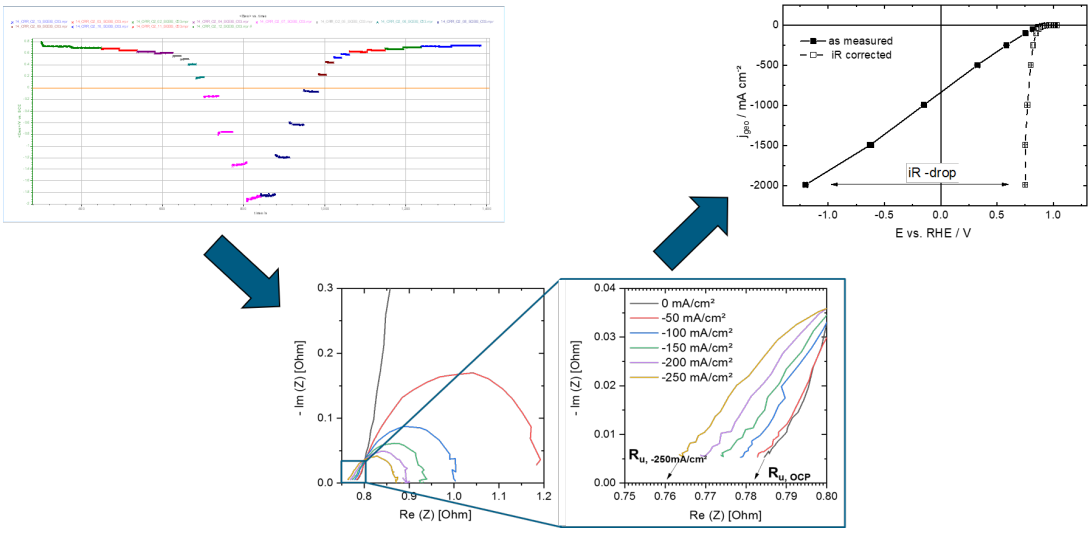

Figure 6.1: The Impact of data correction and the effect of iR leading to high difference in ORR activity

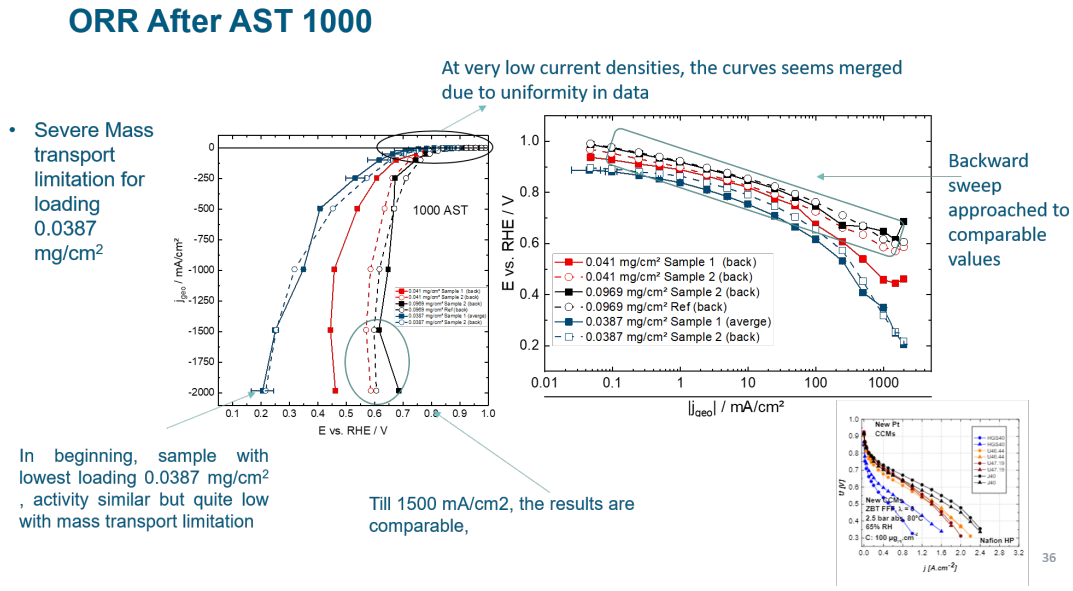

Figure 6.2: The errors during activation procedure of Pt/HGS after 1000 degradation cycles

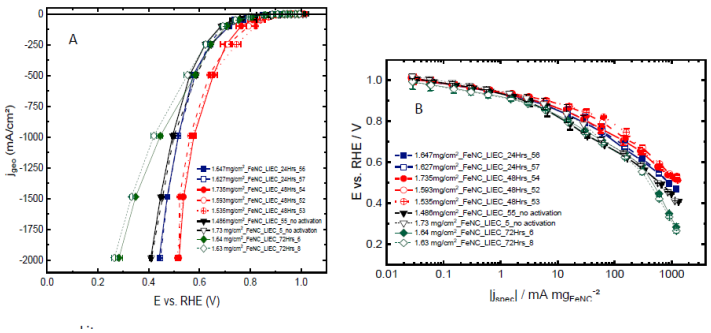

Figure 6.3: Reproducible results of several samples in GDE half cell for Fe-N-C in 1.0M KOH

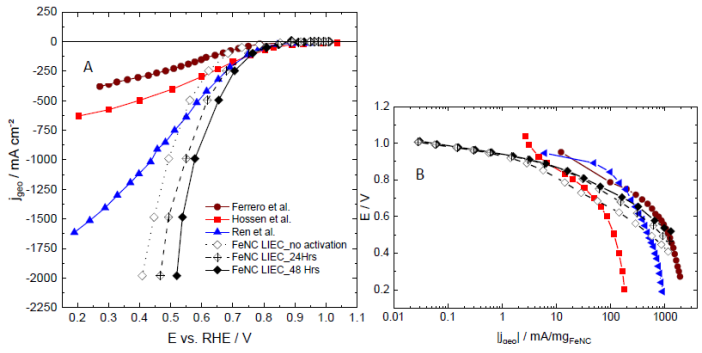

Figure 6.4: Comparison of modified samples Fe-N-C with LIEC activation in GDE half cell to previous research

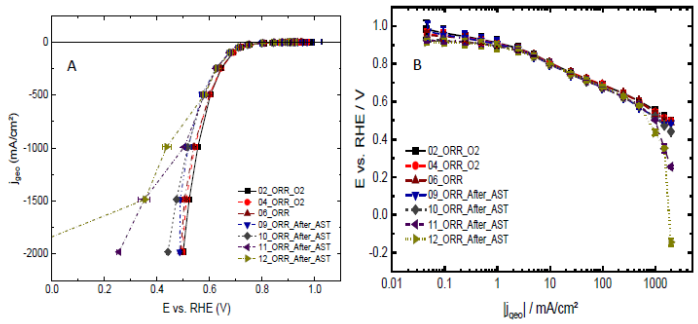

Figure 6.5: Reproducible results of ORR activity in numerous SGIES steps in GDE half cell for Fe-N-C in 1.0M KOH

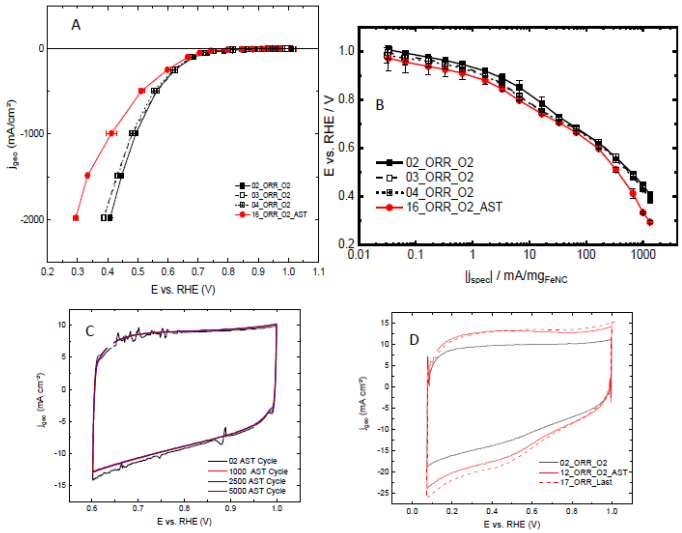

Figure 6.6: The ORR activity effect of non activated Fe-N-C LIEC with degradation cycles in Ar-Multiple test of ORR in O_2

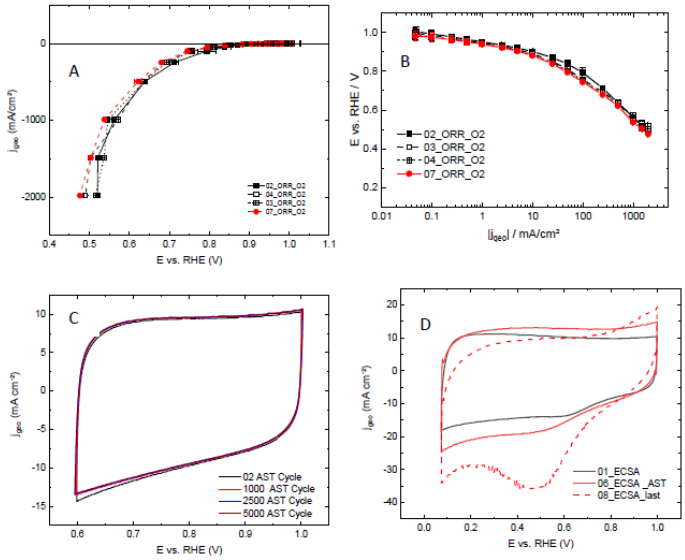

Figure 6.7: The ORR activity effect of highly activated (48Hrs) Fe-N-C LIEC with degradation cycles in Ar-Multiple test of ORR in O_2

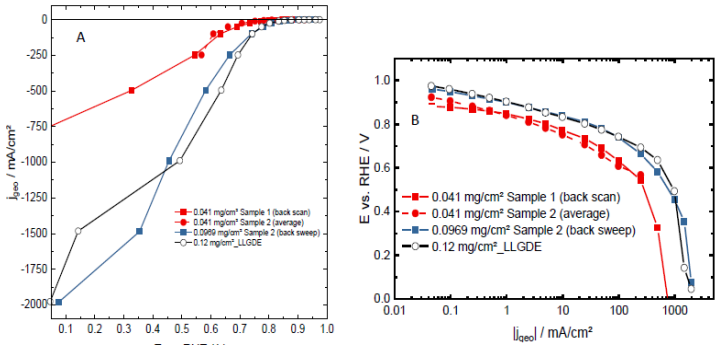

Figure 6.8: Comparison of activity degradation of Pt/HGS in synthetic air with commercial Pt/C catalyst

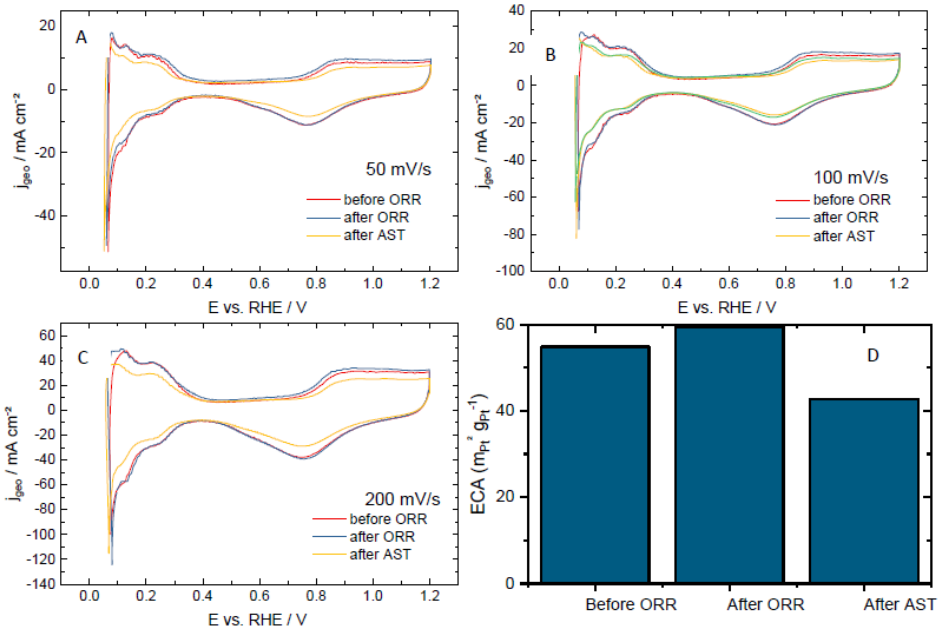

Figure 6.9: Commercial Pt/C HISPEC 4000 recorded voltammogram at 50, 100 and 200 mV/sec with ECSA before and after stress test

7

Publication

Electrochemistry Communications 116 (2020) 106761

Contents lists available at ScienceDirect

Electrochemistry Communications

journal homepage: www.elsevier.com/locate/elecom

Fuel cell catalyst layer evaluation using a gas diffusion electrode half-cell: Oxygen reduction reaction on Fe-N-C in alkaline media

Konrad Ehelebe[a,b,*,1], Talal Ashraf[c,d,1], Simon Hager[a], Dominik Seeberger[a,b], Simon Thiele[a,b], Serhiy Cherevko[a,*]

[a] Forschungszentrum Jülich GmbH, Helmholtz-Institute Erlangen-Nürnberg for Renewable Energy (IEK-11), Egerlandstraße 3, 91058 Erlangen, Germany
[b] Department of Chemical and Biological Engineering, Friedrich-Alexander University Erlangen-Nürnberg, Egerlandstraße 3, 91058 Erlangen, Germany
[c] Instituto Superior Técnico – University of Lisbon, 1049-001 Lisbon, Portugal
[d] AGH University of Science and Technology, 30-059 Kraków, Poland

ARTICLE INFO

Keywords:
Fe-N-C
Oxygen reduction reaction
Gas diffusion electrode
Alkaline fuel cell
Non-noble metal catalyst
Alkaline ionomer

ABSTRACT

Anion exchange membrane fuel cells (AEMFC) are a promising technology to allow the application of non-precious metal catalysts. While many of such catalysts have been identified in numerous recent fundamental research studies, reports evaluating these catalysts in realistic AEMFC catalyst layers together with stability assessments are rare. In the present work we show that fast and reliable evaluation and optimization of Fe-N-C-based oxygen reduction reaction (ORR) catalyst layers can be achieved using a gas diffusion electrode (GDE) half-cell approach. To set a benchmark in such measurements, a commercial Pajarito Powder Fe-N-C catalyst and commercial Aemion^{TM} ionomer are used. It is demonstrated that the ORR performance can be increased significantly by fine-tuning of the ionomer activation time. Furthermore, the optimized Fe-N-C-based catalyst layer shows very high stability with no observable performance deterioration after 5000 cycles in the 0.6–1.0 V vs. RHE potential window.

1. Introduction

After decades of optimization, proton exchange membrane fuel cells (PEMFC) with Pt-group metal (PGM) catalysts have reached commercialization level [1]. However, the price for those devices is still high. The membrane electrode assembly (MEA) with PGM-based catalyst layers accounts for approximately one third of the overall device costs [2]. Therefore, the search for efficient, durable and cheap electrocatalysts and their implementation in real devices are two of the main topics in fuel cell research [3]. Recently, catalysts synthesized from earth-abundant, inexpensive and easily exploited materials as iron, nitrogen, and carbon (Fe-N-C) exhibit promising oxygen reduction reaction (ORR) activities, which opens new opportunities to significantly reduce the overall fuel cell technology costs [4]. Still, for this kind of catalyst the acidic environment of conventional PEMFCs imposes stability challenges, mainly due to Fe dissolution and carbon corrosion [5–7]. When operated in an alkaline environment instead, the durability of non-PGM materials can be improved significantly [8]. Additionally, the intrinsic activity of those materials can be slightly increased at high pH values [9]. Therefore, anion exchange membrane fuel cells (AEMFC) could facilitate the widespread application of non-PGM catalysts and hence significantly reduce overall fuel cell device costs. Recently tremendous progress in AEMFC development has led to performances exceeding power densities of PEMFCs using non-PGM catalyst materials [10]. This progress mainly arises from optimized mass transport of water, OH^- and the reactant gases, which is influenced by (i) membrane and ionomer materials, (ii) catalyst layer design and (iii) operating conditions. For more details, the readers are referred to excellent reviews in the field [10–13]. As those mass transport phenomena have a huge impact on the fuel cell performance, appropriate methods should be established to examine and optimize this influencing parameters both properly and rapidly.

Hitherto Fe-N-C research and development in PEMFC and AEMFC has mainly been conducted with either thin-film rotating disk electrode (TF-RDE) or MEA setups. Both suffer from limitations evaluating catalyst layer effects on the single cell performance. Thin catalytic layers $< 100\ \mu g\ cm^{-2}$ are suggested for a valid application of TF-RDE, but often very high amounts of catalyst are used for those

* Corresponding authors at: Forschungszentrum Jülich GmbH, Helmholtz-Institute Erlangen-Nürnberg for Renewable Energy (IEK-11), Egerlandstraße 3, 91058 Erlangen, Germany.
E-mail addresses: k.ehelebe@fz-juelich.de (K. Ehelebe), s.cherevko@fz-juelich.de (S. Cherevko).
[1] These authors contributed equally to this work.

https://doi.org/10.1016/j.elecom.2020.106761
Received 15 April 2020; Received in revised form 19 May 2020; Accepted 20 May 2020
Available online 31 May 2020

measurements leading to uncontrolled hydrodynamics and potentially misleading intrinsic results [14]. Additionally, the Fe-N-C catalyst most active in RDE, does not automatically lead to the best performance in MEA [15,16], which is not really surprising taking into account the different mass transport effects in a very thin catalyst layer on a solid glassy carbon disk in RDE experiments and a realistic catalyst layer on a gas diffusion layer used in MEA experiments. Especially because experiments with Fe-N-C catalysts in both PEMFC and AEMFC have already revealed the impact of catalyst layer parameters (e.g. type of ionomer, ionomer content and distribution and manufacturing condition) on the morphology and transport behaviour in the electrode and therefore the single cell performance [17–19]. Generally it has to be pointed out, that a fuel cell electrode is a complex structure including catalyst, ionomer and void space, where each one of these plays a crucial role for electrode function [12]. This can only be investigated insufficiently with TF-RDE experiments. Hence MEA experiments are widely used to study catalyst layer effects on the fuel cell performance. But MEA experiments also introduce major drawbacks as they are (i) time and material intensive, (ii) do not allow direct insights into one single electrode (usually lack of a reference electrode) and (iii) are often difficult to compare due to deficiency of standardized test protocols and conditions for the evaluation of non-PGM catalysts. To bridge the gap between RDE and MEA experiments and to combine their advantages, recently different groups have conducted experiments with electrochemical half-cells using gas diffusion electrodes (GDE) as working electrodes [20–22]. Those GDE experiments allow fast and comparable testing at standardized operating conditions and provide dedicated insights into one single electrode with realistic catalyst layer parameters at relevant potential and current ranges. Therefore, this method can be an optimal supplement to drastically shorten the time from successful catalyst synthesis to an operating electrode for fuel cell applications.

In this communication, we present the first implementation of this novel GDE method for non-PGM catalysts in alkaline environment. As the ORR is still the limiting half-cell reaction [12], we focus on cathode catalyst layers and will address anode catalyst layer optimization in further work.

2. Material and methods

2.1. Catalyst ink and electrode preparation

The PGM-free high pH GDE was fabricated from an ink comprised of a total of 20 wt% solids in 1-propanol. The solid fraction was made up by commercial 70 wt% Fe-N-C (PMF-011904, Pajarito Powder) and commercial 30 wt% ionomer (Aemion^{TM} HNN5-00-X, Ionomr) with ion exchange capacity (IEC) ~1.4–1.7 meq g^{-1}. The ionomer was dissolved in the solvent and then added to the catalyst powder. The resulting ink was stirred for one hour, placed in an ultra-sonication bath for one hour, stirred overnight, sonicated again for another hour on the next day and after this, stirred until usage. The ink was applied onto a Freudenberg H23C8 gas diffusion media (4 × 4 cm) with an automated film applicator (ZAA 2300, Zehntner). The wet film thickness was determined by adjusting the gap-height on the doctor blade. It was set to 170 µm, which resulted in an average loading of ~1.3–1.5 mg cm^{-2}. Subsequently the samples were dried at 40 °C for 1 h and at 40 °C under reduced pressure for an additional hour. The Fe-N-C loading of the GDEs was measured by weighing (Sartorius Cubis®, 0.001 mg) the samples before and after the catalyst ink deposition and solvent evaporation.

2.2. GDE half-cell measurements

For the electrochemical measurements the GDE setup, electrochemical components and protocols presented in a previous work [22] were used. For more detailed information, see also Supporting Information. All experiments were carried out in minimum two batches of experiments in 1.0 M KOH (EMSURE®, Merck). Potentials were converted to reversible hydrogen electrode (RHE) reference. Reference electrode potential against RHE was measured before every experiment with the same batch of electrolyte ($E_{Ag/AgCl} = 1.015 - 1.026\ V_{RHE}$).

3. Results and discussion

As described above, GDE half-cell experiments can be used to investigate and optimize single catalyst layer parameters in a fast and dedicated way. One of those parameters is the pre-conditioning or activation of the ionomer used in the catalyst layer. As the ionomer is present in the iodide form, an exchange of those iodide ions with hydroxide ions is required to obtain a hydroxide conductive polymer [23]. In the literature this activation is mostly done by immersing the alkaline electrode into 1 M KOH solution. But different activation protocols have been applied, also varying for different ionomers. Some research groups dip the electrode into the solution for 40–60 min [24,25], 5–6 h [26], 24 h [27] or 48 h [28,29]. However, the impact of immersion time for activation of alkaline electrodes has never been compared. Therefore, the samples were differentially preconditioned by immersing them into 1 M KOH for several intervals (2 × 20 min, 24 h, 48 h and 72 h) and subsequently washed thoroughly with ultrapure water to remove the impurities. In Fig. 1 the polarization curves in O_2 and cyclic voltammograms (CV) in Ar of alkaline Fe-N-C electrodes are compared, which have been activated in 1 M KOH for various timeframes.

From the comparison it can be clearly seen that the activation procedure effects the electrode's performance. While immersing the electrode into 1 M KOH for 2 × 20 min or 24 h does not lead to a significant improvement of the ORR performance, a pre-treatment of the alkaline GDEs in 1 M KOH for 48 h leads to best activities and mass transport properties. Therefore, it can be concluded that using Aemion^{TM} ionomers 48 h of pre-conditioning in 1 M KOH are required to replace all the iodide ions with hydroxide ions and obtain the optimal hydroxide conductivity. Surprisingly a drastic decrease in mass transport properties (but not intrinsic activity, see low-current region in Fig. 1B) can be observed after 72 h of pre-treatment in 1 M KOH. This is probably due to catalyst or ionomer degradation in aqueous alkaline environment.

It has to be noted that this activation data is very specific to the alkaline ionomer which is used for GDE manufacturing. But the example shows how GDE experiments can be used to drastically accelerate electrode evaluation and activation. Whereas one single cell experiment almost takes one day of experiments, due to sophisticated MEA fabrication in alkaline, assembling, heating up, cooling down and disassembling of the cell, all the experiments for this activation study with repetitions could be conducted in less than four working days. Additionally, in half-cell experiments, factors such as anodic reaction limitations and carbonation of the alkaline ionomers [25,30] can be excluded and therefore, the effect of one single parameter can be investigated exclusively.

After the impact of ionomer activation was investigated, the durability of the GDEs in alkaline environment as well as a possible impact of carbonation should be assessed. The carbonation of ionomers can lead to significant problems in AEMFC, mainly due to changes in conductivity behaviour and therefore mass transport limitations, but also electrocatalytic effects [25,30]. Although carbonation of the ionomer mainly occurs when operating AEMFC with ambient air, it can already take place during the manufacturing process or sample storage as the exchange from OH^- to HCO_3^-/CO_3^{2-} occurs very fast. Nevertheless, it has been found out, that at high current densities all HCO_3^-/CO_3^{2-} are exchanged by OH^- again ("self-purging") [30,31]. Therefore, the samples have first been tested towards their ORR activity up to 2 Acm^{-2} three times consecutively to check for any effect of ionomer carbonation on ORR activity determination. Subsequently they have been exposed to a load cycling protocol comprising 5000 triangular cycles between 0.6 and 1.0 V vs. RHE performed at a scan rate of 100 mV s^{-1}

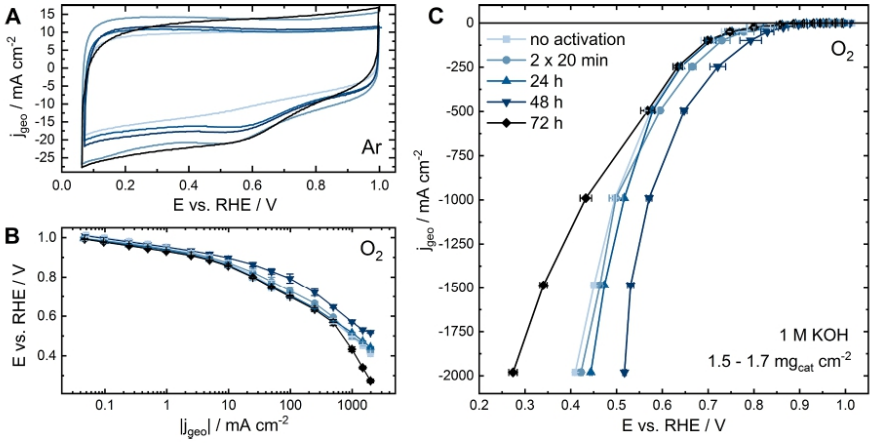

Fig. 1. Comparison of polarization curves of alkaline Fe-N-C cathodes (Pajarito Powder, 1.5–1.7 mg_{cat} cm^{-2}) with Aemion™ ionomer and different pre-treatment procedures applied. Tested in 1.0 M KOH. A: Cyclic voltammograms (100 mV s^{-1}) with Ar. B&C: Tafel plot and polarization curve for the oxygen reduction reaction with pure O_2.

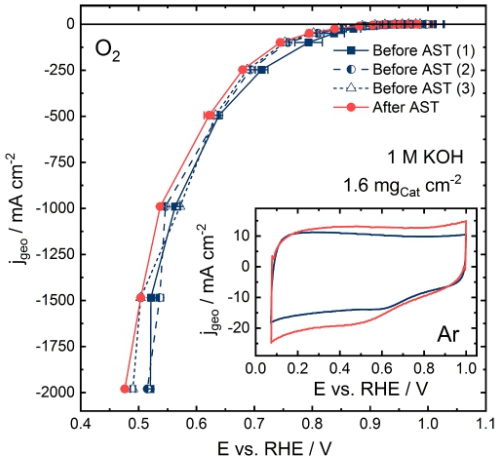

Fig. 2. Comparison of consecutive polarization curves of alkaline Fe-N-C cathodes (Pajarito Powder, 1.6 mg_{cat} cm^{-2}) with Aemion™ ionomer (48 h activated in 1 M KOH) before (blue) and after (red) 5000 degradation cycles (100 mV s^{-1}, 0.6–1.0 V vs. RHE, Ar). Tested in 1.0 M KOH with O_2. Inset: Cyclic voltammograms of same samples in Ar.

in Ar-saturated electrolyte as used in previous degradation studies for non-PGM catalysts [8]. In Fig. 2, the cathode's activity towards ORR during this protocol is compared on the example of one 48 h activated sample. For reasons of clarity only one sample is displayed, but the trends shown in Fig. 2 have been confirmed in all other experiments.

From Fig. 2 two conclusions can be drawn: (i) There is no significant performance loss over 5000 degradation cycles. A slightly worse performance in comparison to the fresh samples can be attested, but the difference is minor and lays very close to the error bars of GDE testing at those high current densities. Therefore, the results from experiments in aqueous electrolyte can be confirmed [8] where Fe-N-C catalysts proved to be suitable for AEMFC applications in terms of durability. (ii) Carbonation does not play a significant role in GDE testing in alkaline environment, as the performance over the first consecutive polarization curves remains stable. This can be attributed to the constant purging of the adjacent aqueous electrolyte with Ar for about 20 min prior to the ORR experiments, when CVs in Ar are recorded. This shows, that GDE experiments are a suitable tool to evaluate the degradation of only one single catalyst layer. The impact of carbonation could be studied further in detail by purging different concentrations of CO_2 into the aqueous electrolyte and thereby facilitate the carbonation of the ionomer.

A catalyst system should always be compared to recent state-of-the-art developments to provide a comprehensive evaluation to the readers. Unfortunately, this is not always done appropriately, which can lead to difficulties in comparing results between different research groups. In Fig. 3 we provide a comparison of the present results to the state-of-the-art performances measured in AEMFC experiments with: (i) the same catalyst, (ii) Fe-N-C catalysts in general and (iii) PGM catalysts.

In previous AEMFC experiments with the commercial Fe-N-C catalyst from Pajarito Powder (empty squares), Hossen et al. [26] have been able to achieve current densities up to approximately 700 mA cm^{-2}. In comparison with our present results with the same catalyst it can be seen that the onset of the polarization curve in the activation region is in a comparable range, even slightly higher at Hossen's single cell experiments, probably due to different operating conditions in AEMFC testing (60 °C, 1.4 bar) and higher catalyst loading (3.5 vs. 1.6 mg_{Cat} cm^{-2}). However, when exceeding low current densities severe reaction limitations can be observed in the high current region. There can be multiple explanations for that: (i) catalytic limitations at the Pt/C anode, (ii) mass transport-limitations in either the cathode's or the anode's catalyst layer, (iii) ohmic resistance in the membrane. And probably each of these factors plays a role in limiting the overall reaction. But in the conducted single cell experiment it is difficult to reveal which effect is the most severe, stressing again the advantage of the presented GDE half-cell method. The benchmark for Fe-N-C catalysts in alkaline environment was just recently set by Firouzjaie et al. [10] using a catalyst from Jaouen's group [8]. The better performance of their catalyst system in comparison with the one presented in the present work can be explained by: (i) their use of a catalyst tuned for alkaline environment, instead of a commercial catalyst developed especially for acidic environment; (ii) improved mass-transport through catalyst layer engineering. Especially Mustain's group has developed methods to drastically improve AEMFC performance through dedicated

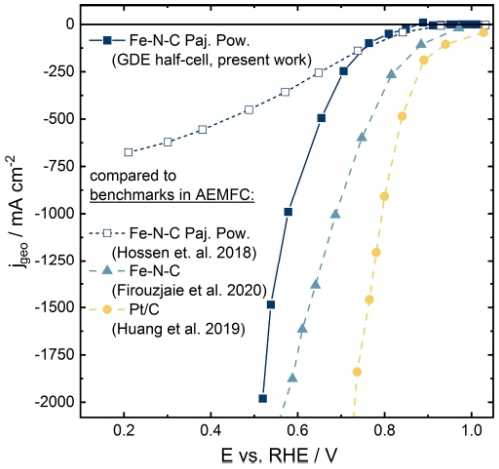

Fig. 3. Comparison of the present work (blue squares, 1.6 $mg_{Fe\text{-}N\text{-}C}$ cm^{-2}) with benchmark results of AEMFC experiments with (a) the same commercial catalyst from Pajarito Powder (empty squares, Fe-N-C cathode: 3.5 $mg_{Fe\text{-}N\text{-}C}$ cm^{-2}, Pt/C anode: 0.2 mg_{Pt} cm^{-2}) [26], (b) Fe-N-C catalysts (light blue triangles, Fe-N-C cathode: 0.9 $mg_{Fe\text{-}N\text{-}C}$ cm^{-2}, PtRu/C anode: 0.6 mg_{PtRu} cm^{-2}) [10] and (c) Pt/C catalyst (yellow, Pt/C cathode: 0.56 mg_{Pt} cm^{-2}, PtRu/C anode: 0.986 mg_{PtRu} cm^{-2}) [32]. (For interpretation of the references to colour in this figure legend, the reader is referred to the web version of this article.)

catalyst layer design [10,12]. This is not only crucial working with non-PGM catalysts, but also in AEMFCs using PGM catalysts, confirmed by the fact that also the benchmark PGM system in AEMFC has been developed by the same group [32]. This again highlights the importance of catalyst layer parameters on AEMFCs performance. However, in single cell experiments it is often difficult to reveal the impact of those parameters and compare with studies from other groups as (i) both half-cell reactions and mass-transport phenomena in the membrane can play a crucial role on the cell's performance and (ii) no standard operating procedure has been established yet, which leads to various different testing protocols and testing parameters complicating a valid comparison between different literature results. Therefore, standardized half-cell experiments using GDE setup could play an important role accelerating the understanding and optimization of catalyst layer parameters to further improve AEMFC performance.

4. Conclusions and outlook

AEMFCs are a promising technology to allow the application of non-PGM catalysts to fuel cells due to their improved stability in alkaline media. Nevertheless, a lot of effort still has to be made in understanding the impact of catalyst layer parameters and subsequently optimizing them. For PEMFC this optimization took decades. Therefore, faster methods should be developed to help accelerating this research. GDE half-cell experiments are proposed as one of such methods to bridge the gap between TF-RDE and MEA testing. Both, RDE and MEA will still play an important role for catalyst synthesis evaluation (RDE) and evaluating operating parameters and full cell phenomena such as water management (MEA). Nevertheless, GDE experiments allow faster and dedicated evaluation of the effect of catalyst layer parameters on AEMFC performance. In this study this has been demonstrated on the examples of (i) ionomer activation, where immersing the GDE with commercial Aemion™ ionomer in 1 M KOH for 48 h leads to the best electrode performance, and (ii) Fe-N-C catalyst stability, where the commercial Pajarito Powder catalyst showed high stability during 5000 load cycles between 0.6 and 1.0 V vs. RHE. Due to the simplicity of the setup this experiments could be conducted in a fraction of the time necessary for MEA testing. The obtained results have been compared to benchmarks in literature. This comparison revealed the importance of understanding and optimizing catalyst layer parameters, such as catalyst loading, type of ionomer, ionomer content and distribution, and the morphology of the catalyst layer. Further work will be dedicated to understanding the impact of those parameters on both anode and cathode performance. Also the effect of carbonation of the ionomer will be addressed by using different CO_2 saturation in the aqueous electrolyte.

CRediT authorship contribution statement

Konrad Ehelebe: Conceptualization, Investigation, Writing - original draft, Writing - review & editing. **Talal Ashraf:** Investigation, Writing - original draft, Writing - review & editing. **Simon Hager:** . **Dominik Seeberger:** Investigation, Writing - review & editing. **Simon Thiele:** Resources, Writing - review & editing. **Serhiy Cherevko Conzeptualization:** Resources, Writing - review & editing, Supervision.

Declaration of Competing Interest

The authors declare that they have no known competing financial interests or personal relationships that could have appeared to influence the work reported in this paper.

Acknowledgements

KE gratefully thanks Heinrich Böll Foundation for financial support.

Appendix A. Supplementary data

Supplementary data to this article can be found online at https://doi.org/10.1016/j.elecom.2020.106761.

References

[1] T. Yoshida, K. Kojima, Electrochem. Soc. Interface 24 (2015) 45–49, https://doi.org/10.1149/2.F03152if.
[2] W. Bernhart, S. Riederle, M. Yoon, W.G. Aulbur, Auto Tech. Rev. 3 (2014) 18–23, https://doi.org/10.1365/s40112-014-0568-z.
[3] D. Banham, S. Ye, ACS Energy Lett. 2 (2017) 629–638, https://doi.org/10.1021/acsenergylett.6b00644.
[4] U. Martinez, S. Komini Babu, E.F. Holby, H.T. Chung, X. Yin, P. Zelenay, Adv. Mater. 31 (2019) 1806545, https://doi.org/10.1002/adma.201806545.
[5] C.H. Choi, W.S. Choi, O. Kasian, A.K. Mechler, M.T. Sougrati, S. Brüller, K. Strickland, Q. Jia, S. Mukerjee, K.J.J. Mayrhofer, F. Jaouen, Angew. Chem. Int. Ed. 56 (2017) 8809–8812, https://doi.org/10.1002/anie.201704356.
[6] U. Martinez, S. Komini Babu, E.F. Holby, P. Zelenay, Curr. Opin. Electrochem. 9 (2018) 224–232, https://doi.org/10.1016/j.coelec.2018.04.010.
[7] Y. Shao, J.-P. Dodelet, G. Wu, P. Zelenay, Adv. Mater. 31 (2019) 1807615, https://doi.org/10.1002/adma.201807615.
[8] P.G. Santori, F.D. Speck, J. Li, A. Zitolo, Q. Jia, S. Mukerjee, S. Cherevko, F. Jaouen, J. Electrochem. Soc. 166 (2019) F3311–F3320, https://doi.org/10.1149/2.0371907jes.
[9] S. Rojas-Carbonell, K. Artyushkova, A. Serov, C. Santoro, I. Matanovic, P. Atanassov, ACS Catal. 8 (2018) 3041–3053, https://doi.org/10.1021/acscatal.7b03991.
[10] H.A. Firouzjaie, W.E. Mustain, ACS Catal. 10 (2020) 225–234, https://doi.org/10.1021/acscatal.9b03892.
[11] A. Serov, I.V. Zenyuk, C.G. Arges, M. Chatenet, J. Power Sources 375 (2018) 149–157, https://doi.org/10.1016/j.jpowsour.2017.09.068.
[12] W.E. Mustain, Curr. Opin. Electrochem. 12 (2018) 233–239, https://doi.org/10.1016/j.coelec.2018.11.010.
[13] S. Gottesfeld, D.R. Dekel, M. Page, C. Bae, Y. Yan, P. Zelenay, Y.S. Kim, J. Power Sources 375 (2018) 170–184, https://doi.org/10.1016/j.jpowsour.2017.08.010.
[14] A.R. Zeradjanin, ChemSusChem 11 (2018) 1278–1284, https://doi.org/10.1002/cssc.201702287.
[15] M.J. Workman, M. Dzara, C. Ngo, S. Pylypenko, A. Serov, S. McKinney, J. Gordon, P. Atanassov, K. Artyushkova, J. Power Sources 348 (2017) 30–39, https://doi.org/10.1016/j.jpowsour.2017.02.067.
[16] F. Jaouen, V. Goellner, M. Lefèvre, J. Herranz, E. Proietti, J.P. Dodelet, Electrochim. Acta 87 (2013) 619–628, https://doi.org/10.1016/j.electacta.2012.09.057.

[17] S. Stariha, K. Artyushkova, M.J. Workman, A. Serov, S. McKinney, B. Halevi, P. Atanassov, J. Power Sources 326 (2016) 43–49, https://doi.org/10.1016/j.jpowsour.2016.06.098.
[18] X. Yin, L. Lin, H.T. Chung, S. Komini Babu, U. Martinez, G.M. Purdy, P. Zelenay, ECS Trans. (2017), https://doi.org/10.1149/07711.1273ecst.
[19] B. Britton, S. Holdcroft, J. Electrochem. Soc. 163 (2016) F353–F358, https://doi.org/10.1149/2.0421605jes.
[20] B.A. Pinaud, A. Bonakdarpour, L. Daniel, J. Sharman, D.P. Wilkinson, J. Electrochem. Soc. 164 (2017) F321–F327, https://doi.org/10.1149/2.0891704jes.
[21] M. Inaba, A.W. Jensen, G.W. Sievers, M. Escudero-Escribano, A. Zana, M. Arenz, Energy Environ. Sci. 11 (2018) 988–994, https://doi.org/10.1039/C8EE00019K.
[22] K. Ehelebe, D. Seeberger, M.T.Y. Paul, S. Thiele, K.J.J. Mayrhofer, S. Cherevko, J. Electrochem. Soc. 166 (2019) F1259–F1268, https://doi.org/10.1149/2.0911915jes.
[23] O.D. Thomas, K.J.W.Y. Soo, T.J. Peckham, M.P. Kulkarni, S. Holdcroft, J. Am. Chem. Soc. 134 (2012) 10753–10756, https://doi.org/10.1021/ja303067t.
[24] T.J. Omasta, Y. Zhang, A.M. Park, X. Peng, B. Pivovar, J.R. Varcoe, W.E. Mustain, J. Electrochem. Soc. 165 (2018) F710–F717, https://doi.org/10.1149/2.1401809jes.
[25] Y. Zheng, T.J. Omasta, X. Peng, L. Wang, J.R. Varcoe, B.S. Pivovar, W.E. Mustain, Energy Environ. Sci. 12 (2019) 2806–2819, https://doi.org/10.1039/C9EE01334B.
[26] M.M. Hossen, K. Artyushkova, P. Atanassov, A. Serov, J. Power Sources 375 (2018) 214–221, https://doi.org/10.1016/j.jpowsour.2017.08.036.
[27] C.G. Arges, J. Parrondo, G. Johnson, A. Nadhan, V. Ramani, J. Mater. Chem. 22 (2012) 3733–3744, https://doi.org/10.1039/C2JM14898F.
[28] N. Ziv, A.N. Mondal, T. Weissbach, S. Holdcroft, D.R. Dekel, J. Membr. Sci. 586 (2019) 140–150, https://doi.org/10.1016/j.memsci.2019.05.053.
[29] A.G. Wright, J. Fan, B. Britton, T. Weissbach, H.-F. Lee, E.A. Kitching, T.J. Peckham, S. Holdcroft, Energy Environ. Sci. 9 (2016) 2130–2142, https://doi.org/10.1039/C6EE00656F.
[30] N. Ziv, W.E. Mustain, D.R. Dekel, ChemSusChem 11 (2018) 1136–1150, https://doi.org/10.1002/cssc.201702330.
[31] N. Ziv, D.R. Dekel, Electrochem. Commun. 88 (2018) 109–113, https://doi.org/10.1016/j.elecom.2018.01.021.
[32] G. Huang, M. Mandal, X. Peng, A.C. Yang-Neyerlin, B.S. Pivovar, W.E. Mustain, P.A. Kohl, J. Electrochem. Soc. 166 (2019) F637–F644, https://doi.org/10.1149/2.1301910jes.